SOIL MOISTURE DYNAMICS IN WATER-LIMITED CROPPING SYSTEMS OF THE SOUTHERN GREAT PLAINS

By

ANDRES PATRIGNANI

Bachelor of Science in Agronomic Engineering
Universidad Nacional de Rosario
Rosario, Santa Fe, Argentina
2008

Master of Science in Plant and Soil Sciences
Oklahoma State University
Stillwater, OK
2011

Submitted to the Faculty of the
Graduate College of the
Oklahoma State University
in partial fulfillment of
the requirements for
the Degree of
DOCTOR OF PHILOSOPHY
December, 2015

SOIL MOISTURE DYNAMICS IN WATER-LIMITED

CROPPING SYSTEMS OF THE

SOUTHERN GREAT PLAINS

Dissertation Approved:

Dr. Tyson E. Ochsner

Dissertation Adviser

Dr. Jeffrey T. Edwards

Dr. Jason Warren

Dr. Duncan Wilson

.

ACKNOWLEDGEMENTS

I dedicate this dissertation to my family who has provided unconditional support at a great distance. I would also like to acknowledge the members of my committee: Drs. Jeff Edwards, Jason Warren, and Duncan Wilson who have always provided valuable feedback and challenging questions. I also want to extend my gratitude to all the undergraduate and graduate students of the soil physics team that have helped me during the past four years and from whom I learned invaluable lessons. Finally, I want to thank Dr. Tyson E. Ochsner for shaping my professional career like no one else has ever done.

Name: ANDRES PATRIGNANI

Date of Degree: DECEMBER, 2015

Title of Study: SOIL MOISTURE DYNAMICS IN WATER-LIMITED CROPPING SYSTEMS OF THE SOUTHERN GREAT PLAINS

Major Field: SOIL SCIENCE

Abstract:

In this dissertation we present and discuss four research questions about the role of water in the water-limited cropping systems of the southern Great Plains. i) Why are wheat yields near stagnation in the southern Great Plains? Grain yield and growing season rainfall for a total of 19 Oklahoma counties were analyzed. Current yields represent 74% of the maximum attainable yield but only 30% of water-limited potential yield at state level. Wheat yields were often limited by factors other than growing season rainfall amount. ii) Is it possible to develop a simple and accurate tool to measure in situ vegetation conditions to inform crop models and in-season management decisions? A new tool called Canopeo was designed to quantify green canopy cover from digital images and videos. The rapid image processing and the accurate values of green canopy cover make Canopeo a useful tool with potential to better manage grazing and improve soil moisture estimations in winter wheat cropping systems. iii) Can we directly use soil moisture observations under grassland to represent the soil moisture condition of nearby wheat cropland? Grassland and winter wheat soil moisture dynamics were analyzed for 78 Oklahoma Mesonet stations. The use of a neural network as an observation operator proved to be effective to capture the main soil moisture dynamics under winter wheat cropland. This study revealed that there is inscribed information in the soil moisture time series under grassland vegetation that allow estimates of soil moisture in nearby cropland. iv) Do plants growing in the same soil start to decline the transpiration rate at higher soil water contents under higher atmospheric demands? What is the nature of that relationship? Corn plants were grown in a controlled-environment chamber under atmospheric demands of 4.8 and 8.4 mm d^{-1} reference evapotranspiration. Relative plant transpiration rate (actual rate/potential rate) started to consistently decline at a soil matric potential similar to that at the inflection point of the soil water retention curve, regardless of the atmospheric demand. A double exponential function proved effective to describe the relationship between relative transpiration and soil matric potential for different soil and atmospheric demands.

TABLE OF CONTENTS

LIST OF TABLES

TABLES IN CHAPTER II

Table Page

TABLES IN CHAPTER III

TABLES IN CHAPTER IV

TABLES IN CHAPTER V

LIST OF FIGURES

FIGURES IN CHAPTER II

Figure Page

FIGURES IN CHAPTER III

FIGURES IN CHAPTER IV

FIGURES IN CHAPTER V

CHAPTER I

GENERAL INTRODUCTION

Winter wheat (*Triticum aestivum* L.) is the most widely cultivated crop worldwide with over 200 million hectares harvested every year (FAO, 2015). Wheat is considered the third largest crop worldwide from the production stand point with a total of 716 million Mg yr^{-1} (FAO, 2013), only behind corn and paddy rice. The United States of America is the third largest wheat producing country and has a total of about 22 million hectares of wheat planted every year (USDA-NASS, 2015). The southern Great Plains states of Kansas, Oklahoma, and Texas account for about 40% of the total planted area in the US (USDA-NASS, 2015), making winter wheat a major player in the economy of the region. Furthermore, in states such as Oklahoma, winter wheat represents ~70% of the total cropland area (USDA-NASS, 2015), making it a major player in the hydrology of many watersheds of the southern Great Plains. In this region, winter wheat is predominantly grown in rainfed environments where frequent soil water stress is among the most important limitations to crop production. In order to better understand the dynamics of winter wheat systems under water-limited conditions, we investigate in this dissertation four main questions from which we expect to gain useful agronomic and hydrologic insights.

i) From the late 1800s until the 1950s wheat yields across the southern Great Plains were constant at about 0.8 Mg ha^{-1} (USDA-NASS, 2015). The development of semi-dwarf varieties that increased the proportion of grain relative to total crop biomass (i.e. harvest index) and improved fertilization strategies caused a dramatic rise of wheat yields in the mid-1950s. By the.

end of the 1980s, wheat yields in the region were topping a new level near 2.0 Mg ha^{-1}. Nonetheless, since the 1980s wheat yields have remained stagnant in the state of Oklahoma and near stagnant in the southern Great Plains. Current research shows that yield stagnation is often due to a narrow gap between current grain yields and potential yields (Cassman, 1999; Lobell et al., 2009; Grassini et al., 2011; Ittersum et al., 2013), but the magnitude and reasons of the yield gap for winter wheat in the southern Great Plains remains unknown. Why are wheat yields near stagnation in the southern Great Plains? Are current grain yields close to water-limited potential yields? Is the limited-growing season rainfall a driving factor for yield stagnation?

ii) Crop models for prediction of grain yield and root-zone soil moisture use local weather observations and soil properties. Despite the high sensitivity of vegetation dynamics to local weather and soil conditions, plant simulation routines typically rely on species-specific parameters without accounting for local interactions. This is of particular interest in dual purpose (i.e. grazing and grain) and wheat systems of the southern Great Plains, where wheat biomass dynamics dramatically change with each grazing event. Tools that can measure the crop condition can be used to correct simulated crop growth leading to better soil moisture and grain yield estimations. In addition, dual purpose wheat systems require careful management of the stocking rate, and careful management of the entry and termination of the grazing period for dual purpose wheat fields is essential to avoid a penalty in the final grain yield as a consequence of overgrazing. Research conducted in the state of Oklahoma shows that final grain yield is closely linked to the amount of green canopy cover that is maintained during grazing (Butchee and Edwards, 2012). The authors found that maintaining about 50 to 60% green canopy cover is necessary before grazing termination in order to maintain 95% of the grain yield compared to grain-only systems. Therefore, a tool capable of easily measuring green canopy cover has the potential to be used not only to correct crop models but also to aid wheat producers in better dual purpose management, but such as tool has not previously existed. Is it possible to develop a

simple and accurate tool to measure in situ vegetation conditions at high spatial and temporal resolutions? Can these observations feedback to inform crop models and in-season management decisions?

iii) In water-limited environments, soil moisture monitoring is crucial for early detection and accurate assessment of agricultural droughts (Mozny et al., 2012; Torres et al., 2013), improved hydrological model simulations (Houser et al., 1998), and development of better adapted cropping strategies (Peterson et al., 1996; Nielsen et al., 2005). The state of Oklahoma is one of the most intensively instrumented regions for weather and soil moisture monitoring in the world (Mohanty and Skaggs, 2001; McPherson et al., 2007). Nonetheless, monitoring stations have almost exclusively been deployed in grasslands dominated by warm season grasses. Although meteorological variables are representative of the surrounding environment, the extrapolation of soil moisture observations to adjacent but contrasting land covers can bias landscape estimations of soil moisture. The questions arising from this context are: can we directly use soil moisture observations under grassland to represent the soil moisture condition of nearby wheat cropland? If not, is there information in the soil moisture observations under grassland that can be exploited to estimate soil moisture under wheat cropland? Using grassland soil moisture observations to represent the soil moisture condition of other land covers nearby will enhance the value and broaden the applications large-scale monitoring networks.

iv) Quantitative responses of plant transpiration to soil drying are imperative to model plant growth in environments with frequent soil water stress. Due to the complexity of the soil-plant-atmosphere continuum, quantitative responses are empirical and have been studied in field (Muchow et al., 1986; Bennett et al., 1987; Sadras et al., 1993), greenhouse (Gholipoor et al., 2010), or growth chamber pot experiments (Ray et al., 2002; Fletcher et al., 2007) documenting the relative transpiration rate as a function of soil moisture. To represent the degree of soil moisture, multiple variables have been proposed in the literature. Perhaps, the most common

concept is that of plant available water, in which soil moisture is considered to be available for plant uptake only between an upper (i.e. field capacity) and a lower (i.e. permanent wilting point) limit. The empiricism and the difficulties for consistent determination of these limits across field, pot, and laboratory settings can lead to researcher bias and may hinder the extrapolation to field conditions (Ratliff et al., 1983). In addition, most quantitative responses have been developed for low to moderate atmospheric demands (Sadras and Milroy, 1996). Our objective is to study the transpiration response at high atmospheric demands typical during the summer periods in the southern Great Plains. We also explore alternative stress functions that do not rely on arbitrary limits to represent soil water availability.

DISSERTATION ORGANIZATION

This dissertation consists of a total of six chapters. The first and last chapters are a general introduction (**Chapter I**) and conclusion (**Chapter VI**) that lay out the research questions and most important findings. The remaining four chapters address different questions and objectives related to the role of water in cropping systems of the southern Great Plains.

Chapter II investigates possible reasons for winter wheat yield stagnation in the region. Grain yield and growing season rainfall for a total of 19 Oklahoma counties were analyzed to determine the magnitude and possible reasons of winter wheat yield and production gaps in the southern Great Plains.

Chapter III describes a new tool called Canopeo, which was designed to quantify green canopy cover from digital images and videos. This chapter describes Canopeo's working principle, its classification accuracy relative to other software products, potential applications, and limitations of this tool.

Chapter IV introduces an innovative way to use soil moisture observations under grassland vegetation to estimate soil moisture under adjacent winter wheat fields. This chapter describes the advantages and limitations of this method relative to traditional crop models. An example to demonstrate the applications of this method are presented using a grid cell of the recently launched Soil Moisture Active Passive satellite (SMAP) mission.

Chapter V studies the transpiration response to soil drying under moderate and high atmospheric demands. It also explores the use of the inflection point of the soil water retention curve to describe the response of plants to soil water stress without using arbitrary upper and lower limits.

REFERENCES

Bennett, J.M., T.R. Sinclair, R.C. Muchow, and S.R. Costello. 1987. dependence of stomatal conductance on leaf water potential, turgor potential, and relative water content in field-grown soybean and maize. Crop Sci. 27(5): 984

Butchee, J.D., and J.T. Edwards. 2013. Dual-purpose wheat grain yield as affected by growth habit and simulated grazing intensity. Crop Sci. 53(4): 1686.

Cassman, K.G. 1999. Ecological intensification of cereal production systems: yield potential, soil quality, and precision agriculture. Proc. Natl. Acad. Sci. U. S. A. 96(11): 5952–5959.

Fletcher, A.L., T.R. Sinclair, and L.H. Allen. 2007. Transpiration responses to vapor pressure deficit in well-watered "slow-wilting" and commercial soybean. Environ. Exp. Bot. 61(2): 145–151.

FAO, Food and Agriculture Organization of the United Nations Statistics Division. http://faostat3. fao.org/home/E. Accessed online 31 Oct. 2015.

Gholipoor, M., P.V.V. Prasad, R.N. Mutava, and T.R. Sinclair. 2010. Genetic variability of transpiration response to vapor pressure deficit among sorghum genotypes. Field. Crop. Res. 119(1): 85–90

Grassini, P., J. Thorburn, C. Burr, and K.G. Cassman. 2011. High-yield irrigated maize in the Western U.S. Corn Belt: I. On-farm yield, yield potential, and impact of agronomic practices. F. Crop. Res. 120(1): 142–150.

Houser, P.R., W.J. Shuttleworth, J.S. Famiglietti, H. V. Gupta, K.H. Syed, and D.C. Goodrich. 1998. Integration of soil moisture remote sensing and hydrologic modeling using data assimilation. Water Resour. Res. 34(12): 3405.

Lobell, D.B., K.G. Cassman, and C.B. Field. 2009. Crop yield gaps: Their importance, magnitudes, and causes. Annu. Rev. Environ. Resour. 34: 179–204.

McPherson, R.A., C.A. Fiebrich, K.C. Crawford, R.L. Elliott, J.R. Kilby, D.L. Grimsley, J.E. Martinez, J.B. Basara, B.G. Illston, D.A. Morris, K.A. Kloesel, S.J. Stadler, A.D. Melvin, A.J. Sutherland, H. Shrivastava, J.D. Carlson, J.M. Wolfinbarger, J.P. Bostic, and D.B. Demko. 2007. Statewide monitoring of the mesoscale environment: A technical update on the Oklahoma Mesonet. J. Atmos. Ocean. Technol. 24(3): 301–321.

Mohanty, B.P., and T.H. Skaggs. 2001. Spatio-temporal evolution and time-stable characteristics of soil moisture within remote sensing footprints with varying soil, slope, and vegetation. Adv. Water Resour. 24(9-10): 1051–1067.

Mozny, M., M. Trnka, Z. Zalud, P. Hlavinka, J. Nekovar, V. Potop, and M. Virag. 2012. Use of a soil moisture network for drought monitoring in the Czech Republic. Theor. Appl. Climatol. 107(1-2): 99–111.

Muchow, R.C., T.R. Sinclair, J.M. Bennett, and L.C. Hammond. 1986. Response of leaf growth, leaf nitrogen, and stomatal conductance to water deficits during vegetative growth of field-grown soybean. Crop Sci. 26(6): 1190–1195.

Nielsen, D.C., P.W. Unger, and P.R. Miller. 2005. Efficient water use in dryland cropping systems in the Great Plains. Agron. J. 97(2): 364–372.

Peterson, G.A., A. J. Schlegel, D.L. Tanaka, and O.R. Jones. 1996. Precipitation use efficiency as affected by cropping and tillage systems. J. Prod. Agric. 9(2): 180–186.

Ratliff, L.F., J.T. Ritchie, and D.K. Cassel. 1983. Field-measured limits of soil water availability as related to laboratory-measured properties. Soil Sci. Soc. Am. J. 47(4): 770.

Ray, J.D., R.W. Gesch, T.R. Sinclair, and L. Hartwell Allen. 2002. The effect of vapor pressure deficit on maize transpiration response to a drying soil. Plant Soil 239: 113–121.

Sadras, V.O., and S.P. Milroy. 1996. Soil-water thresholds for the responses of leaf expansion and gas exchange: A review. Field. Crop. Res. 47(2-3): 253–266.

Sadras, V.O., F.J. Villalobos, E. Fereres, and D.W. Wolfe. 1993. Leaf responses to soil water deficits: Comparative sensitivity of leaf expansion rate and leaf conductance in field-grown sunflower (Helianthus annuus L.). Plant Soil 153(2): 189–194.

Torres, G.M., R.P. Lollato, and T.E. Ochsner. 2013. Comparison of drought probability assessments based on atmospheric water deficit and soil water deficit. Agron. J. 105(2): 428.

USDA-NASS. 2015. USDA-NASS. www.nass.usda.gov/Statistics_by_State/Oklahoma/Publications/County_Estimates/index.asp (accessed 31 Oct 2015).

van Ittersum, M.K., K.G. Cassman, P. Grassini, J. Wolf, P. Tittonell, Z., and Hochman. 2013. Yield gap Analysis with local to global relevance- A review. Field. Crop. Res. 143: 4–17

CHAPTER II

This chapter shows the most recent data analysis. A prior version with minor differences was published in Agronomy Journal Vol. 106, p. 1329–1339 (2014)

YIELD GAP AND PRODUCTION GAP OF RAINFED WINTER WHEAT IN THE SOUTHERN GREAT PLAINS

Andres Patrignani, Romulo P. Lollato, Tyson E. Ochsner, Chad B. Godsey, and Jeff. T. Edwards

ABSTRACT

Since 1980, average wheat (*Triticum aestivum* L.) yields have remained nearly stagnant in the southern Great Plains (SGP) and stagnant in the state of Oklahoma. Yield stagnation can sometimes be attributed to a relatively small gap between current and potential yields, but the magnitude of the yield gap for this region has not been well quantified. The objective of this study was to determine the wheat yield and production gaps in Oklahoma at state and county levels. This involved estimation of attainable yield (Ya) using a frontier yield function and water-limited potential yield (Yp) using estimated transpiration and transpiration efficiency. Yield gap and production gap relative to Ya and Yp were calculated using grain yields and harvested area for 19 counties. Current average yield (Yc) was 2.06 Mg ha^{-1} at the state level, well below the maximum recorded yield at the plot level of 6.59 Mg ha^{-1}. The Yp of current wheat varieties is far above Yc in Oklahoma, and Yc represents 74% of Ya but only 30% of Yp at state level. For growing season rainfall (GSRF) amount <250 mm wheat yields were often water-limited.

However, average GSRF was 471 mm, and yield was typically limited by factors other than GSRF amount. Production exhibited greater temporal variability than yield, and production gap may be a better indicator than yield gap for regions with highest potential to increase production. Low yields and yield stagnation in Oklahoma cannot be attributed to a small remaining yield gap relative to water-limited potential yields, nor to inadequate GSRF amount.

INTRODUCTION

Hard red winter wheat is the dominant crop in the SGP (Kansas, Oklahoma, and Texas), with around 8 million hectares planted every year. In this region, wheat grain yields increased from 1955 to 1980 at an average rate of 34.9 kg ha^{-1} yr^{-1} (Fig. 1A) (USDA-NASS, 2012). In the same period, the state of Oklahoma showed similar wheat yield gains (34.3 kg ha^{-1} yr^{-1}) (Fig. 1B). However, from 1980 to 2012, wheat yields have remained nearly stagnant for the SGP (Δ6.6 kg ha^{-1} yr^{-1}), and stagnant in the state of Oklahoma (Δ –1.1 kg ha^{-1} yr^{-1}). Wheat yield stagnation is not confined to the SGP, but has also been observed in other parts of the world. In the North China Plains, winter wheat yields have stagnated at 5 Mg ha^{-1} (Wu et al., 2006), and in France, wheat yield has not increased since 1996 (Brisson et al., 2010). Evidence also exists for wheat yield stagnation in Japan, Tunisia, and Canada (Calderini and Slafer, 1998). Given wheat's significance as a global food grain and the rising global food demand, there is need to identify the causes of yield stagnation in several of the world's wheat-producing regions. This research is a first step toward identifying the causes of yield stagnation in Oklahoma, an important wheat producing region in the United States, where yields are low and stagnation is pronounced.

In the state of Oklahoma approximately 2 million hectares are cultivated annually with winter wheat, which represents roughly 75% of the state's total cropland. A majority of the winter wheat in this region is produced using conventional tillage under rainfed conditions (Vitale et al., 2011). Annual rainfall ranges from <400 mm in the Panhandle region (western Oklahoma) to >1000 mm in the eastern portion of the state. Growing season rainfall, defined as the total rainfall from 1 October to 15 June, ranges from ~200 mm in the Panhandle region up to ~800 mm in eastern Oklahoma. Growing season reference evapotranspiration is high, ranging from 1050 mm in the Panhandle to 740 mm in eastern Oklahoma, and drought is a frequent concern for wheat producers in the state (Mariger and Kelsey, 2003).

The rise of wheat yield in both the SGP and the state of Oklahoma from 1955 to 1980 may have been a consequence of improved management, such as the adoption of N-based

fertilizers; and improved genetics, including semi-dwarf wheat cultivars (Bell et al., 1995; Brancourt-Hulmel et al., 2003). The percentage of hectares receiving N-based fertilization increased from 60 to 95% from 1964 to 2009 in Oklahoma. Similarly, the average rate of N-based fertilization increased from 35 up to ~65 kg N ha^{-1} for the same period (USDA Economic Research Service Staff, 2013). Yield gain due to genetic improvements in wheat varieties in Oklahoma has been estimated at 18.8 kg ha^{-1} yr^{-1} from 1919 to 1997 by Khalil et al. (2002) and 11.03 kg ha^{-1} yr^{-1} from 1971 to 2008 by Battenfield et al. (2013). However, Graybosch and Peterson (2010) found no statistically significant genetic gains in experimental wheat yields from 1984 to 2008 in the SGP. There is a clear need to understand why continued efforts to improve management and genetics have failed to increase state average yields in Oklahoma since 1980. Here we test the hypothesis that wheat yield stagnation in Oklahoma is occurring because current wheat yields (Yc) are close to the water-limited potential yields (Yp).

When actual yields are ~70% of water-limited potential yields, stagnation is reached and further increases in grain yield may be difficult (Cassman, 1999). In a global analysis, current winter wheat yields in the SGP were estimated to represent only 25 to 50% of water-limited potential yields (Licker et al., 2010). If that result is correct, yields might be expected to increase over time, nonetheless, as shown in Fig. 1A and 1B, wheat yields have not increased appreciably since the 1980s. Licker et al. (2010) noticed that the yield gaps of winter wheat in the SGP and in the eastern Canadian plains were exceptionally large relative to other crops in developed countries such as United States and Canada, but the causes of this phenomenon were not identified.

Exclusive reliance on yield gap to compare the remaining potential yield increases across regions can potentially lead to misguided conclusions when comparing areas with varying total grain production. Calculating the production gap along with the yield gap may be particularly important since some regions may show large yield gaps, but small areas cultivated with wheat,

which may lead to low production gaps. Calculating the production gap may allow a more accurate estimation of the potential increase in wheat production for a given region, serving at the same time as an indicator to target research and outreach efforts. Although van Wart et al. (2013) suggested a method for yield gap estimation that accounts for 40 to 50% of the harvested area of the region being studied, we are not aware of any prior studies which have examined production gaps along with yield gaps.

The causes of winter wheat yield stagnation in Oklahoma, as well as in the rest of the southern Great Plains, remain unknown. To better elucidate the reasons for yield stagnation and to more precisely quantify the magnitude of the remaining exploitable wheat yield gap in Oklahoma, more detailed knowledge of both current yield and water-limited potential yield is needed. The objective of this study was to determine the state and county wheat yield and production gaps in Oklahoma.

MATERIALS AND METHODS

Overview

Water-limited potential yield is here defined as the maximum yield that can be obtained by an adapted variety in a specific rainfed environment if no nutritional limitations are present (Hochman et al., 2009; Lobell et al., 2009), and attainable yield (Ya) is defined as the maximum yield ever achieved in a specific environment (i.e., plot, county, or state) for a given GSRF (Connor, 2004; Connor et al., 2011). Water-limited potential yield is a theoretical maximum yield, while attainable yield is based on recorded data at a specific spatial level. Current yield, defined as the average wheat yield of the last 10 years (Anderson, 2010), is typically below water-limited potential yield because the latter requires almost perfect understanding and management of agronomic variables (Lobell et al., 2009). The difference between Yp and Yc or Ya and Yc is widely known as the yield gap, and is used to describe the remaining potential for yield increase of the crop under study in a specific environment. The yield gap calculated relative

to either Ya or Yp has been used to detect whether management or genetic potential are limiting grain yield in a given environment (Anderson, 2010; Calvino and Sadras, 2002; French and Schultz, 1984; Neumann et al., 2010; Sadras and Angus, 2006).

Water-limited potential yields can be estimated using crop simulation models or by the use of a linear approach based on estimated transpiration, transpiration efficiency (TE), GSRF, and grain yield data (French and Schultz, 1984). A distinct advantage of the linear approach is the use of actual data collected from farms, which easily allows the incorporation of grain yield spatial variability into the analysis. Even though the linear approach does not account for within season rainfall distribution, which is related to seasonal yield variability (Asseng et al., 2001; van Ittersum et al., 2013), reported wheat yields compared well with simulated yields when GSRF was below 500 mm (Angus and van Herwaarden, 2001). This method has been widely adopted by Australian wheat researchers, producers, and consultants to calculate water-limited potential yield and yield gap (Angus and van Herwaarden, 2001) due to its simplicity (Sadras and Angus, 2006). Therefore, the linear approach was employed in this study for water-limited potential yield estimation. Attainable yields at a given spatial scale, management (i.e., crop rotations), and technology level, can be estimated using a frontier yield function (Coelli and Rao, 2005; Neumann et al., 2010). Here we adapt this approach to describe the maximum grain yield ever achieved for a given amount of input resources, in this case GSRF.

Data Collection

State level winter wheat grain yield data from 1894 to 2012 were obtained from the National Agricultural Statistic Service (USDA-NASS, 2012). County level wheat grain yield data from 1919 to 2011 for 19 counties in Oklahoma were collected using the same source. For each county, geographic coordinates and elevation of the county seat, 10-yr GSRF, growing season mean air temperature, and cumulative thermal units (base temperature = 0°C) in the growing season, are presented in Table 1. The 19 counties assessed in this study encompassed 1,261,961

ha or 73% of Oklahoma's winter wheat harvested area during the 2011–2012 growing season (Fig. 2). This is important since a minimum of 40 to 50% coverage of the area of interest is needed to ensure representative results when estimating regional yield gaps (van Wart et al., 2013). All available monthly rainfall totals for each selected county were obtained from the Oklahoma Climate Survey (OCS, 2013). Missing monthly rainfall values from 1994 to 2011 were obtained from the Oklahoma Mesonet, a network of automated weather stations across Oklahoma (McPherson et al., 2007). Years previous to 1994 with missing monthly rainfall values were not included in the analysis.

A total of 15 counties from central-western Oklahoma, with a minimum of 40 yr of pairwise growing season rainfall amount and wheat grain yield were selected for the estimation of attainable yield at different levels of GSRF. Growing season rainfall amount was defined as the amount of precipitation from 1 October to 15 June, which corresponds to typical sowing and harvesting dates of winter wheat in Oklahoma. Two counties from the Panhandle region (western Oklahoma) and two counties from eastern Oklahoma were also selected following the same standards to extend the comparison to portions of the state with different precipitation regimes (Table 1).

To identify the predominant agricultural soil series for each county, we found the soil series with the greatest areal extent in each county using the Web Soil Survey (USDA-NRCS, 2013b). Then, we used the official soil series description to corroborate that the main land use of the selected soil series was wheat cropland (USDA-NRCS, 2013a). If the land use of the previously selected soil series was not wheat cropland, then the second most predominant soil for that county was selected and subjected to the same scrutiny. This process continued until we found the predominant soil series in which wheat cropland was the main land use. Soils with slope >5% were not included in the analysis. Typical land capability class and soil texture corresponding to the top horizon were obtained for the selected soil profiles.

Yield and Production Gap Determination

Yield gaps were estimated using three different yield calculations in this study: (i) At the county level, current yield was estimated as the average grain yield of the most recent 10 yr of available data for each county. At the state level, current yield was calculated as the state-average grain yield of the most recent 10 yr. Only 10 yr of data were used in the calculation of current yield to avoid temporal effects of advances in technology or possible climate change, which would affect yield estimates averaged over a longer period (e.g., 30 yr), while still containing adequate data to average out much of the year-to-year variability in grain yield (van Ittersum et al., 2013); (ii) At the county level, attainable yield was determined for each county as the maximum grain yield ever achieved at the average GSRF of last 10 yr using a frontier yield function approach (Fig. 3). The attainable yield for the state of Oklahoma was estimated as the maximum yield ever recorded at state level; and (iii) The water-limited potential yield was determined by the linear approach using estimated transpiration and TE (Fig. 4) (French and Schultz, 1984).

Frontier yield functions relating grain yield to GSRF have been considered a reliable approach for estimating attainable yield across a wide range of environments (van Ittersum et al., 2013). The frontier yield function for each county was constructed by: (i) plotting all pairwise GSRF and wheat yields of a given county; (ii) dividing the GSRF in as many ranges or bins of log-spaced width as possible without generating any bins lacking wheat grain yield values. Log-spaced bins were used to increase the selection of data at low and average GSRF, a range in which our data set is rich in information; (iii) selecting the highest grain yield from each bin, and (iv) fitting the selected yields using the following logarithmic equation:

$$y = a + b\ \ln x + c\ (\ln x)^2, \quad x > 0$$

where a, b, and c are fitting parameters, y is wheat grain yield, and x is growing season rainfall. The 10-yr average GSRF for each county was calculated using climate records and then matched with the frontier production function to obtain the attainable yield (see Ya in Fig. 3). A

logarithmic frontier yield function, such as the Cobb–Douglas equation, has been successfully used for attainable yield estimation by Neumann et al. (2010). The equation we used in this study (i.e., Eq. [1]) to determine the frontier yield allows for the estimation of possible yield decrease due to excessive growing season rainfall amount, something that has not been reported by prior studies using the same approach (Neumann et al., 2010). The yield gap relative to attainable yield (YGa) was calculated as the difference between Ya and Yc (Fig. 3). Data was analyzed using Matlab R2013a (The Mathworks Inc., 2012).

The linear approach framework is based on the assumption that when soil water storage during the fallow period preceding the wheat crop is low, the GSRF can be used as an estimate of the water used by the crop. However, not all water is used by the crop, and losses likely occur. Minimum water losses are typically estimated by the x-intercept of the linear regression of yield vs. GSRF whereas the slope provides an estimation of the transpiration efficiency (Fig. 4). Then:

$$Y_p = TE(GSRF - L)$$

where TE is transpiration efficiency, GSRF is growing season rainfall, and L is the minimum water losses. The term (GSRF-L) represents an estimation of water-limited potential transpiration.

In this study, minimum water losses for each county were estimated by the x-intercept of the frontier yield function. Transpiration efficiency was determined for central-western Oklahoma and the Panhandle region under the assumption that counties within the same region have the same TE. The reason behind grouping counties within the same region was to ensure that enough pairwise data points were used to obtain a robust TE estimation. Also, we added pairwise yield and GSRF data from wheat variety trials within each region to further improve TE estimates. The TE was determined by dividing GSRF up to 400 mm (value at which yields do not appear to be limited by water) into as many possible evenly-spaced bins without generating empty bins, and then selecting the maximum wheat yield in each bin to make the linear fit. Similar approaches

have been reported using the 95th percentile instead of the maximum value (Cade and Noon, 2003; Grassini et al., 2009). Since our study covers 73% of Oklahoma's wheat cropland, the water-limited potential yields at county level were weighted by the last 10-yr average harvested area of each county to estimate state level water-limited potential yield. The linear approach was only used in counties with GSRF from 0 to 500 mm as suggested by previous investigators (French and Schultz, 1984; Sadras and Angus, 2006). In counties with GSRF >500 mm, water-limited potential yield was set equal to 8.0 Mg ha^{-1}, which is the maximum yield value we found reported for the southern Great Plains under irrigated conditions (Musick et al., 1994). The estimation of water-limited potential yield by the linear approach using GSRF more than 500 mm leads to unrealistic water-limited potential yields for this region. Yield gaps respective to water-limited potential yield (YGp) were calculated by subtracting Yc from Yp for each county.

Current production for each county was estimated as the average production of the most recent 10 yr with available data (USDA-NASS, 2012). Attainable production was calculated as the product of the attainable yield and the average harvested area of the most recent 10 yr with available data. In the same way, potential production was calculated as the product between potential yield and harvested area. Wheat production gap relative to attainable production (PGa) was calculated by subtracting current from attainable production for each county. Production gap respective to water-limited production (PGp) was calculated by subtracting current from potential production for each county.

RESULTS AND DISCUSSION

Site Characteristics

As expected, GSRF increased from west to east, with average GSRF values ranging from 233 mm yr^{-1} in the Panhandle region to 835 mm yr^{-1} in counties located in eastern Oklahoma (Table 1). For the 15 counties in central-western Oklahoma, the 10-yr average GSRF ranged from 357 mm in Kiowa county to 595 mm in Kay county, with most of the counties in the range of 410

to 515 mm. Counties located in the Southwest region of the state, such as Tillman and Jackson, averaged higher mean growing season temperatures, resulting in >3500 °C-day total cumulative thermal units. Counties in North-Central Oklahoma, such as Kay, Alfalfa, and Woods, had lower mean growing season temperatures, and therefore cumulative thermal units in the growing season rarely surpassed 3200 °C-day. Although soil types vary considerably across and within counties, the predominant soil classifications of Oklahoma's agricultural land were Argiustolls and Paleustolls (Table 2). Surface soil texture was predominantly silt loam (11 out of 19 counties), but ranged from fine sandy loam to silty clay loam. A total of 15 counties have predominant agricultural soils with moderate to severe limitations to crop production (land capabilities classes II and III), and the most recurring limitation in this study was soil erosion (11 out of 19). Only soils with <5% slope were considered in this assessment. Soil erosion might be an even greater concern if soils with steeper slopes, which are sometimes used for crop production, were considered in the analysis.

State Level Yield and Production Gaps

State level current yield was 2.06 Mg ha^{-1} (Fig. 5), a value similar to the average current yield weighed by the harvested area of the 19 counties reported in Table 3, 2.0 Mg ha^{-1}. On the other hand, attainable yield at state level was 2.5 Mg ha^{-1} and water-limited potential yield was 7.3 Mg ha^{-1} (Table 3). The difference between Yc and Ya at state level was 0.5 Mg ha^{-1}, and assuming the value of 7.3 Mg ha^{-1} as an approximation to water-limited potential yield at state level, the difference between Yc and Yp was ~5.3 Mg ha^{-1} with current yield representing 80% of attainable yield and 27% of water-limited potential yield (Fig. 5). Similarly, Licker et al. (2010) estimated that current yield was 25 to 50% of water-limited potential yield for wheat in the southern Great Plains. Neumann et al. (2010) reported that current yield was 64% of attainable yield for winter wheat at global scale, indicating a larger yield gap than we observed for Oklahoma. Clearly, there is a large difference between water-limited potential and attainable

yield in this region, and considering water-limited potential yield could lead to unrealistic conclusions about remaining potential for grain yield increases, at least in the short term. However, it is evident that attainable yield changes over time and the yield gap relative to attainable yield may only be valid for short periods of time when wheat varieties, management, and technology remain almost constant. For the long term, yield gap relative to water-limited potential yield may be a more reliable indicator for remaining yield increase potential for this region.

Average wheat yield at state level has not changed in last 30 yr (Fig. 1B). Similarly, wheat yields have stabilized in other regions of the world in the last 10 to 15 yr (Calderini and Slafer, 1998). While genetic yield potential may be increasing (Battenfield et al., 2013), these genetic gains are not reflected in state level yield trends. Lack of adoption of improved varieties does not seem to be an adequate explanation, as improved varieties were planted on 47% of Oklahoma's wheat land areas in 2013 (USDA-NASS, 2013). With approximately 75% of Oklahoma's cropland planted to wheat each year, lack of crop rotation is likely one factor contributing to the large yield gap. Wheat yields in winter wheat–winter canola (*Brassica napus L.*) rotation were 10 to 22% higher than yields under continuous wheat in a recent study (Bushong et al., 2012).

Another factor that has been widely suggested as a limitation for grain yield and a key factor in strategic management toward closing the yield gap is poor soil quality (Anderson, 2010; Cassman, 1999). The land capability class is one indicator of soil quality for agricultural purposes. Notably, 11 out of the 19 counties considered in this study have predominant soil series with erosion limitations (land capability classes IIe and IIIe, Table 2). In addition, conventional tillage is the most common tillage practice in Oklahoma (Vitale et al., 2011), and one which can lead to high erosion rates (Berg et al., 1988). Therefore, past and present topsoil erosion in Oklahoma's cropland is likely contributing to yield stagnation by, for instance, decreasing soil fertility and available water holding capacity. Another factor that may contribute to the yield

stagnation in Oklahoma is the fact that producers may not pursue water-limited potential yields but actually may seek the yield that maximizes profitability or minimizes risk. This issue is especially relevant in regions such as the SGP where climate is highly variable and uncertain (Lobell et al., 2009).

County Level Yield Gaps

Wheat grain yield at county level across all 19 counties in this study ranged from 0.23 to 3.57 Mg ha^{-1} in the period from 1919 to 2011. Rainfall during the growing season ranged from 56 to 1119 mm. Plotting pairwise GSRF and wheat yields for those counties with <500 mm GSRF allowed us to create a frontier yield function that can be compared with the linear approach proposed by French and Schultz (1984) to estimate water-limited potential yield. In the frontier yield function approach, points below the curve denotes that yield was limited by environmental factors (e.g., high air temperatures and unfavorable rainfall distribution), or management practices (e.g., inadequate fertilization, early or late sowing). The ascending part of the frontier yield function near the minimum GSRF value has a similar slope (which is equivalent to TE) as the linear approach (Fig. 6). Previous studies have shown TE ranging from 16.7 kg ha^{-1} mm^{-1} in the southern Great Plains to 22.3 kg ha–1 mm–1 in the China Loess Plateau and southeastern Australia (Sadras and Angus, 2006; Zhang et al., 2013). In this study TE was 23 kg ha^{-1} mm^{-1} in central-western Oklahoma and 17 kg ha^{-1} mm^{-1} in the Panhandle, values that are close to the maximum reported TE in China and southeastern Australia, and higher than the value of 16.7 kg mm^{-1} previously reported for the SGP (Sadras and Angus, 2006). For the eastern region of Oklahoma a linear approach was not used to estimate water-limited potential yield since growing season rainfall is typically more than 500 mm, a range for which the linear approach has not yet been compared to actual data.

When the difference between GSRF and minimum water losses was lower than 100 to 150 mm, grain yields were water limited (Fig. 6). Minimum water losses in the Panhandle region

were as low as 38 mm and in central-western Oklahoma were around 140 mm, both values fall within the range found by French and Schultz (1984) for southeastern Australia of 30 to 170 mm. Also, a decreasing trend in grain yields was observed when GSRF was >700 mm. We have two hypotheses for this yield reduction at high GSRF. First, grain yield reduction at increasing GSRF may be a consequence of not having enough records in the GSRF range from 700 to 1200 mm to accurately define the frontier yield function (i.e., N > 700 = 144 out of N = 1053). Second, grain yield may be reduced at high GSRF amounts as the result of higher disease pressure, and possibly water logging, lodging, and leaching of N fertilizers. Passioura and Angus (2010) suggested that for rainfall amounts >500 mm, radiation rather than water is the main limiting factor for wheat production in southeastern Australia. However, we did not find obvious differences in total growing season radiation between years with high and low GSRF (data not shown).

The GSRF amount is typically in the range of 400 to 500 (median equal to 451 mm and average equal to 473 mm) in the central-western region of Oklahoma, a range in which wheat grain yields were shown to be not greatly limited by GSRF amount. However, rainfall distribution within the growing season (particularly short water stress periods) still remains to be addressed, especially considering that small individual rainfall events result in large losses of water by direct evaporation from the soil, canopy interception, and residue cover interception (Sadras, 2003). Analysis of daily GSRF data from 1994 to 2011 for central-western counties in Oklahoma involving 25 weather stations and 36,932 daily precipitation values, resulted in a 75th percentile of 11.4 mm, and ~73% of daily rainfall totals were smaller than 10 mm on days with measurable rainfall. Therefore, evaporation from soil, canopy, and residue, may account for a significant amount of water loss in this region. Management practices that increase infiltration and reduce water losses from light rainfall events may result in increased grain yields (Li et al., 2001). Also, management practices that reduce bare soil evaporation, such as residue mulching, can result in greater water use efficiency and yields in such regions (Deng et al., 2006). Given the high proportion of small rainfall events in this part of the SGP and the implementation of successful

management strategies to mitigate evaporation in other parts of the world, there is a need to determine the extent to which improved management practices could increase current yields in this region by reducing evaporative losses.

Increased yield gap relative to water-limited potential yield was observed with increased GSRF amount (Fig. 7). A GSRF of 476 mm resulted in YGp of almost 6.1 Mg ha^{-1} in Blaine County, while GSRF amount of 184 mm resulted in YGp of 0.9 Mg ha^{-1} in Cimarron county. For these 15 counties in Oklahoma the slope of the linear regression of YGp vs GSRF was 20 kg ha^{-1} mm^{-1} with minimum water losses of 125 mm during the growing season as indicated by the x-intercept of the regression. These results are in agreement with a study conducted by Anderson (2010) for different shires in southeastern Australia, which resulted in yield gap relative to water-limited potential yield slope of 11 kg ha^{-1} mm^{-1}, with minimum growing season water loss of approximately 110 mm.

To compare Yc, Ya, and Yp, with current wheat varieties' genetic potential, wheat variety trials from 2005 to 2012 were analyzed to find the maximum yield at plot level across the state. A yield of 6.59 Mg ha^{-1} was recorded at Balko, OK, in 2007 and a yield of 5.99 Mg ha^{-1} was recorded at Lahoma, OK, in 2003 under rainfed conditions (Edwards et al., 2007; Raun et al., 2011). We also examined recent wheat variety trial reports from surrounding states, selecting the highest yielding hard red winter wheat variety either under irrigated or rainfed conditions. Results in Table 4 shows a maximum yield of 7.69 Mg ha^{-1} in the state of New Mexico under irrigated conditions, and a regional average maximum variety trial yield of 7.14 Mg ha^{-1} including irrigated and rainfed conditions. These maximum yields are consistent with yields reported by Musick et al. (1994) in Bushland, TX, where irrigated wheat yielded between 6 and 8 Mg ha^{-1}. Evidently, genetic potential yield per se is not a limitation to grain yield in Oklahoma as current wheat varieties have much higher yield potential than average or maximum recorded yields for any county in the state. This finding agrees with results found in southeastern Australia where

environment accounted for a greater proportion of grain yield variation than management practices or cultivars (Anderson, 2010; Anderson et al., 2005).

Another issue especially important in some environments of the SGP is the use of winter wheat for both forage (i.e., dual purpose) and grain (i.e., grain-only). A 12-yr study at the plot level in Marshall, OK, showed that dual purpose wheat yields were on average 14% lower than wheat yields under grain-only management (Edwards et al., 2011). These results were obtained when wheat yields under grain-only management were ≤5.0 Mg ha–1, a level representative of most of the wheat cropland across the SGP. The effects of grazing in higher-yielding environments remain unknown (Edwards et al., 2011).

County Level Production Gaps

Although the determination of the yield gap is a crucial step in determining the regional potential to increase food production, examining the production gap provides a different and complementary perspective. The production gap highlights the fact that counties with a large yield gap relative to attainable yield, may not have a large potential to increase wheat production as a result of a small area cultivated with wheat, assuming that major changes in wheat acreage are not expected or desired. For example, Sequoyah county in eastern Oklahoma had a relatively large yield gap, YGa of 0.5 Mg ha^{-1}, but an almost negligible production gap, PGa of 1 Gg (Fig. 8). On the other hand, in Garfield county YGa was around 0.6 Mg ha^{-1}, but resulted in a PGa of approximately 91 Gg, which is due to a relatively large area cultivated with wheat. By accounting for differences in harvested areas, the production gap may be a better indicator than yield gap for identifying regions with potential to increase grain production. Accounting for a representative area as specified in van Wart et al. (2013) is important for reliable estimations of the yield gap in a given region, but the sole use of the yield gap may not provide sufficient information about the potential production increase of that region in a larger context (i.e., nationwide, worldwide). We are not aware of any prior studies which have examined production gaps.

By examining production data, we found that wheat production in Oklahoma has greater temporal variability than grain yield. The 5-yr coefficient of variation (CV) of statewide grain production was greater than the 5-yr CV for grain yield during most of the period analyzed (Fig. 9). This phenomenon is caused by the yearly variation in harvested area (Singh and Byerlee, 1990). In adverse growing seasons, harvested area declines along with a lower average grain yield, therefore production (the product of the two) declines relatively more than does yield. The fraction of all planted area which is harvested declines in adverse growing seasons, and the areas which are harvested are likely the better croplands in the region. As a result, the average grain yield at the county or state level does not decline as markedly as it would if all the area was harvested, since average yields are computed only using harvested area. For these reasons, grain yield does not vary year-to-year as much as production. Likely, the primary cause of variation in both production and grain yield in the SGP is weather. Since grain production fluctuates more than grain yield, there is a need to study the influence of weather on regional wheat production to better understand and forecast the role of the SGP region in global food security and economics (Lobell et al., 2008; Wichelns, 2001).

CONCLUSION

In the SGP states of Oklahoma, Texas, and Kansas, state average hard red winter wheat yields have not surpassed the barrier of 3.0 Mg ha^{-1}. Despite some reports of ongoing experimental yield gains due to genetic improvements, the state average yield in Oklahoma has been stagnant for more than 30 yr. Current winter wheat varieties reached experimental yields as high as 6.59 Mg ha–1 in Oklahoma under rainfed conditions, and a maximum of 7.69 Mg ha^{-1} under irrigated conditions in the SGP, while current state yield is only ∼2.0 Mg ha^{-1}. Thus, winter wheat yields at the state level are not limited by genetic potential, per se.

In Oklahoma, when growing season rainfall amount was <250 mm, grain yield was often water-limited, but in the more common range of 400 to 600 mm, yields were rarely limited by

growing season rainfall amount. Additionally, in years with growing season rainfall amount >700 mm grain yields appeared to decrease with increasing rainfall. State average yield gap relative to attainable yield and water-limited potential yield was 0.5 and 5.3 Mg ha^{-1}, respectively. Current grain yield at the state level in Oklahoma represents 80% of attainable yield but only 27% of water-limited potential yield. Current state level production is 81% of attainable production, and 28% of water-limited production of the state. Therefore, we reject the hypothesis that wheat yields in Oklahoma are stagnant due to a narrow yield gap relative to water-limited potential yields, and we suggest that poor soil quality, reflected by the land capability class, may be an important yield limiting factor in this region. The state level production gap relative to attainable yield and water-limited potential yield was 588 and 6719 Gg, respectively. We found that the production gap may be a better indicator than yield gap to elucidate counties within the state with greater potential to increase wheat production. Four out of the top five counties with highest production gap were located in North-Central Oklahoma, where research and outreach efforts should perhaps be focused if the goal is to increase statewide wheat production.

REFERENCES

W.K. Anderson 2010. Closing the gap between actual and potential yield of rainfed wheat. The impacts of environment, management and cultivar. Field Crops Res. 116:14–22. doi:10.1016/j.fcr.2009.11.016

Anderson, W.K., M.A. Hamza, D.L. Sharma, M.F. D'Antuono, F.C. Hoyle, and N. Hill. 2005. The role of management in yield improvement of the wheat crop-A review with special emphasis on Western Australia. Aust. J. Agric. Res. 56:1137–1149. doi:10.1071/AR05077

Angus, J.F., and A.F. van Herwaarden. 2001. Increasing water use and water use efficiency in dryland wheat. Agron. J. 93:290–298. doi:10.2134/agronj2001.932290x

Asseng, S., N.C. Turner, and B.A. Keating. 2001. Analysis of water- and nitrogen-use efficiency of wheat in a Mediterranean climate. Plant Soil 233:127–143. doi:10.1023/A:1010381602223

Battenfield, S.D., A.R. Klatt, and W.R. Raun. 2013. Genetic yield potential improvement of semidwarf winter wheat in the Great Plains. Crop Sci. 53:946–955. doi:10.2135/cropsci2012.03.0158

Bell, M.A., R.A. Fischer, D. Byerlee, and K. Sayre. 1995. Genetic and agronomic contributions to yield gains: A case study for wheat. Field Crops Res. 44:55–65. doi:10.1016/0378-4290(95)00049-6

Berg, W.A., S.J. Smith, and G.A. Coleman. 1988. Management effects on runoff, soil, and nutrient losses from highly erodible soils in the Southern Plains. J. Soil Water Conserv. 43:407–410.

Brancourt-Hulmel, M., G. Doussinault, C. Lecomte, P. Berard, B. Le Buanec, and M. Trottet. 2003. Genetic improvement of agronomic traits of winter wheat cultivars released in France from 1946 to 1992. Crop Sci. 43:37–45. doi:10.2135/cropsci2003.0037

Brisson, N., P. Gate, D. Gouache, G. Charmet, F.X. Oury, and F. Huard. 2010. Why are wheat yields stagnating in Europe? A comprehensive data analysis for France. Field Crops Res. 119:201–212. doi:10.1016/j.fcr.2010.07.012

Bushong, J.A., A.P. Griffith, T.F. Peeper, and F.M. Epplin. 2012. Continuous winter wheat versus a winter canola–winter wheat rotation. Agron. J. 104:324–330. doi:10.2134/agronj2011.0244

Cade, B.S., and B.R. Noon. 2003. A gentle introduction to quantile regression for ecologists. Front. Ecol. Environ 1:412–420. doi:10.1890/1540-9295(2003)001[0412:AGITQR]2.0.CO;2

Calderini, D.F., and G.A. Slafer. 1998. Changes in yield and yield stability in wheat during the 20th century. Field Crops Res. 57:335–347. doi:10.1016/S0378-4290(98)00080-X

Calvino, P., and V. Sadras. 2002. On-farm assessment of constraints to wheat yield in the south-eastern Pampas. Field Crops Res. 74:1–11. doi:10.1016/S0378-4290(01)00193-9

K.G. Cassman 1999. Ecological intensification of cereal production systems: Yield potential, soil quality, and precision agriculture. Proc. Natl. Acad. Sci. USA 96:5952–5959. doi:10.1073/pnas.96.11.5952

Coelli, T.J., and D.S.P. Rao. 2005. Total factor productivity growth in agriculture: A Malmquist index analysis of 93 countries, 1980–2000. Agric. Econ. 32:115–134. doi:10.1111/j.0169-5150.2004.00018.x

D.J. Connor 2004. Designing cropping systems for efficient use of limited water in southern Australia. Eur. J. Agron. 21:419–431. doi:10.1016/j.eja.2004.07.004

Connor, D.J., R.S. Loomis, and K.G. Cassman. 2011. Crop ecology: Productivity and management in agricultural systems. Cambridge Univ. Press, Cambridge.

Deng, X.P., L. Shan, H.P. Zhang, and N.C. Turner. 2006. Improving agricultural water use efficiency in and and semiarid areas of China. Agric. Water Manage. 80:23–40. doi:10.1016/j.agwat.2005.07.021

Edwards, J.T., B.F. Carver, G.W. Horn, and M.E. Payton. 2011. Impact of dual-purpose management on wheat grain yield. Crop Sci. 51:2181–2185. doi:10.2135/cropsci2011.01.0043

Edwards, J.T., R.D. Kochenower, R.E. Austin, J.D. Ladd, B.F. Carver, and R.M. Hunger. 2007. Winter wheat variety performance tests 2006–2007. Production Technol. Rep. PT-2007-6. Vol. 19. No. 6. Dep. of Plant and Soil Sci., Oklahoma State Univ., Stillwater.

French, R.J., and J.E. Schultz. 1984. Water-use efficiency of wheat in a Mediterranean-type environment.1. The relation between yield, water-use and climate. Aust. J. Agric. Res. 35:743–764. doi:10.1071/AR9840743

Grassini, P., H.S. Yang, and K.G. Cassman. 2009. Limits to maize productivity in Western Corn-Belt: A simulation analysis for fully irrigated and rainfed conditions. Agric. For. Meteorol. 149:1254–1265. doi:10.1016/j.agrformet.2009.02.012

Graybosch, R.A., and C.J. Peterson. 2010. Genetic improvement in winter wheat yields in the Great Plains of North America, 1959–2008. Crop Sci. 50:1882–1890. doi:10.2135/cropsci2009.11.0685

Hochman, Z., D. Holzworth, and J.R. Hunt. 2009. Potential to improve on-farm wheat yield and WUE in Australia. Crop Pasture Sci. 60:708–716. doi:10.1071/CP09064

Khalil, I.H., B.F. Carver, E.G. Krenzer, C.T. MacKown, and G.W. Horn. 2002. Genetic trends in winter wheat yield and test weight under dual-purpose and grain-only management systems. Crop Sci. 42:710–715. doi:10.2135/cropsci2002.0710

Li, X.Y., J.D. Gong, Q.Z. Gao, and F.R. Li. 2001. Incorporation of ridge and furrow method of rainfall harvesting with mulching for crop production under semiarid conditions. Agric. Water Manage. 50:173–183. doi:10.1016/S0378-3774(01)00105-6

Licker, R., M. Johnston, J.A. Foley, C. Barford, C.J. Kucharik, C. Monfreda, and N. Ramankutty. 2010. Mind the gap: How do climate and agricultural management explain

the ‘yield gap’ of croplands around the world? Glob. Ecol. Biogeogr. 19:769–782. doi:10.1111/j.1466-8238.2010.00563.x

Lobell, D.B., M.B. Burke, C. Tebaldi, M.D. Mastrandrea, W.P. Falcon, and R.L. Naylor. 2008. Prioritizing climate change adaptation needs for food security in 2030. Science (Washington, DC) 319:607–610. doi:10.1126/science.1152339

Lobell, D.B., K.G. Cassman, and C.B. Field. 2009. Crop yield gaps: Their importance, magnitudes, and causes. Annu. Rev. Environ. Resour. 34:179–204. doi:10.1146/annurev.environ.041008.093740

Mariger, S.C., and K.D. Kelsey. 2003. Determining the research, education, and extension needs of Oklahoma wheat producers. J. South. Agric. Educ. Res. 53:47–58.

The Mathworks Inc. 2012. Matlab version R2013a for Windows. The MathWorks Inc., Natick, MA.

McPherson, R.A., C.A. Fiebrich, K.C. Crawford, R.L. Elliott, J.R. Kilby, and D.L. Grimsley. 2007. Statewide monitoring of the mesoscale environment: A technical update on the Oklahoma Mesonet. J. Atmos. Ocean. Technol. 24:301–321. doi:10.1175/JTECH1976.1

Musick, J.T., O.R. Jones, B.A. Stewart, and D.A. Dusek. 1994. Water-yield relationships for irrigated and dryland wheat in the US Southern Plains. Agron. J. 86:980–986. doi:10.2134/agronj1994.00021962008600060010x

Neumann, K., P.H. Verburg, E. Stehfest, and C. Muller. 2010. The yield gap of global grain production: A spatial analysis. Agric. Syst. 103:316–326. doi:10.1016/j.agsy.2010.02.004

OCS. 2013. Oklahoma climatological survey. Oklahoma Climatological Survey Staff. http://climate.ok.gov (accessed 15 Apr. 2012).

Passioura, J.B., and J.F. Angus. 2010. Improving productivity of crops in water-limited environments. Adv. Agron. 106(106):37–75. doi:10.1016/S0065-2113(10)06002-5

Raun, W.R., J.B. Solie, and M.L. Stone. 2011. Independence of yield potential and crop nitrogen response. Precis. Agric. 12:508–518. doi:10.1007/s11119-010-9196-z

V.O. Sadras 2003. Influence of size of rainfall events on water-driven processes- I. Water budget of wheat crops in south-eastern Australia. Aust. J. Agric. Res. 54:341–351. doi:10.1071/AR02112

Sadras, V.O., and J.F. Angus. 2006. Benchmarking water-use efficiency of rainfed wheat in dry environments. Aust. J. Agric. Res. 57:847–856. doi:10.1071/AR05359

Singh, A.J., and D. Byerlee. 1990. Relative variability in wheat yields across countries and over time. J. Agric. Econ. 41:21–32. doi:10.1111/j.1477-9552.1990.tb00616.x

USDA Economic Research Service Staff. 2013. Fertilizer use and price. USDA. www.ers.usda .gov/data-products/fertilizer-use-and-price.aspx#26727 (accessed 6 Dec. 2013).

USDA-NASS. 2012. USDA-NASS. www.nass.usda.gov/Statistics_by_State/Oklahoma /Publications /County_Estimates/index.asp (accessed 1 July 2012).

USDA-NASS. 2013. Oklahoma wheat variety. Oklahoma Field Office, Oklahoma City.

USDA-NRCS. 2013a. Official soil series descriptions. Soil Survey Staff. USDA-NRCS, Lincoln, NE. soils.usda.gov/technical/classification/osd/index.html (accessed 1 Nov. 2013).

USDA-NRCS. 2013b. Web soil survey. Soil Survey Staff. USDA-NRCS, Lincoln, NE. http://websoilsurvey.nrcs.usda.gov/(accessed 15 Apr. 2013).

van Ittersum, M.K., K.G. Cassman, P. Grassini, J. Wolf, P. Tittonell, and Z. Hochman. 2013. Yield gap analysis with local to global relevance-A review. Field Crops Res. 143:4–17. doi:10.1016/j.fcr.2012.09.009

van Wart, J., K.C. Kersebaum, S.B. Peng, M. Milne, and K.G. Cassman. 2013. Estimating crop yield potential at regional to national scales. Field Crops Res. 143:34–43. doi:10.1016/j.fcr.2012.11.018

Vitale, J.D., C. Godsey, J. Edwards, and R. Taylor. 2011. The adoption of conservation tillage practices in Oklahoma: Findings from a producer survey. J. Soil Water Conserv. 66:250–264. doi:10.2489/jswc.66.4.250

D. Wichelns 2001. The role of ‘virtual water’ in efforts to achieve food security and other national goals, with an example from Egypt. Agric. Water Manage. 49:131–151. doi:10.1016/S0378-3774(00)00134-7

Wu, D.R., Q. Yu, C.H. Lu, and H. Hengsdijk. 2006. Quantifying production potentials of winter wheat in the North China Plain. Eur. J. Agron. 24:226–235. doi:10.1016/j.eja.2005.06.001

Zhang, S., V. Sadras, X. Chen, and F. Zhang. 2013. Water use efficiency of dryland wheat in the Loess Plateau in response to soil and crop management. Field Crops Res. 151:9–18. doi:10.1016/j.fcr.2013.07.005

Table 1. Location and description of key weather variables for 19 counties in the state of Oklahoma. Location of each site is specified by latitude, longitude, and elevation of the county seat. Weather variables are 10-yr average rainfall during the winter wheat growing season, average growing period temperature, and average cumulative thermal units during the growing season.

County	Latitude	Longitude	Elevation	10-yr Average Season Rainfall	Minimum Water Losses	Growing season mean Temperature	Cumulative Season Thermal Units
	N	W	m	mm	mm	°C	Cd
Kiowa	35.02˚	99.09˚	473	357	120	11	3619
Garfield	36.39˚	98.09˚	380	369	134	9	3215
Jackson	34.66˚	99.31˚	426	385	134	11	3674
Tillman	34.23˚	98.69˚	345	428	137	12	3750
Woods	36.8˚	98.67˚	411	432	44	9	3149
Major	36.27˚	98.48˚	397	449	183	10	3401
Washita	35.38˚	98.98˚	473	450	152	10	3387
Caddo	35.1˚	98.44˚	382	467	121	10	3343
Alfalfa	36.53˚	98.28˚	411	475	91	9	3158
Blaine	35.85˚	98.42˚	472	476	154	10	3336
Custer	35.54˚	98.69˚	504	480	152	10	3418
Canadian	35.54˚	97.96˚	414	482	194	10	3321
Grant	36.8˚	97.74˚	333	505	96	9	3183
Payne	36.14˚	97.07˚	273	586	220	10	3419
Kay	36.8˚	97.3˚	309	595	186	9	3162
Western counties							
Cimarron	36.73˚	102.5˚	1270	184	38	9	2907
Beaver	36.82˚	100.5˚	751	282	105	8	2932
Eastern counties							
Sequoyah	35.46˚	94.81˚	162	816	334	11	3514
Leflore	34.97˚	94.72˚	148	853	344	12	3735

Table 2. Predominant agricultural soil series, classification of predominant soil series, typical land capability class, and typical surface soil textures (0 to 20 cm) for 19 counties across the state of Oklahoma.

County	Predominant agricultural soil series	Predominant soil classification	Land capability class[†]	Soil texture
Garfield	Kirkland	Paleustoll	IIe	Silt loam
Woods	Pond Creek	Argiustolls	I	Silt loam
Kiowa	Hollister	Haplusterts	IIs	Silty clay loam
Jackson	Hollister	Haplusterts	IIs	Silty clay loam
Major	Tillman	Paleustolls	IIe	Clay loam
Tillman	Tipton	Argiustolls	I	Loam
Washita	St. Paul	Argiustolls	IIe	Silt loam
Custer	St. Paul	Argiustolls	IIe	Silt loam
Alfalfa	Pond Creek	Argiustolls	I	Silt loam
Blaine	Lovedale	Argiustolls	IIe	Fine sandy loam
Caddo	Pond Creek	Argiustolls	IIe	Silt loam
Grant	Kirkland	Paleustolls	IIIe	Silt loam
Canadian	Norge	Paleustolls	IIe	Silt loam
Payne	Renfrow	Paleustolls	IIIe	Silt loam
Kay	Kirkland	Paleustolls	IIIe	Silt loam
Western counties				
Cimarron	Sherm	Paleustolls	IIc	Clay loam
Beaver	Dalhart	Haplustalfs	IIIc	Fine sandy loam
Eastern counties				
Sequoyah	Coushatta	Eutrudepts	I	Silt loam
Leflore	Sallisaw	Paleudalfs	IIe	Loam

[†] Class I: Soils have few limitations for cultivation.
Class II: Soils have limitations that require moderate conservation practices.
Class III: Soils have severe limitations that require special conservation practices.
e: Soil erosion is the dominant limitation
s: Soil limitations within the root zone such as low water holding capacity, shallow soil, or rocks.
c: Climatic limitation such as low or high temperature and low soil moisture.
Source: USDA-NRCS Agriculture handbook No. 20. 1961.

Table 3. Current winter wheat yield (Y_c), attainable yield (Y_a), and water-limited potential yield (Y_p), yield and production gap relative to Y_a (YG_a and PG_a), yield and production gap relative to Y_p (YG_p and PG_p), as well as current production (P_c), attainable production (P_a), water-limited potential production (P_p), and harvested area (HA) for 19 counties in the state of Oklahoma.

County	Y_c[a]	Y_a[b]	Y_p[c]	YG_a	YG_p	P_c	P_a	P_p	PG_a	PG_p	HA
	Mg					Gg					1000 ha
Kiowa	1.9	2.0	6.0	0.1	4.1	164	174	522	10	358	88
Garfield	2.1	2.8	6.3	0.6	4.1	303	393	884	91	582	141
Jackson	2.0	2.6	6.6	0.5	4.6	118	148	383	30	265	58
Tillman	1.8	2.3	7.6	0.5	5.8	95	121	399	26	304	52
Woods	2.1	2.8	7.7	0.6	5.6	175	225	632	51	458	82
Major	1.9	2.4	8.0	0.5	6.1	124	156	522	32	398	65
Washita	1.9	2.3	8.0	0.4	6.1	153	183	633	31	480	79
Caddo	2.0	2.6	8.0	0.6	6.0	119	156	476	38	358	60
Alfalfa	2.3	2.6	8.0	0.3	5.7	231	263	800	32	569	100
Blaine	1.9	2.3	8.0	0.5	6.1	141	176	604	35	463	76
Custer	2.0	2.6	8.0	0.5	6.0	166	208	648	42	482	81
Canadian	2.1	2.4	8.0	0.3	5.9	143	164	556	21	413	70
Grant	2.1	2.6	8.0	0.4	5.9	293	354	1109	61	816	139
Payne	1.8	2.5	8.0	0.7	6.2	20	27	87	7	67	11
Kay	2.0	2.7	8.0	0.6	6.0	186	244	734	58	548	92
Western counties											
Cimarron	2.0	2.0	2.9	0.1	0.9	67	69	96	2	29	34
Beaver	1.8	2.3	4.6	0.5	2.8	73	95	186	22	112	41
Eastern counties											
Sequoyah	2.6	3.1	8.0	0.5	5.4	3	4	11	1	7	1
Leflore	2.4	2.5	8.0	0.1	5.6	5	5	16	0	11	2
State	2.0	2.5	7.3	0.5	5.3	2579	3167	9298	588	6719	1269

† Current yield was calculated as the average of the last ten years for each county with data obtained from NASS.

‡ Attainable yield was calculated using the frontier yield function.

§ Potential yield was calculated using the French and Schultz (1984) linear approach. Counties with growing season rainfall >500 mm were set to 8 Mg ha^{-1}

¶ For Y_c, Y_a, Y_p, YG_a, and YG_p state values are the weighted average of each column. For P_c, P_a, P_p, PG_a, PG_p, and HA, state values are the sum of each column.

Table 4. State, location, and date for the maximum recorded winter wheat yields found in variety trial networks in the Southern Great Plains under irrigated (I) and rainfed (R) conditions.

State	Location	Cultivar	Year	Yield
				Mg ha^{-1}
Texas (I)[†]	McGregor	Duster	2008/09	6.38
New Mexico (I)[†]	Clovis	Winterhawk	2011/12	7.69
Arkansas (I)[‡]	Rohwer	AGS2038	2010/11	7.58
Kansas (I)[§]	Colby	WB-Cedar	2011/12	7.46
Oklahoma (R)[¶]	Balko	Danby	2006/07	6.59
Average				7.14

[†] Managed by Texas A&M. Soil and Crop Sciences. Small Grains division.
[‡] Managed by University of Arkansas. Division of Agriculture. Small Grains division.
[§] Managed by Kansas State University. Extension Agronomy.
[¶] Managed by Oklahoma State University. Plant and Soil Sciences. Small Grains Extension.

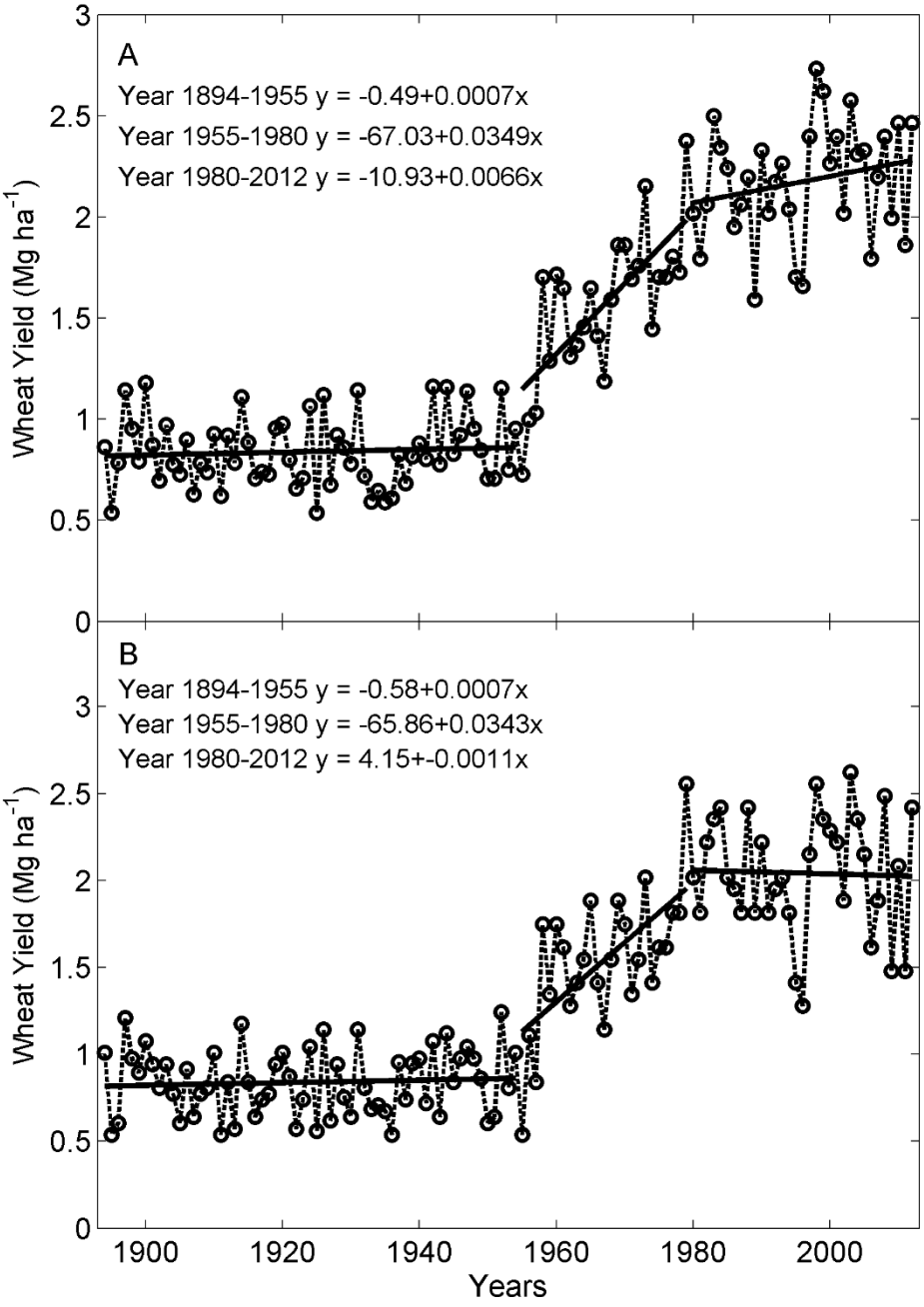

Figure 1. Timeline showing the evolution of winter wheat grain yield in the (A) southern Great Plains (SGP), and (B) Oklahoma. Data spans the period from 1894 to 2012. Trend lines were calculated for the period of 1894 to 1955, 1955 to 1980, and 1980 to 2012. Data were obtained from the USDA National Agricultural Statistics Service.

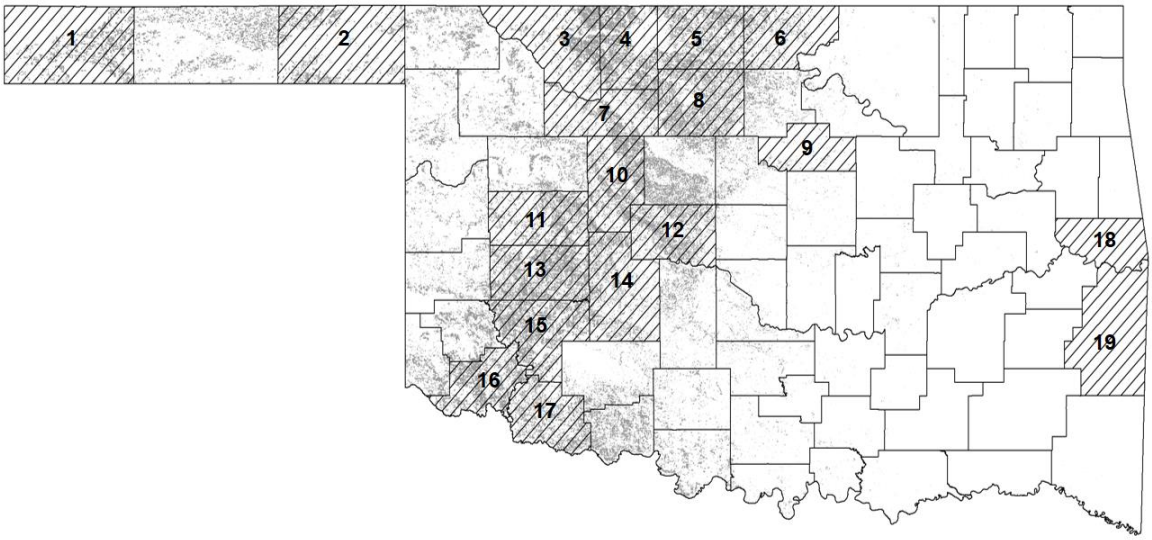

Figure 2. Map of the state of Oklahoma showing wheat fields in 2010 (grey dots) (2010 land cover map, USDA Data Gateway) and the selected counties in this study (hatched areas). Counties are: Cimarron (1), Beaver (2), Woods (3), Alfalfa (4), Grant (5), Kay (6), Major (7), Garfield (8), Payne (9), Blaine (10), Custer (11), Canadian (12), Washita (13), Caddo (14), Kiowa (15), Jackson (16), Tillman (17), Sequoyah (18), and Le Flore (19).

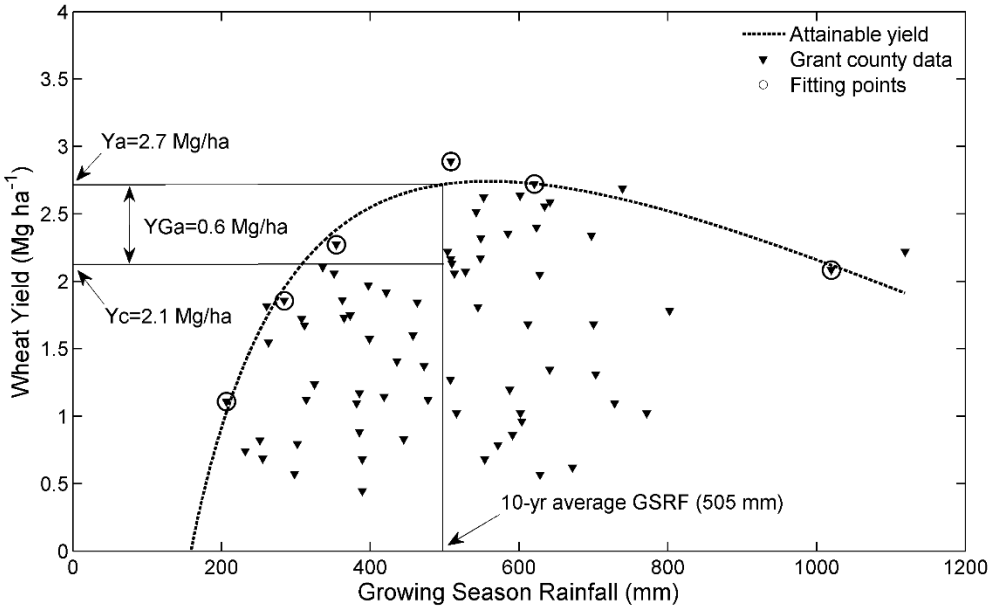

Figure 3. Example of the construction of the frontier yield function for Grant county. Black inverted triangles represent pairwise GSRF and wheat yield for Grant county, and circled data represent the points selected to make the fit. The difference between the attainable yield (Ya) and the current yield (Yc) represents the yield gap relative to Ya (YGa).

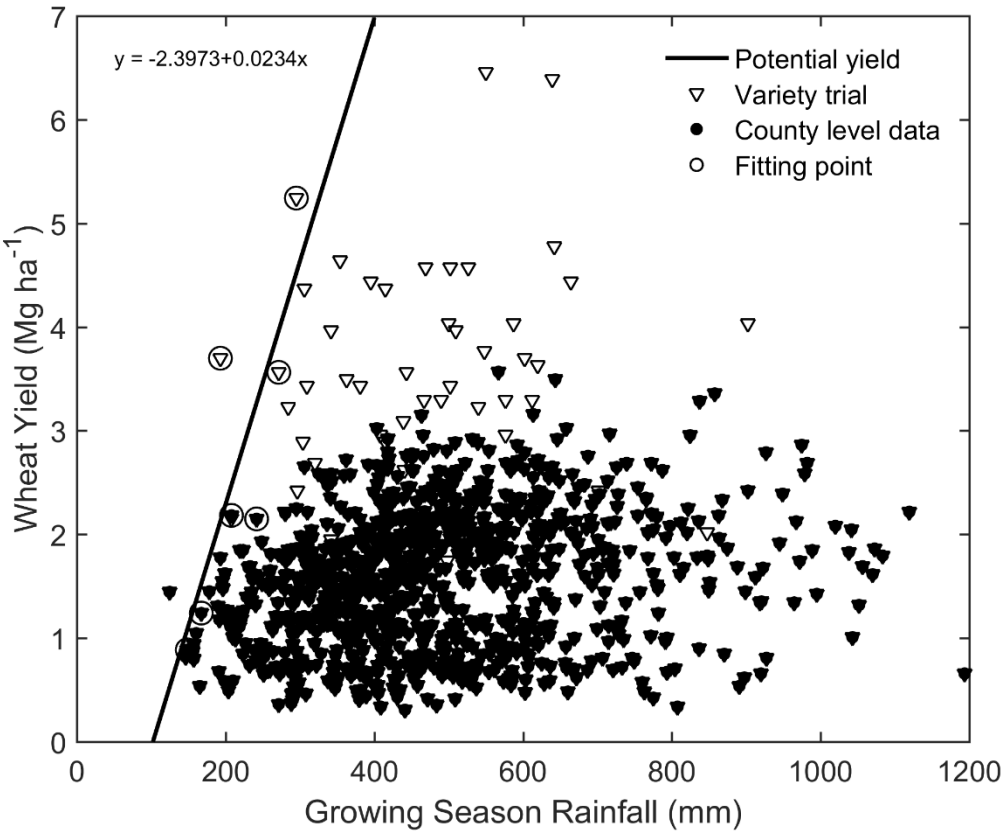

Figure 4. Example of the construction of the linear approach used to estimate the potential yield in central-western Oklahoma. Black inverted triangles represent pairwise growing season rainfall (GSRF) and yield from counties in central-western Oklahoma, white diamonds represent pairwise data from wheat variety trials, and circled data represent the points selected to make the fit.

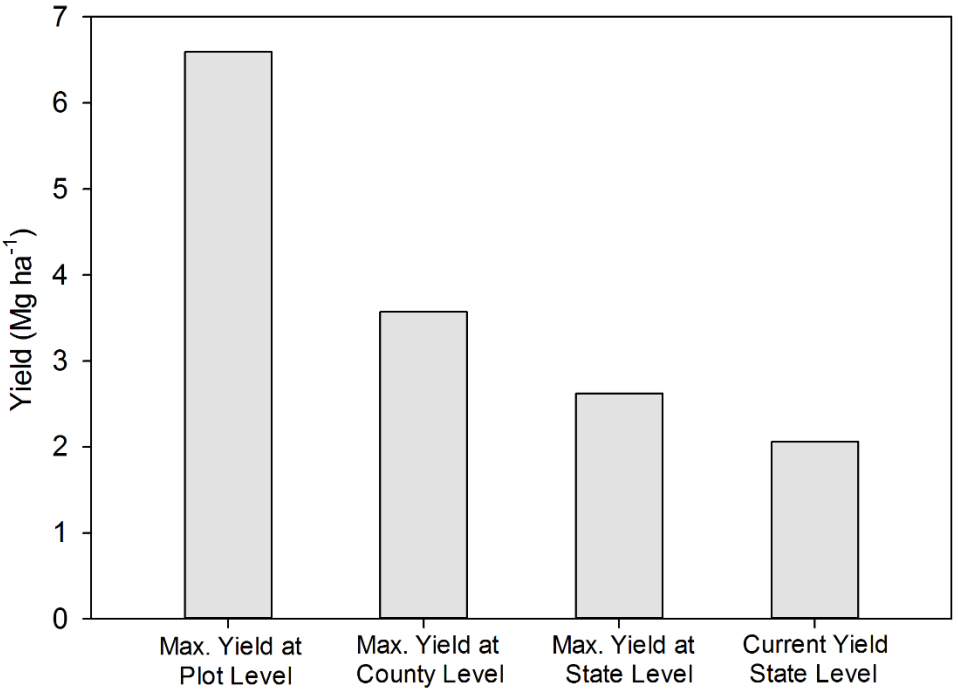

Figure 5. Comparison among wheat grain yield at different spatiotemporal scales for the state of Oklahoma.

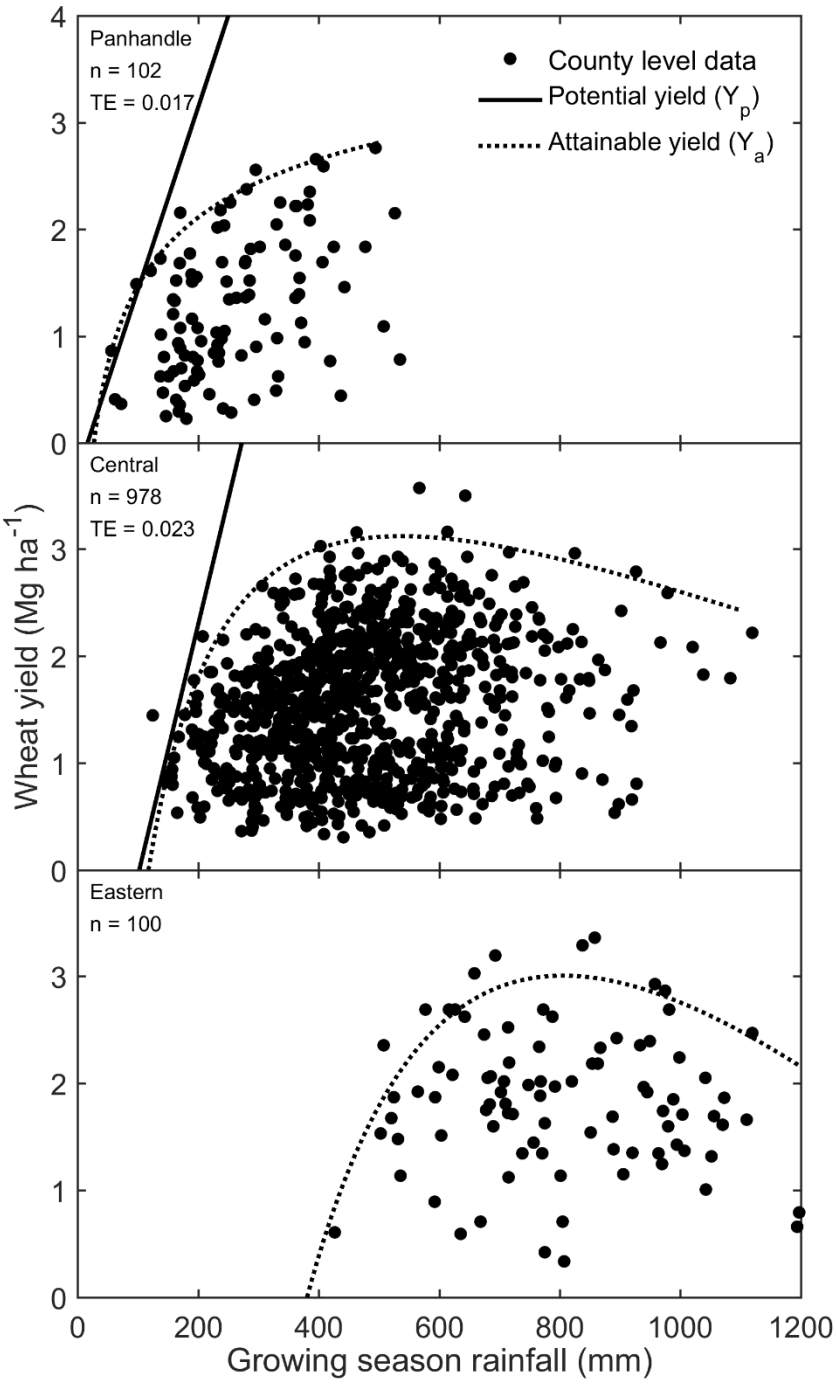

Figure 6. Pairwise growing season rainfall amount and wheat grain yield for 93 yr across 19 counties in Oklahoma. The frontier yield approach was used to estimate attainable yield (Ya) and a linear approach using transpiration efficiency was used to calculate water-limited potential yield (Yp).

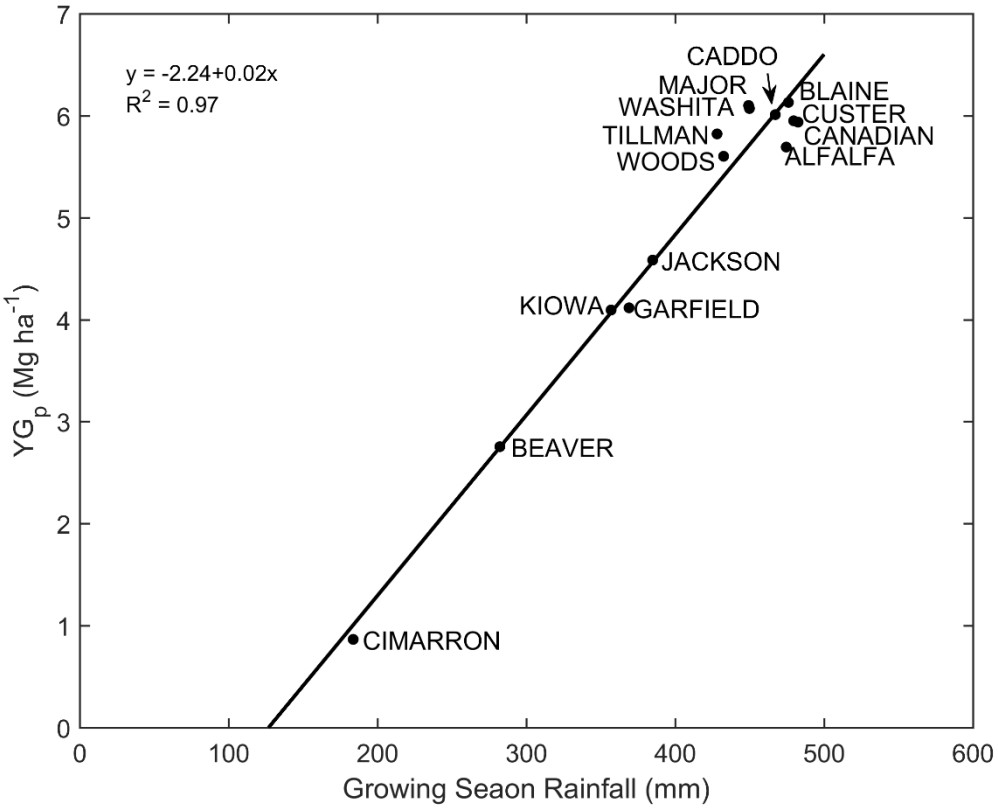

Figure 7. Yield gap relative to water-limited yield potential (YGp) for all counties in central-western Oklahoma with <500 mm growing season rainfall.

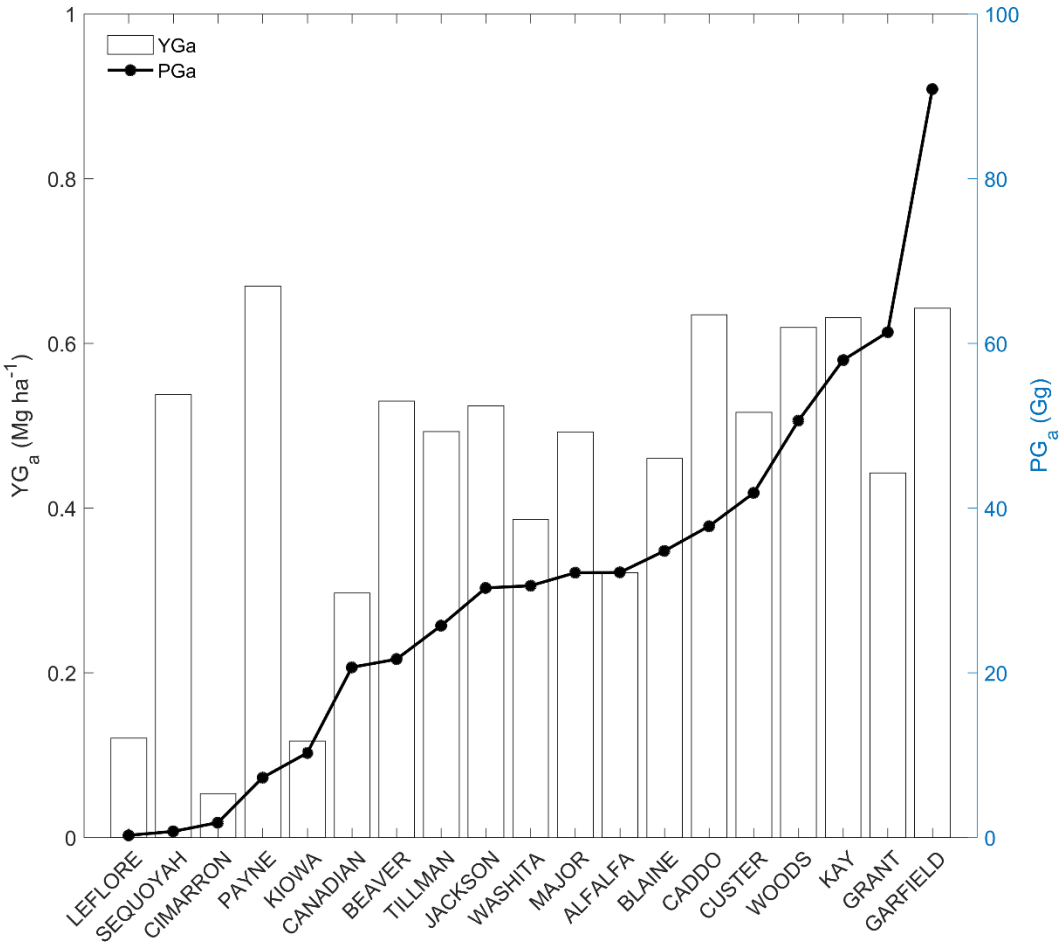

Figure 8. Comparison between yield gap relative to attainable yield (YGa) and production gap relative to attainable yield (PGa).

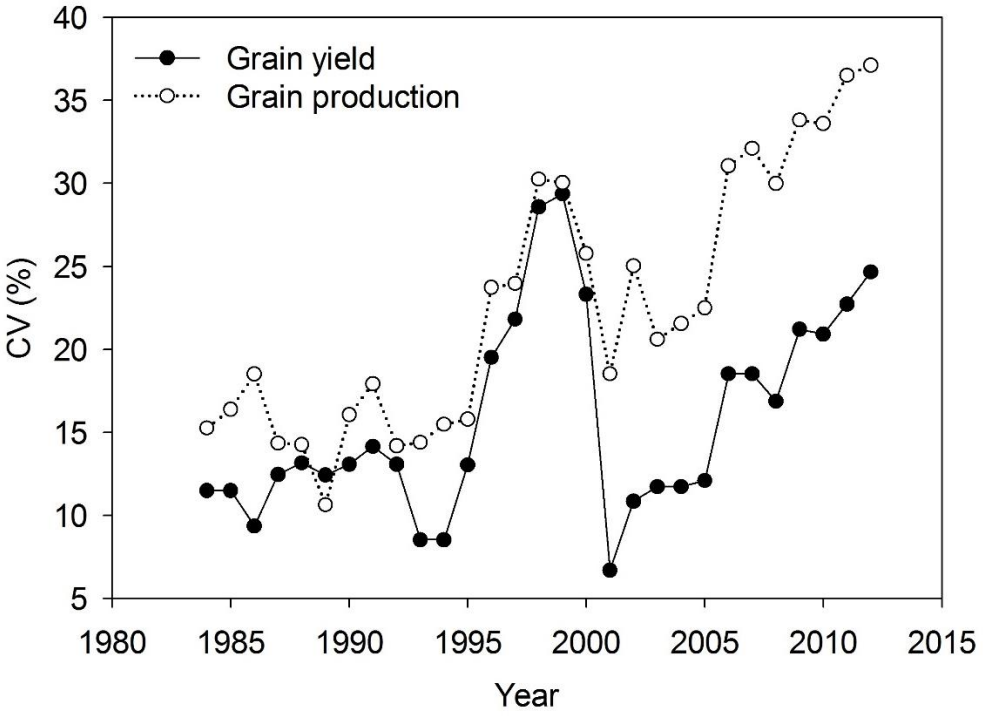

Figure 9. Time series of the 5-yr coefficient of variation (CV) of Oklahoma hard red winter wheat yield and production. Data are plotted as the CV for the preceding 5 yr.

CHAPTER III

Manuscript published in Agronomy Journal Vol. 107, p. 2312–2320 (2015)

CANOPEO: A POWERFUL NEW TOOL FOR MEASURING FRACTIONAL GREEN CANOPY COVER

Andres Patrignani and Tyson E. Ochsner

ABSTRACT

Fractional green canopy cover (FGCC) is a key diagnostic variable that can be used to estimate canopy development, light interception, and evapotranspiration partitioning. Available image analysis tools for quantifying FGCC are time-consuming or expensive, and cannot analyze video. Our objective was to develop a simple, accurate, and rapid tool to analyze FGCC from images and videos. This tool, called Canopeo, was developed using Matlab and is based on color ratios of red to green (R/G) and blue to green (B/G) and an excess green index (2G–R–B). The output from this tool was compared to that from two software packages widely used to analyze FGCC, SamplePoint, and SigmaScan Pro. Canopeo's image processing speed was 20 to 130 times faster than SigmaScan and 75 to 2500 times faster than SamplePoint. Canopeo correctly classified 90% of pixels when compared to SamplePoint. Root mean squared difference (RMSD) values for Canopeo FGCC vs. FGCC determined by SamplePoint and SigmaScan ranged from 0.04 to 0.12, with an average RMSD of 0.073 across several sets of images of corn (*Zea mays* L.), forage sorghum [*Sorghum bicolor* (L.) Moench], bermuda grass [*Cynodon dactylon* (L.) Pers.], and

switchgrass (*Panicum virgatum* L.). Analysis of video recordings of transects over crop canopies proved to be useful to minimize sampling error and to quantify FGCC spatial variability. This analysis was simple and rapid with Canopeo but not possible with SamplePoint or SigmaScan. The Canopeo app for Matlab and for iOS and Android mobile devices can be downloaded at www.canopeoapp.com.

INTRODUCTION

Active plant canopies play an important role in the Earth's atmospheric dynamics, surface energy balance, and soil water balance (Wittich and Hansing, 1995). To measure the extent of canopy development numerous indices such as spectral vegetation indices, Leaf Area Index (LAI), and Fractional Green Canopy Cover (FGCC) have been developed. Fractional green canopy cover has emerged as a non-destructive and relatively easy-to-measure variable that is employed in disciplines such as ecology, environmental science, and agronomy to quantify active vegetative land cover at different scales in space and time. For instance, FGCC was used to measure forest land cover of Scots pine and Norway spruce by Korhonen et al. (2006). Also, a relationship between FGCC and light interception was developed to estimate the proportion of green and senescing leaves in soybean (Purcell, 2000). The use of FGCC has also been examined to measure the color and percent land cover in turf (Karcher and Richardson, 2003; Richardson et al., 2001), and to measure growth rate of weeds after tillage events (Rasmussen et al., 2010). Sharma and Ritchie (2015) used FGCC along with crop height and normalized difference vegetation index (NDVI) to monitor cotton (*Gossypium hirsutum* L.) growth under different irrigation regimes in high-throughput phenotyping studies in Texas. Statistical correlations between FGCC, LAI, NDVI, and above ground biomass have also been developed by multiple researchers (Carlson and Ripley, 1997; Lati et al., 2011; Lukina et al., 1999; Nielsen et al., 2012; Rundquist, 2002). Crop FGCC is a key variable in soil-plant-atmosphere models such as Aquacrop (Hsiao et al., 2009; Raes et al., 2009; Steduto et al., 2009), in which FGCC is used to estimate crop water use.

Canopy cover has traditionally been measured using subjective methods (Richardson et al., 2001; Robson et al., 2013). The projection of images on a grid or transparency for point classification helped to reduce subjectivity, but these methods are not efficient when analyzing large sets of images (Corak et al., 1993; Ribeiro et al., 2011). In recent decades, improvements in the quality of images produced by affordable digital cameras and mobile devices propelled the

use of digital images for FGCC measurements. At the same time, numerous image processing methods (Behrens and Diepenbrock, 2006; Shrestha and Steward, 2002; Thorp and Dierig, 2011; Thorp et al., 2008) and software packages (Ewing and Horton, 1999; Purcell, 2000; Rasmussen et al., 2007) have been developed to analyze digital images of plants for a variety of applications.

Currently available green canopy cover software packages can be classified in two groups according to their pixel classification principle: manual pixel classification (MPC) and automatic color threshold (ACT) classification. The first type uses a set of randomly selected pixels (usually less than 250 random points), which have to be manually classified by a trained user. The manual classification of pixels has high accuracy, but it is time consuming because the user typically classifies 100 to 250 pixels per image. Sampling error is also a concern with MPC methods because only a miniscule fraction of the millions of pixels in a typical image are actually classified. MPC methods are particularly useful when calibrating ACT methods (Booth et al., 2006) or when calculating the proportion of various plant species or other components such as plant residue, soil, or rocks that are not easily distinguishable using color threshold settings. An example of a widely used MPC product is SamplePoint, a program developed by Booth et al. (2006). Applications of SamplePoint have included monitoring ground cover in cropping systems research (Krueger et al., 2012), monitoring plant phenology (Crimmins and Crimmins, 2008), studying grazing intensity and spatial variability in grasslands (Augustine et al., 2012), and developing relationships between FGCC and LAI in crops for its use in the Aquacrop simulation model (Nielsen et al., 2012).

The ACT type of software requires the specification of color thresholds or color ratios to select the desired portion of the image. This type of software is advantageous because a computer does the pixel classification, and therefore image processing time is markedly reduced. Another benefit of ACT methods is that all pixels in the image are classified. However, undesired pixels may be selected, leading to under or over estimation of the variable of interest. An example of a widely used ACT software package in agronomy is SigmaScan Pro 5, a product of Systat

software (Chicago, IL, US). This software requires user-specified hue (range from 0 to 360) and saturation values (range from 0 to 100) (Purcell, 2000). This software has been used to analyze canopy cover and light interception in soybean (Purcell, 2000), percent turf coverage (Karcher and Richardson, 2005; Richardson et al., 2001), and turf color (Karcher and Richardson, 2003). Even though this software can be significantly faster than SamplePoint, high resolution images can result in processing times >30 seconds per image. Traditionally, a small number of images have been taken to represent research plots or experimental fields, however, available technology is generating a growing interest for high spatial and temporal monitoring of plant growth, generating large datasets that require faster image processing tools. In addition, the user cannot visualize the effects of the chosen threshold values prior to batch image processing in SigmaScan, nor can SigmaScan analyze video recordings.

Given the limitations of current software to quantify FGCC, there is a need to develop new tools that overcome those limitations and provide convenient and accurate methods to analyze FGCC. The objectives of this study were i) to develop an interactive, simple, and accurate tool capable of rapidly analyzing high resolution digital images and video recordings to quantify FGCC, and ii) to evaluate the accuracy and image processing speed of that tool relative to two software packages widely used in agronomic research.

MATERIALS AND METHODS

Canopeo description

Canopeo is an ACT image analysis tool developed in the Matlab programming language (Mathworks, Inc., Natick, MA) using color values in the Red-Green-Blue (RGB) system. Canopeo analyzes and classifies all pixels in the image. The analysis is based on the selection of pixels according to ratios of red to green (R/G), blue to green (B/G) (Liang et al., 2012, Paruelo et al., 2000), and the excess green index (2G-R-B) (Chen et al., 2010; Richardson et al., 2007). The result of the analysis is a binary image where white pixels correspond to the pixels that satisfied

the selection criteria (green canopy) and black pixels correspond to the pixels that did not meet the selection criteria (not green canopy). Fractional green canopy cover ranges from zero (no green canopy cover) to 1 (100% green canopy cover). The classification of green canopy is based on the following criteria:

$$R/G < P_1 \text{ and } B/G < P_2 \text{ and } 2G-R-B > P_3$$

where P_1 and P_2 are parameters that typically have a value near 1 (Paruelo et al., 2000) in order to classify pixels that are predominantly in the green band (~500-570 nm), and P_3 is a parameter that sets the minimum excess green index, which typically has a value around 20 to select green vegetation (Meyer and Neto, 2008; Richardson et al., 2007). The default parameter values for Canopeo are $P_1 = 0.95$, $P_2 = 0.95$, and $P_3 = 20$.

Canopeo allows the user to preview the effectiveness of the settings prior to starting image analysis, which is especially helpful when analyzing a large set of images or videos. Having the opportunity to set, test, and modify threshold R/G and B/G values for several test images selected from the set of images to be analyzed gives the user more confidence in the chosen threshold values. The threshold value for the excess green index was set constant at a value of 20, and cannot be changed by the user. The excess green index effectively classifies dark or gray pixels that cannot be adequately discriminated using the R/G and B/G ratios alone. Canopeo also has the capability to reduce noise by removing isolated green pixels. Isolated pixels that meet the color ratio specifications can sometimes occur in other objects and are not exclusively part of green canopy (Lati et al., 2011). For instance, some isolated pixels in residue shadows may have R/G and B/G ratios similar to those found in green canopies. Canopeo can remove these pixels or small clusters of pixels (e.g. small weeds in a row crop) by analyzing connected neighboring pixels. The user-adjustable noise reduction value in Canopeo determines the minimum number of 4-connected pixels that any area in the binary (i.e. classified) image must have to avoid being deleted.

In Canopeo a subset of frames from a given video can be extracted according to user specifications, and then each frame is analyzed as a separate image. Canopeo saves a spreadsheet (Microsoft Excel format) file with the settings used in the image analysis (R/G threshold, B/G threshold, and noise reduction), directory, image file name, and FGCC value for each image. In the case of video, Canopeo saves the video file name, frame number, FGCC values, average, standard deviation, coefficient of variation of FGCC in the video, and the minimum number of images that were necessary to estimate the mean with a 95% confidence interval of 0.05 FGCC for each video. The supported video formats are .avi (Audio Video Interleaved format), .wmv (Windows Video Media format), .mp4 (MPEG-4 format), and .mov (QuickTime multimedia file format). Canopeo is available as a free Matlab app, but requires prior installation of a properly licensed copy of Matlab R2013a or later and Matlab image processing toolbox 8.2 or newer. The Canopeo Matlab app can be downloaded by following the link at www.canopeoapp.com. To install Canopeo, first launch Matlab, then open the Apps tab, and finally install the downloaded app. Versions of Canopeo for iOS and Android mobile devices are also available through links at that same website.

Evaluation

Images for the evaluation were typically taken from 1000 to 1400 h on sunny to partially cloudy days during the years 2009-2012 from experimental plots in Oklahoma, USA. Nadir (i.e. downward-facing) images were taken from random areas of experimental plots using inexpensive "point and shoot" type digital cameras such as the Canon Powershot SD1200 IS (10 MPX). The camera was kept at about 1.5 m from the top of the canopy using a 1.5 m monopod. Maintaining adequate distance from the camera to the top of the canopy is critical in order to minimize overestimation of FGCC caused by the top leaves of the canopy being too close to the lens of the camera and by crop rows that are not orthogonal with the lens of the camera (Hoyos-Villegas et al., 2014).

Canopeo was compared against SamplePoint (i.e. MPC) version 1.56 and SigmaScan Pro 5 (i.e. ACT) to test accuracy and image processing speed. In this study the pixel-level accuracy of Canopeo was evaluated by using SamplePoint as the "gold standard" (i.e. best available benchmark). For each test image, each pixel in an automatically-created, uniformly-spaced 10 by 10 grid (i.e. 100 pixels) was manually classified as "Green" or "Not-Green". SamplePoint automatically selects the grid spacing, based on the image resolution, so that the grid spans the majority of the image. For this accuracy test, a set of 20 images with resolution of 8 MPX (3264 by 2448 pixels) and with FGCC ranging from 0.07 to 0.89 (based on values obtained using SamplePoint) for different crops (i.e. wheat, soybean, corn, canola, and grain sorghum) and backgrounds (i.e. no-till and conventional till) was used. A total of 2000 pixels (100 pixels per image x 20 images) resulted in a wide gamut of colors for testing Canopeo's classification accuracy.

The same set of 20 images was classified in SamplePoint by three trained users to account for different perceptions of green canopy cover. Because only two classification outcomes were possible (i.e. "Green" and "Not Green"), the final pixel classification was decided upon the decision of two out of the three users (i.e. decision of the majority). Pixel classification by the trained users was based on two criteria: 1) color of the central pixel selected by SamplePoint and 2) surrounding context of the selected pixel. Examination of the context around the pixel (i.e. zooming out from pixel to leaf or plant level) can sometimes reveal that the selected pixel represents green canopy cover, particularly in portions of the image that display shaded canopy. Pixels were classified as "Green" only if the surrounding context of the pixel allowed the user to unambiguously determine that the pixel was representing green canopy cover, otherwise the pixel was classified as "Not-Green".

The same set of 20 images was also analyzed with Canopeo. We developed a Matlab script that matched the pixels selected by SamplePoint with the corresponding pixels classified by Canopeo. Because our pixel classification had a binomial outcome (i.e. "Green" and "Not-

Green"), we evaluated Canopeo's accuracy using the concept of sensitivity and specificity. Sensitivity evaluates the proportion of true positive cases (i.e. "Green" pixels defined by SamplePoint), while specificity evaluates the proportion of true negative cases (i.e. "Not-Green" pixels defined by SamplePoint) cases. Additionally, 50 or more images for corn, forage sorghum, switchgrass, and bermuda grass collected under natural lighting conditions in various fields were analyzed to extend our comparisons of the FGCC values from the three software packages across diverse vegetation, soil, and lighting conditions. We used the root mean squared difference (RMSD) to describe the performance of Canopeo relative to SamplePoint and SigmaScan.

The Canopeo speed test was performed against SigmaScan using a computer with an Intel Core duo2 processor with a speed of 2.66 GHz and 3 GB of RAM. Three sets of 72 images per set were used to evaluate the processing speed using the macro for batch image analysis developed by Karcher and Richardson (2005). The processing speed was measured dividing the total image processing time by the total number of images in the set (i.e. 72 images). For SigmaScan we used a digital stopwatch to measure the processing time of the 72 images, while for Canopeo we used Matlab's stopwatch timer functions (i.e. tic and toc functions). The three sets of images had resolutions of 0.3 MPX (640 by 480 pixels), 3.1 MPX (2048 by 1536 pixels), and 8 MPX (3264 by 2448 pixels), with an approximate image sizes of 150 KB, 1.7 MB, and 3.5 MB, respectively. The approximate pixel size for each image resolution assuming a field of view of 1.2 m^2 at the top of the canopy was 4, 0.4, and 0.15 mm^2, respectively.

For SigmaScan, we employed threshold values similar to those used by Purcell (2000), with hue values ranging from 25 to 150 and saturation values ranging from 10 to 115 (Table 1). The hue and saturation values for SigmaScan were optimized based on visual inspection of the classification performance of three to five images within each image set. The threshold values for the R/G and B/G ratios in Canopeo were optimized in the same way, but varied over a smaller range and required less adjustment. The R/G and B/G threshold ratios are independent of each other, and for FGCC the optimal values for both ratios typically ranged between 0.9 and 1. The

noise reduction parameter in Canopeo was set to one (effectively disabling the function) in order to provide a more fair comparison against the other software packages (Table 1).

In order to demonstrate the spatial variability of FGCC, and how this spatial variability could be assessed by using video recordings, a power analysis statistical procedure was used to calculate the minimum number of images required to obtain a 95% confidence interval of $\pm$ 0.05 FGCC about the population mean along a 40-m transect in a wheat field (crop stage Feekes 3.0) and a grain sorghum field (crop stage V10). The population mean was calculated as the average FGCC of all images in a video. The minimum number of samples was calculated using the following equation (Clewer and Scarisbrick, 2001):

$$n = \left(\frac{1.96\,\sigma}{\delta}\right)^2$$

where *n* is the number of samples needed to estimate μ, the population mean, within δ=0.05 FGCC with 95% confidence using standard deviation σ, which is calculated from all images in a given video. This comes from the fact that $\overline{x} \pm 1.96\left(\sigma/\sqrt{n}\right)$ defines a sample mean with 95% confidence interval assuming a known σ. The value of δ=0.05 FGCC is an arbitrary but reasonable confidence interval width for our purposes.

RESULTS AND DISCUSSION

The combination of the R/G and B/G ratios with the excess green index (2G-R-B) resulted in effective and rapid classification of FGCC from digital images. Live green vegetation was effectively separated from the background by using the R/G and B/G ratios, which have been proven useful to quantify aboveground live biomass in a perennial shortgrass steppe in northcentral Colorado (Paruelo et al., 2000). The excess green index was used to set a minimum pixel greenness in order for a given pixel to be considered green canopy. The excess green index was particularly effective for classifying green canopy cover under dark conditions. The addition of the excess green index avoided mis-classifying dark pixels that otherwise would have been

selected by solely using the R/G and B/G ratios. The excess green index can be seen as a variable similar to that of saturation in the hue-saturation-brightness color framework. The excess green index has previously proven useful to track canopy green-up in a deciduous broadleaf forest located in northeastern US (Richardson et al., 2007).

The classification process using the R/G and B/G ratios is illustrated using an image of no-till canola (Fig. 1A). This image was processed with R/G and B/G thresholds set to 0.95, the excess green index threshold set to 20, and the noise reduction parameter set to 1.0, resulting in FGCC = 0.54. Varying the R/G and B/G thresholds independently between 0.9 and 1.0 resulted in FGCC values from 0.52 to 0.56, highlighting the narrow variability in FGCC when adjusting the R/G and B/G thresholds within this range. The bivariate histogram (Fig. 1B) for this image revealed the formation of two clusters, which represent the green vegetation and the background. The cluster located on the left side of Figure 1B (Cluster 1) consists of pixels that were classified as “Green”, while the pixels in the cluster on the right side of Figure 1B (Cluster 2) consists of pixels belonging to the background (e.g. soil, crop residue, etc.). The clusters in Figure 1B are mainly a consequence of the bimodal distribution of the R/G ratio (Fig. 1C), which allows for selecting a clear FGCC classification threshold (R/G=0.95). Nonetheless, the inclusion of the B/G ratio (Fig. 1D) increases the robustness of the classification so that it can be used in more diverse field scenarios such as analyzing zenith (i.e. upward-facing) images where the color of the sky may need to be filtered (Fuentes et al., 2014).

The accuracy test revealed that Canopeo had a sensitivity of 864/(864+89) = 0.91 and specificity of 933/(933+114) = 0.89 (Table 2). These values mean that Canopeo correctly classified 91% of the pixels defined as “Green” (i.e. true positives) and 89% of the pixels defined as “Not Green” (i.e. true negatives) by SamplePoint. The fact that the specificity was 2% lower than the sensitivity shows that Canopeo had a slight tendency to classify pixels as “Green” even though the trained users classified them as “Not Green” (i.e. false positive, type I error). Overall, Canopeo accurately classified 90% of the pixels (i.e. [864+933]/2000). Manual pixel

classification with SamplePoint was used as the pixel-level "gold standard" for comparison in this study, but subjectivity in classification cannot be completely eliminated. At the pixel level, there is sometimes no clear distinction of green canopy cover from background due to pixelation, poor lighting, or other complicating factors.

Canopeo was 20-130 times faster than SigmaScan and 75-2500 times faster than SamplePoint (Table 3). Image resolution more severely impacted the image processing speed of SigmaScan than that of Canopeo. At the lowest resolution (640 by 480 pixels), Canopeo required 0.12 s per image, and at the highest resolution (3264 by 2448 pixels), 1.6 s per image. On the other hand, SigmaScan required 2.4 s per image at the lowest image resolution and 49 s per image at the highest resolution. The relatively low processing speed of SigmaScan may justify the use of video graphics array (VGA) image resolution, i.e. 640 by 480 pixels, when analyzing FGCC with SigmaScan (Purcell, 2000). In SamplePoint, image processing time ranged from 2-5 minutes. Because SamplePoint requires pixel classification by a trained user, the processing speed highly depends on the ability of the user to keep focus on the analysis. The high image processing speed achieved by Canopeo is a result of Matlab's efficiency in matrix manipulation.

The use of Matlab for agronomic image analysis has been reported in other studies. Lati et al. (2011) provided a thorough analysis of the performance of an image segmentation approach based on a hue-invariant transformation to quantify weed biomass and leaf-cover area. The strength of the hue-invariant segmentation approach is the excellent performance under different illumination conditions and camera positions. However, this approach requires a reference point, and was only tested on Purple nutsedge (*Cyperus rotundus* L.) under simple background conditions (i.e. conventional tillage). On the other hand, a study by Robson et al. (2013) used red and green/blue adjustable thresholds to quantify canopy establishment in biofuel crops such as *Miscanthus* (Robson et al., 2013). However, the studies by both Lati et al. (2011) and Robson et al. (2013) were based on single plant species and do not provide detailed information about accuracy and processing time relative to commercially available software packages.

For several crops, Canopeo resulted in FGCC values similar to those obtained using SamplePoint and SigmaScan (Fig. 2). Root mean squared differences (RMSD) for the FGCC values between Canopeo and SamplePoint ranged from 0.056 to 0.123 with an average of 0.086 (Fig. 2). SamplePoint whole-image FGCC estimates cannot be considered as a "gold standard" in this context (i.e. Fig. 2) because the resulting FGCC in SamplePoint was obtained from the analysis of only a small fraction of the pixels in each image (i.e. 100 pixels) whereas the FGCC in Canopeo was calculated by classifying all the pixels. Therefore, the RMSD values shown for the comparisons between Canopeo and SamplePoint result from errors in both approaches. The comparison between SigmaScan and SamplePoint (data not shown) resulted in RMSD of 0.051 for corn, 0.066 for sorghum, 0.096 for turf, and 0.115 for switchgrass, values that are similar to those observed between Canopeo and SamplePoint. The RMSD between FGCC values for Canopeo and SigmaScan ranged from 0.04 to 0.076 with an average of 0.050. These RMSD values are lower than those obtained by comparing either of the ACT methods to SamplePoint, likely due to the fact that both Canopeo and SigmaScan classify every pixel in the image.

Corn and sorghum images with FGCC near a value of one had a combination of both green leaves fully exposed to the sun light and shaded leaves close to ground level. Despite the challenge of accurately identifying leaves under these difficult lighting conditions, Canopeo detected all green parts of plants exposed to sun light, and a great portion of shaded leaves. For example, see the circled portions of Fig. 3C and 3D. Some shaded lower leaves of the corn canopy are barely visible in the raw image (Fig. 3D) but are accurately identified by Canopeo (Fig. 3C). The Canopeo classification approach demonstrated robust performance even for imperfect images such as when the user's feet or the camera monopod's shadow were present in the images (e.g. Sharma and Ritchie, 2015). Previously, the G/R ratio was used by Adamsen et al. (1999) to measure senesced leaves in wheat (*Triticum aestivum* L.) and by Ritchie (2010) and Sharma and Ritchie (2015) to measure FGCC in cotton. Also, a greenness index using the G/B ratio was developed by Crimmins and Crimmins (2008) to monitor plant phenology. The use of

the R/G and B/G ratios together with the excess green index has not been widely reported, but it seems to be highly effective for selecting FGCC of numerous plant species across diverse backgrounds and light conditions without the need for a reference board (Lati et al., 2011).

SigmaScan uses the hue-saturation-brightness (HSB) system instead of the RGB system because the red and blue levels alter pixel greenness (Ewing and Horton, 1999). Many ACT approaches are based on the selection of saturation and hue threshold values, but finding the optimal thresholds is difficult, and threshold settings differ when using images taken under different light intensities and backgrounds (Karcher and Richardson, 2005). Furthermore, in SigmaScan the user cannot pre-visualize the effects of the selected hue and saturation values before running an entire batch of images.

For the batch of turf images, Canopeo had excellent agreement with SigmaScan (Fig. 2, RMSD=0.041), showing the potential of Canopeo to be applied in turf research and management. On the other hand, greater discrepancies were observed when comparing SamplePoint and Canopeo for turf (Fig. 2, RMSD=0.092). The grid size of 100 points used in SamplePoint may be inadequate for precise FGCC estimation for images containing turf plugs growing radially from the center of the image (Fig. 4A). Switchgrass FGCC measurement presented a challenge to all three programs because green parts of the plant were mixed with senesced leaves creating a wide range of color tones (Fig. 4B). In fact, close inspection at the pixel level revealed that gray-green and gray-reddish pixels (e.g. R=90 G=80 B=92) were common in actively growing switchgrass leaves, requiring R/G and B/G ratios to be slightly larger than 1 (i.e. R/G=1.1 and B/G=1.1, Table 1) to select live vegetation. In this case, SamplePoint may be able to provide the most accurate results, but to achieve good precision for these highly heterogeneous images, a larger grid size (i.e. 225 pixels) may be necessary.

The thresholds were easy to set in Canopeo due to its interactive functionality that allows the user to preview and compare with the original image the effect of the selected R/G and B/G threshold values. This interactive capability allows the user to set proper ratios even under

difficult scenarios. Often, no-till cropping systems with low FGCC values are difficult to analyze accurately because crop residue does not offer adequate background contrast. However, Canopeo effectively selected FGCC in no-till crops with low FGCC and complex backgrounds with high crop residue levels (Fig. 5).

Canopeo, as any other measurement tool, relies on proper operation by the end user, and it cannot compensate for some user operational errors. As an example, the images in Figure 5C and 5G would result in different FGCC if the camera lens had been positioned at different heights from the top of the canopy. In Figure 5C, the soybean rows on both sides of the image may have been excluded if the camera lens were closer to the canopy. On the other hand, in Figure 5G additional sunflower rows would have been included in the image if the camera lens was positioned at a greater height above the top of the canopy. While the position of the camera lens can affect the portion of the crop being captured in the image, the classification accuracy of Canopeo remains unaltered.

Perhaps the most unique capability of Canopeo compared to current software packages for quantifying FGCC is the possibility to analyze video recordings. Analyzing video recordings to quantify FGCC can help minimize sampling error in plots or fields with high FGCC spatial variability by allowing the user to record a large number of images in a small amount of time. Video recordings have been used by other researchers to study the severity of foliar plant disease by monitoring necrotic and intact leaves in real-time (Lindow and Webb, 1983). Video was also used to analyze real-time Lepidoptera defoliation in traditional and *Bacillus thuringiensis* (Bt) transgenic cotton in the laboratory, allowing the inclusion of feeding activities in the analysis (Alchanatis et al., 2000). A Matlab tool was used by Fuentes et al. (2014) to estimate LAI in grapevine canopies by recording zenith (i.e. upward-facing) videos. Using zenith images and videos to estimate LAI or FGCC ensures good contrast between live vegetation and its background, which facilitates pixel classification, but operational data acquisition in agricultural fields can be challenging. Shrestha and Steward (2003) developed a vehicle-mounted video

system to quantify plant population in Iowa corn fields at a speed of 1 to 2 m/s. This approach has later been used by Thorp et al. (2007) to relate airborne hyperspectral remote sensing to ground machine-vision measurements of plant population of corn. In this context, measurement of FGCC from videos has the potential to be integrated with other data streams (e.g. multi-spectral or hyperspectral reflectance, plant height sensing) for high throughput phenotyping of plants.

Recording videos in the field did not take longer than taking still images. About 30 seconds were required per plot to record a 15-s video, covering an approximate area of 15 m^2. Fifteen seconds of video using a Canon Powershot SD1200 IS (10 MPX) camera at 30 frames per second resulted in 450 frames. Even though each frame had VGA resolution, each frame is equivalent to an image. Also, many digital cameras allow for high definition video recordings. In the presence of spatial variability of FGCC, videos allow the FGCC of a field or experimental plot to be estimated more accurately by obtaining values close to the FGCC population mean rather than estimating FGCC based on a few images. This advantage is especially significant in plots or fields where FGCC shows large spatial variability and many images may be required to obtain a representative mean.

An example FGCC transect of ~40 m length in a grain sorghum field in growth stage V10 is presented in Figure 6A. The mean FGCC of the transect using ~2000 images was 0.63 with a standard deviation of 0.06 and a coefficient of variation of 9.5%. Using power analysis, we determined that six images were required to have a 95% confidence interval of $\pm$ 0.05 FGCC about the mean (Fig. 6B). On the other hand, a transect of ~40 m in a wheat field in growth stage Feekes 3.0 had a mean of 0.46 FGCC and substantial spatial variability across the recorded transect with a standard deviation of 0.17 and coefficient of variation of 37% (Fig. 6C). The minimum number of images needed to have a 95% confidence interval of $\pm$ 0.05 FGCC about the mean was 45 (Fig. 6D). This shows the importance of large sample sizes in estimating FGCC for heterogeneous canopies and how the use of transect video recordings can help minimize sampling error. Also, the possibility of analyzing FGCC from videos is useful for overcoming the need to

choose “representative” locations in heterogeneous canopies and, therefore, minimizing researcher bias.

CONCLUSIONS

Canopeo is capable of detecting FGCC at high speed relative to the available software packages tested in this study without sacrificing accuracy. The video feature present in this tool is a novel addition to software packages that are used to measure FGCC, allowing the user to record a large number of images and therefore minimize sampling error. One limitation of Canopeo (and other FGCC methods based on digital images) is the need to keep the camera an adequate height above the canopy. For vegetation taller than about 2.5 m, this may require the use of aerial images or special equipment. It may be possible to use the R/G and B/G ratios together with the excess green index to detect other components of digital images, but this possibility requires further research. It is important to highlight that MPC programs such as SamplePoint are invaluable for calibration and when there is need for simultaneous estimation of more complex variables other than FGCC. The Canopeo app for Matlab, as well as versions for iOS and Android mobile devices, can be downloaded at www.canopeoapp.com. The mobile apps are powerful tools which allow producers, crop consultants, researchers, and other end users to easily acquire and process digital images in the field and obtain real-time, geo-referenced green canopy cover estimates.

REFERENCES

Alchanatis, V., A. Navon, I. Glazer, S. Levski. 2000. An image analysis system for measuring insect feeding effects caused by biopesticides. J. Agr. Eng. Res. 77:289-296.

Adamsen, F.J., P.J. Pinter, E.M. Barnes, R.L. LaMorte, G.W. Wall, S.W. Leavitt and B.A. Kimball. 1999. Measuring wheat senescence with a digital camera. Crop Sci. 39:719–724.

Augustine, D.J., D.T. Booth, S.E. Cox and J.D. Derner. 2012. Grazing intensity and spatial heterogeneity in bare soil in a grazing-resistant grassland. Rangeland Ecol. Manag. 65:39–46.

Beherens, T. and W. Diepenbrock. 2006. Using digital image analysis to describe canopies of winter oilseed rape (*Brassica napus* L.) during vegetative developmental stages. J. Agron. and Crop Sci. 192:295–302.

Booth, D.T., S.E. Cox, and R.D. Berryman. 2006. Point sampling digital imagery with "SamplePoint'. Environ. Monit. Assess. 123:97–108.

Carlson, T.N. and D.A. Ripley. 1997. On the relation between NDVI, fractional vegetation cover, and leaf area index. Remote Sens. Environ. 62:241–252.

Chen, L., J. Zhang, H. Su, and W. Guo. 2010. Weed identification method based on probabilistic neural network in the corn seedling field. Proceedings of the Ninth International Conference on Machine Learning and Cybernetics, Qingdao, 11–14 July 2010.

Clewer, A.G. and Scarisbrick, D.H. 2001. Practical statistics and experimental design for plant and crop science. John Wiley and Sons, Ltd, Baffins Lane, Chichester, West Sussex, England.

Corak, S.J., T.C. Kaspar and D.W. Meek. 1993. Evaluating methods for measuring residue cover. J. Soil Water Conserv. 48:70–74.

Crimmins, M.A. and T.M. Crimmins. 2008. Monitoring plant phenology using digital repeat photography. Environ. Manage. 41:949–958.

Ewing, R.P. and R. Horton. 1999. Quantitative color image analysis of agronomic images. Agron. J. 91:148–153.

Fuentes, S., C. Poblete-Echeverria, S. Ortega-Farias, S. Tyerman, and R. De Bei. 2014. Automated estimation of leaf area index from grapevine canopies using cover photography, video and computational analysis methods. Aust. J. Grape Wine R. 20:465–473.

Hoyos-Villegas, V., J.H. Houx, S.K. Singh, and F.B. Fritschi. 2014. Ground-based digital imaging as a tool to assess soybean growth and yield. Crop Sci. 54:1756–1768.

Hsiao, T.C., L. Heng, P. Steduto, B. Rojas-Lara, D. Raes and E. Fereres. 2009. AquaCrop-The FAO crop model to simulate yield response to water: III. Parameterization and testing for maize. Agron. J. 101:448–459.

Karcher, D.E. and M.D. Richardson. 2003. Quantifying turfgrass color using digital image analysis. Crop Sci. 43:943–951.

Karcher, D.E. and M.D. Richardson. 2005. Batch analysis of digital images to evaluate turfgrass characteristics. Crop Sci. 45:1536–1539.

Korhonen, L., K.T. Korhonen, M. Rautiainen and P. Stenberg. 2006. Estimation of forest canopy cover: A comparison of field measurement techniques. Silva Fenn 40:577–588.

Krueger, E.S., T.E. Ochsner, J.M. Baker, P.M. Porter and D.C. Reicosky. 2012. Rye–corn silage double-cropping reduces corn yield but improves environmental impacts. Agron. J. 104: 888-896..

Lati, R.N., S. Filin and H. Eizenberg. 2011. Robust methods for measurement of leaf-cover area and biomass from image data. Weed Sci. 59:276–284.

Liang, L., M.D. Schwartz, and S. Fei. 2012. Photographic assessment of temperate forest understory phenology in relation to springtime meteorological drivers. Int. J. Biometeorol. 56:343–355.

Lindow, S.E., R.R. Webb. 1983. Quantification of foliar plant-disease symptoms by microcomputer-digitized video image-analysis. Phytopathology. 73:520–524.

Lukina, E.V., M.L. Stone and W.R. Rann. 1999. Estimating vegetation coverage in wheat using digital images. J. Plant Nutr. 22:341–350.

Meyer, G.E. and J.C. Neto. 2008. Verification of color vegetation indices for automated crop imaging applications. Comput. Electron. Agr. 63:282-293.

Nielsen, D.C., J.J. Miceli-Garcia and D.J. Lyon. 2012. Canopy cover and leaf area index relationships for wheat, triticale, and corn. Agron. J. 104:1569–1573.

Paruelo, J.M., W.K. Lauenroth, and P.A. Roset. 2000.Technical note: Estimating aboveground plant biomass using a photo-graphic technique. J. Range Manage. 53:190–193.

Purcell, L.C. 2000. Soybean canopy coverage and light interception measurements using digital imagery. Crop Sci. 40:834–837.

Raes, D., P. Steduto, T.C. Hsiao and E. Fereres. 2009. AquaCrop-The FAO crop model to simulate yield response to water: II. Main algorithms and software description. Agron. J. 101:438–447.

Rasmussen, J., H. Mathiasen and B.M. Bibby. 2010. Timing of post-emergence weed harrowing. Weed Res. 50:436–446.

Rasmussen, J., M. Norremark and B.M. Bibby. 2007. Assessment of leaf cover and crop soil cover in weed harrowing research using digital images. Weed Res. 47:299–310.

Ribeiro, A., J. Ranz, X.P. Burgos-Artizzu, G. Pajares, M.J.S. del Arco and L. Navarrete. 2011. An image segmentation based on a genetic algorithm for determining soil coverage by crop residues. Sensors-Basel 11:6480–6492.

Richardson, M.D., D.E. Karcher and L.C. Purcell. 2001. Quantifying turfgrass cover using digital image analysis. Crop Sci. 41:1884–1888.

Richardson A.D., J.P. Jenkins, B.H. Braswell, D.Y. Hollinger, S.V. Ollinger, M.L. Smith. 2007. Use of digital webcam images to track spring green-up in a deciduous broadleaf forest. Oecologia. DOI 10.1007/s00442-006-0657-z.

Ritchie G.L., Sullivan, D.G., Vencill W.K., Bednarz C.W. and J.E. Hook. 2010. Sensitivities of normalized difference vegetation index and a green/red ratio index to cotton ground cover fraction. Crop Sci. 50:1000–1010.

Robson, P.R.H., K. Farrar, A.P. Gay, E.F. Jensen, J.C. Clifton-Brown and I.S. Donnison. 2013. Variation in canopy duration in the perennial biofuel crop Miscanthus reveals complex associations with yield. J. Exp. Bot. 64:2373–2383.

Rundquist, B.C. 2002. The influence of canopy green vegetation fraction on spectral measurements over native tallgrass prairie. Remote Sens. Environ. 81:129–135.

Sharma, B. and G.L. Ritchie. 2015. High-throughput phenotyping of cotton in multiple irrigation environments. Crop Sci. 55:958–969.

Steduto, P., T.C. Hsiao, D. Raes and E. Fereres. 2009. AquaCrop-The FAO crop model to simulate yield response to water: I. Concepts and underlying principles. Agron. J. 101:426–437.

Shrestha, D.S. and B.L. 2003. Steward. Automatic corn plant population measurement using machine vision. Transactions of the ASAE. 46:559–565.

Thorp, K.R. and D.A. Dierig. 2011. Color image segmentation approach to monitor flowering in lesquerella. Ind. Crops Prod. 34:1150–1159.

Thorp, K.R., B.L. Steward, A.L. Kaleita, and W.D. Batchelor. 2008. Using aerial hyperspectral remote sensing imagery to estimate corn plant stand density. Transactions of the ASABE. 51:311–320.

Wittich, K.P. and O. Hansing. 1995. Area-averaged vegetative cover fraction estimated from satellite data. Int. J. Biometeorol. 38:209–215.

Table 1. Software settings used to analyze each batch of images.

Software	Settings	Corn	Forage sorghum	Turf	Switchgrass
Canopeo	R/G	0.97	0.97	0.99	1.1
	B/G	0.97	0.97	0.99	1.1
	Noise reduction	1	1	1	1
SigmaScan	Hue range	40-140	40-140	40-140	50-180
	Saturation range	15-100	15-100	15-100	10-100
SamplePoint	Number of pixels	100	100	100	100

Table 2. Comparison of pixel-level classification by Canopeo and SamplePoint using a total of 2000 pixels selected from 20 images with different crops, backgrounds, and light conditions.

	Canopeo Green	Canopeo Not Green	% Correct
SamplePoint Green	864 (true positives)	89 (type II error)	0.91†
SamplePoint Not Green	114 (type I error)	933 (true negatives)	0.89‡
Correctly classified pixels			0.90

† Sensitivity
‡ Specificity

Table 3. Comparison of pixel classification method, processing speed, cost, number of pixels included in the image analysis, and flexibility of Canopeo, SigmaScan, and SamplePoint.

Characteristics	**Canopeo**	**SamplePoint**	**SigmaScan**
Pixel classification	Computer	Manual	Computer
Speed† (sec. per image)			
640 x 480 pixels	0.12	120-300‡	2.4
2048 x 1536 pixels	0.18	120-300	24
3264 x 2448 pixels	1.62	120-300	49.2
Cost (US$)	Free§	Free	$999#
Number of pixels analyzed	All	50 to 225	All
Ability to classify other than green	Limited	Highly flexible	Limited

† Tested with a set of 72 images per level of resolution.

‡ Maximum of 50 to 70 images per day per user.

§ Matlab software needs to be previously installed. Individual academic license was US$ 500 and image processing toolbox was US$ 200 in September, 2014.

Academic price. Commercial price was US$ 1,499 on August, 2014.

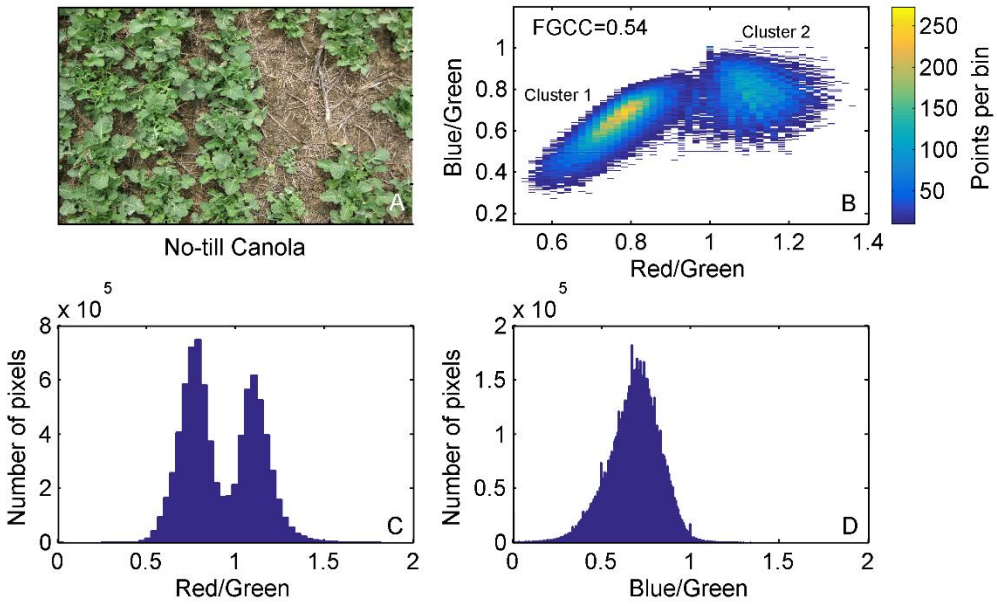

Figure 1: Histograms of the red/green (R/G) and blue/green (B/G) ratios used to classify fractional green canopy cover (FGCC). Example is presented for an image of no-till canola (A) using a bivariate histogram (B) and the one-dimensional R/G (C) and B/G (D) histograms.

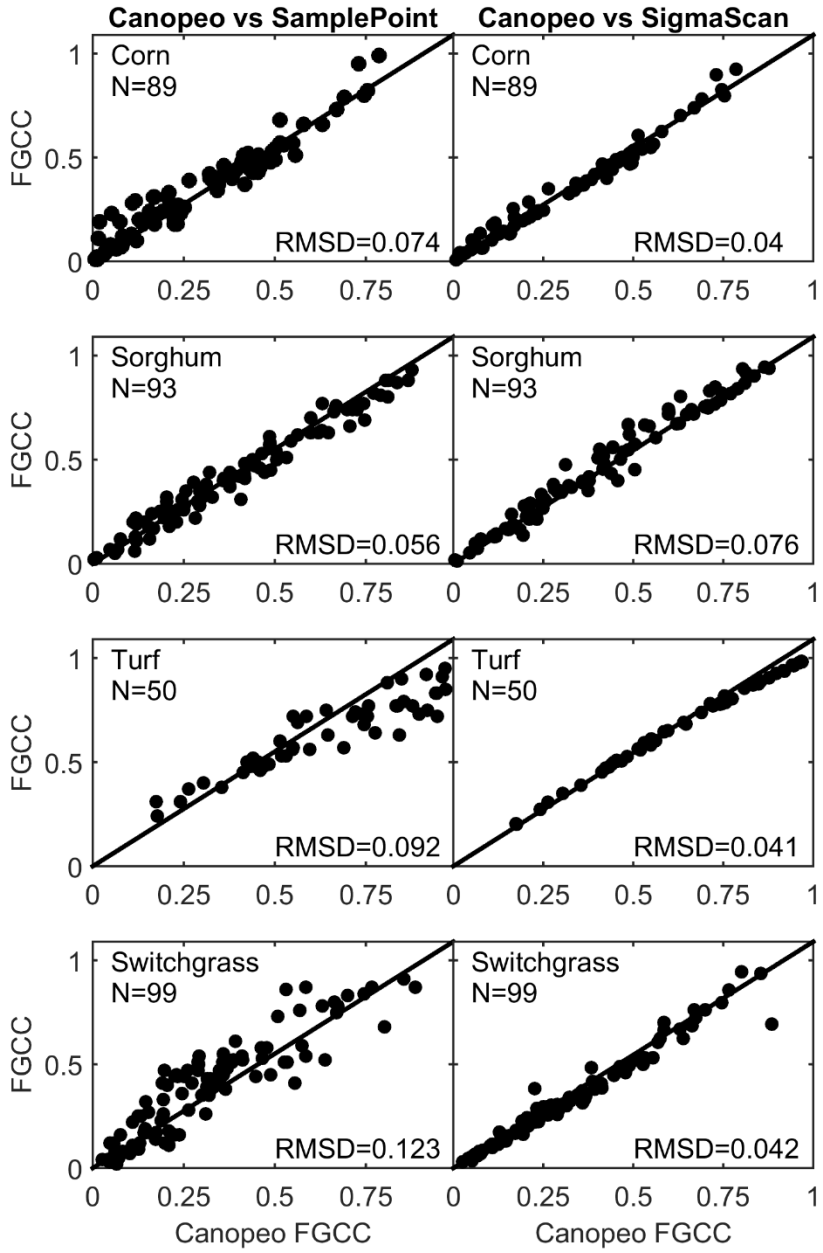

Figure 2: Comparison of fractional green canopy cover (FGCC) for corn, forage sorghum, turf, and switchgrass using Canopeo, SigmaScan, and SamplePoint. The solid line in each subplot represents the 1:1 line.

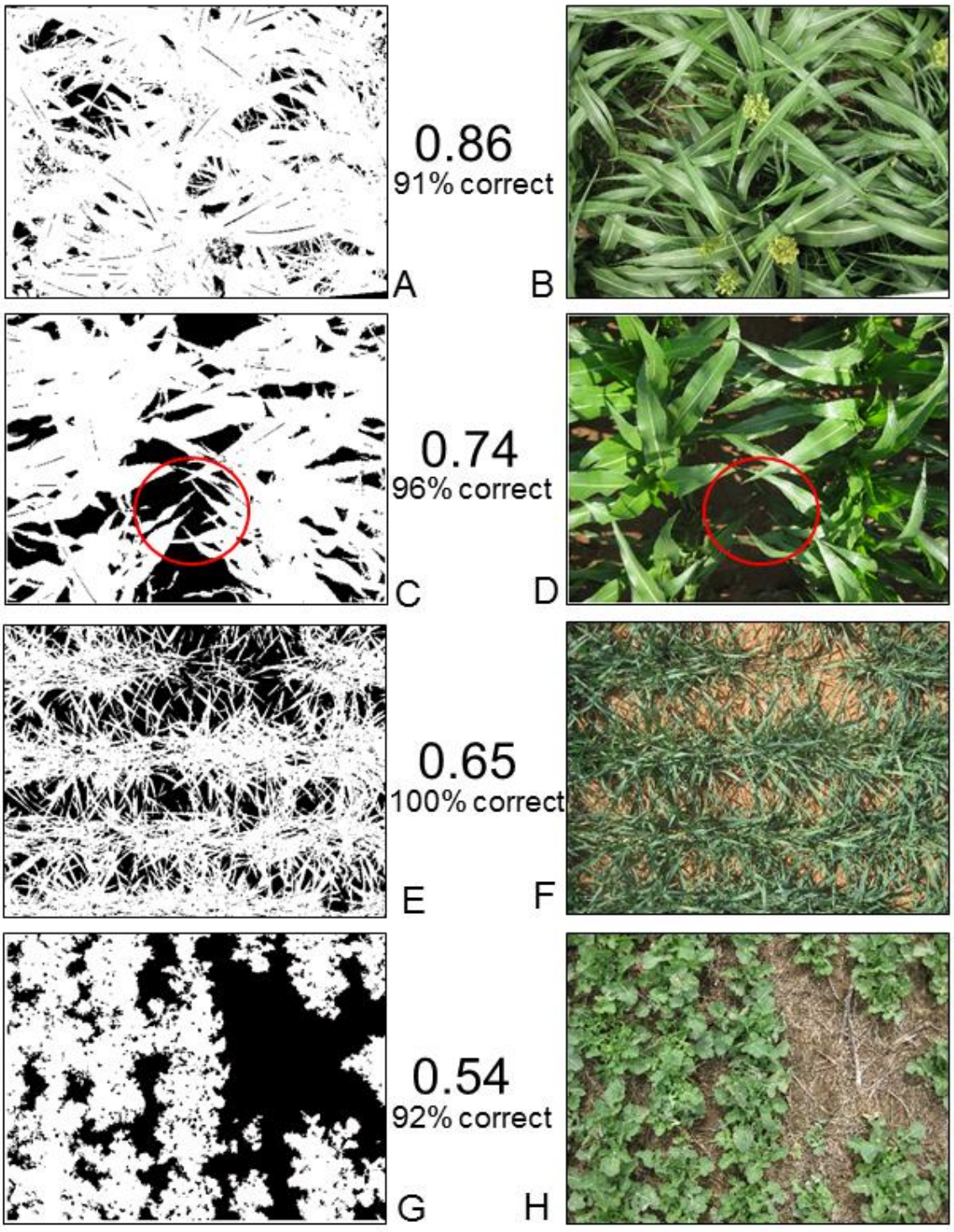

Figure 3. From top to bottom, digital images of no-till grain sorghum (A, B), no-till corn (C, D), conventional till wheat (E, F), and no-till canola (G, H) are shown after the digital image was analyzed (left) relative to the original image (right). Area in white represents green pixels selected by Canopeo. The fractional green canopy cover from Canopeo and the percent of correctly classified pixels relative to SamplePoint are shown between the images. Area within red circle shows lower leaves in the canopy.

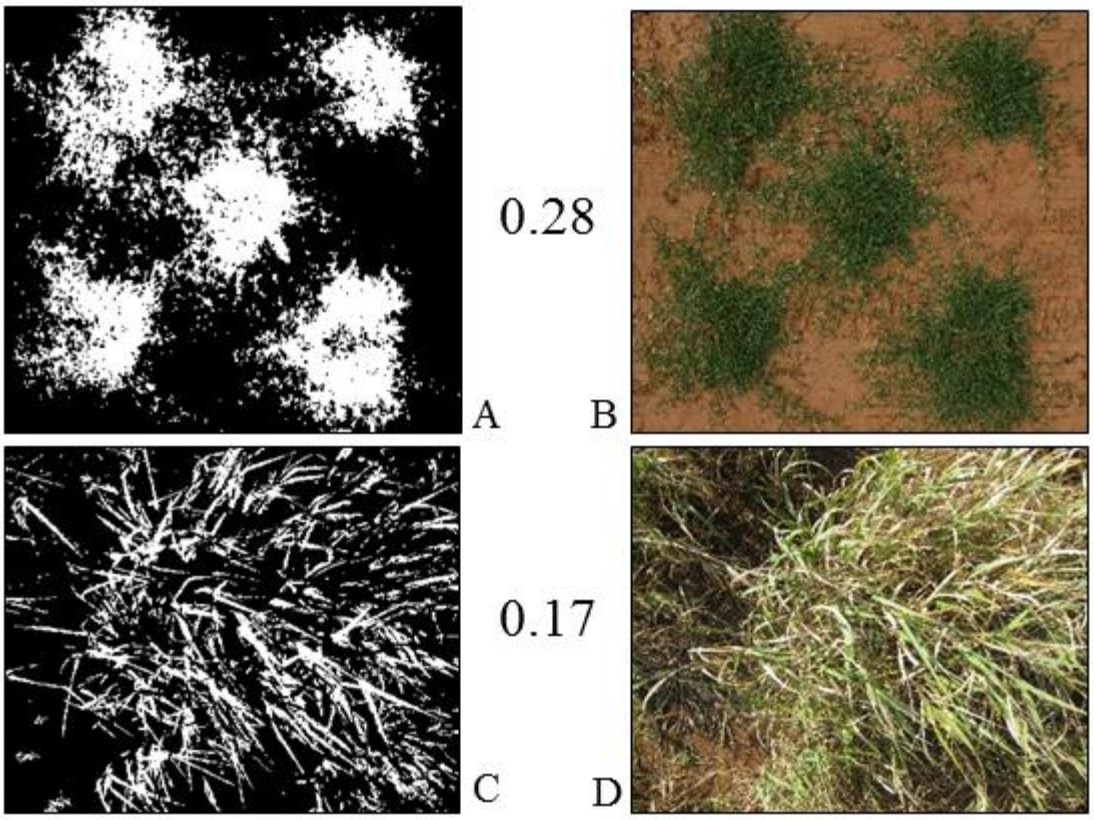

Figure 4. From top to bottom, digital images of turf (A, B) and switchgrass (C, D) are shown after the digital image was analyzed (left) relative to the original image (right). The fractional green canopy cover from Canopeo is shown between the images.

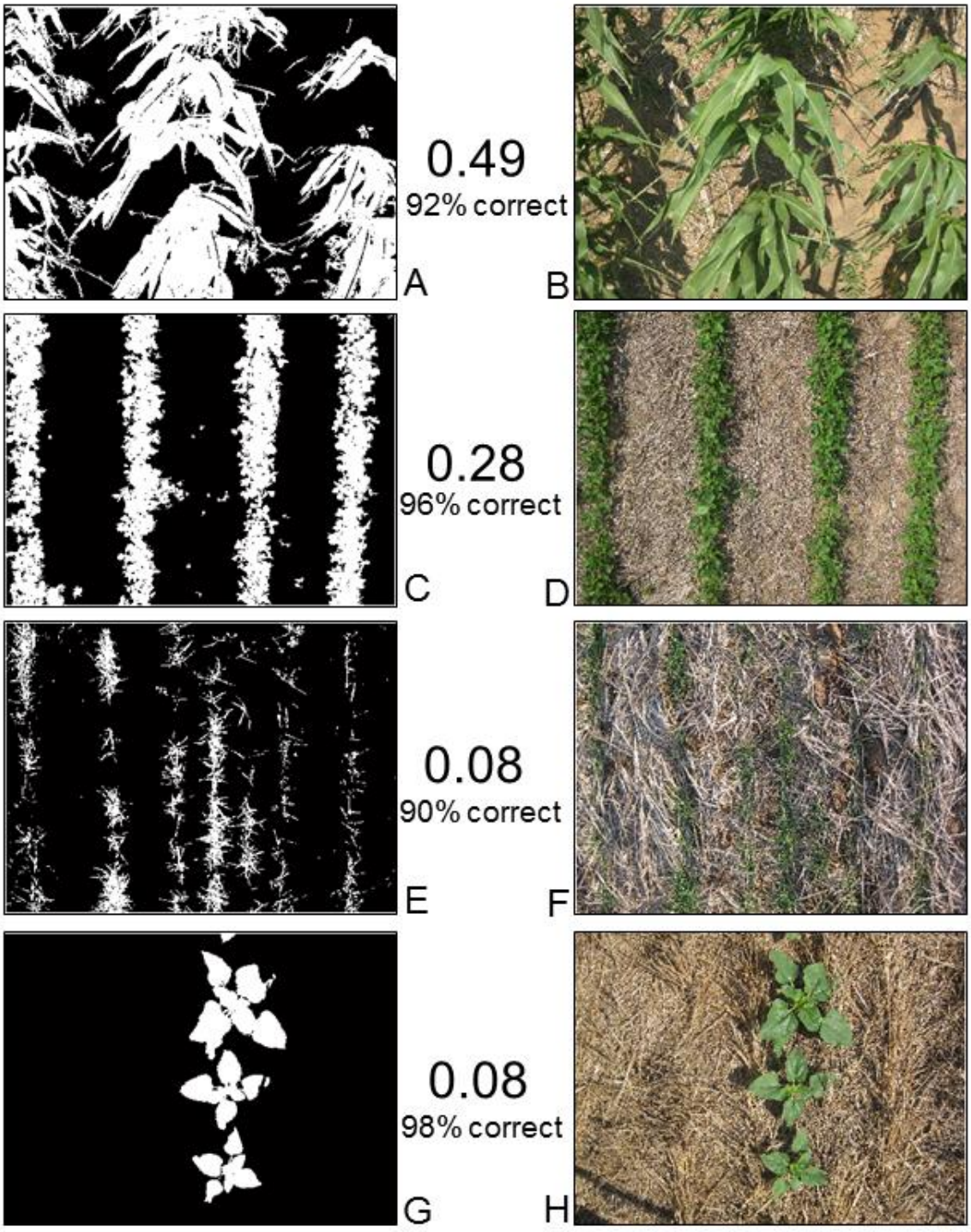

Figure 5. From top to bottom, digital images of no-till grain sorghum (A, B), no-till soybean (C, D), no-till wheat (E, F), and no-till sunflower (G, H) are shown after the digital image was analyzed (left) relative to the original image (right). Area in white represents green pixels selected by Canopeo. The fractional green canopy cover from Canopeo and the percent of correctly classified pixels relative to SamplePoint are shown between the images.

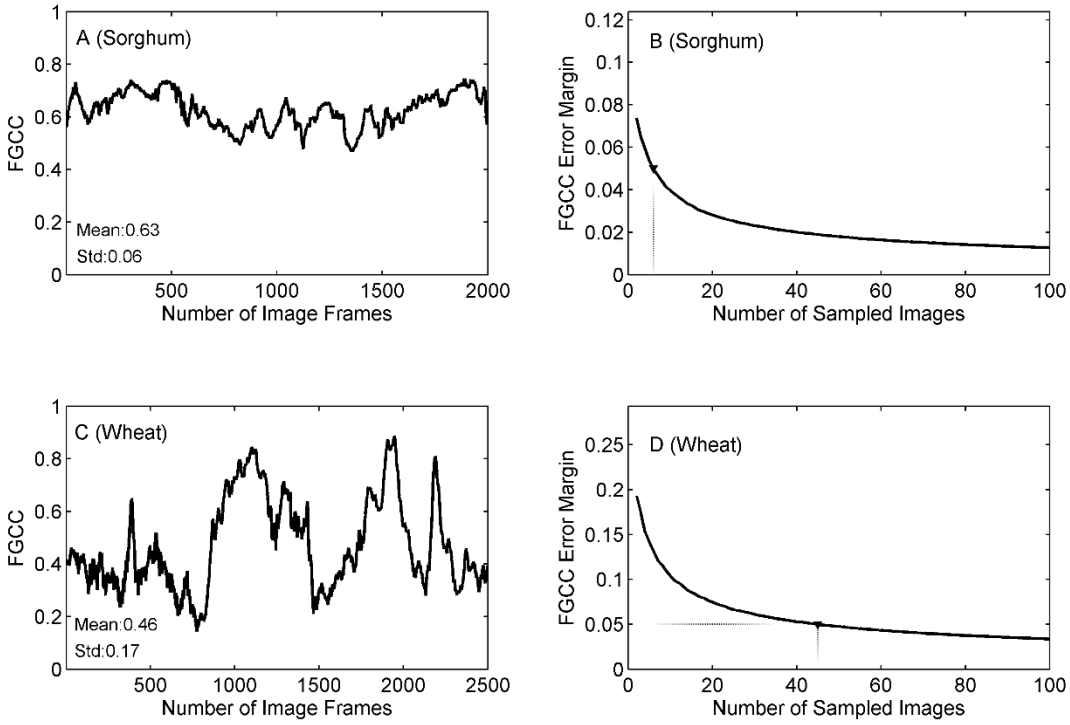

Figure 6: Fractional green canopy cover (FGCC) showing the variability along a transect in a grain sorghum field at phenological stage V10 (A) and a wheat field in stage Feekes 3.0 (C). The minimum number of images required to have a 95% confidence interval of $\pm$ 0.05 about the mean FGCC is shown in B and D.

CHAPTER IV

Manuscript to be submitted to Journal of Hydrology

MODELING TRANSIENT ROOT-ZONE SOIL MOISTURE DICHOTOMIES IN LANDSCAPES WITH INTERMIXED LAND COVERS

Andres Patrignani and Tyson E. Ochsner

ABSTRACT

Although large-scale in situ soil moisture monitoring networks are becoming increasingly valuable research tools, deficiencies of many existing networks include the small spatial support of each station, the low spatial density of stations, and the almost exclusive deployment of stations in grassland vegetation. These grassland soil moisture observations may not adequately represent the real soil moisture patterns in landscapes with intermixed land cover types. The objectives of this study were i) to compare root-zone soil moisture dynamics of two dominant vegetation types across Oklahoma, grassland (observed) and winter wheat cropland (simulated); ii) to relate the soil moisture dynamics of grassland and cropland vegetation using an artificial neural network (ANN) as a the observation operator; and iii) to use the resulting ANN to estimate the soil moisture spatial patterns for a landscape of intermixed grassland and wheat cropland. Root-zone soil moisture was represented by plant available water (PAW) in the top 0.8 m of the soil profile. PAW under grassland was calculated from 18 years of soil moisture

observations at 78 stations of the Oklahoma Mesonet, whereas PAW under winter wheat was simulated for the same 78 locations using a soil water balance model. Then, we trained an ANN to reproduce the simulated PAW under winter wheat using only seven inputs: day of the year, latitude and longitude, measured PAW under grassland, and percent sand, silt, and clay. The resulting ANN was used, along with grassland soil moisture observations, to estimate the detailed soil moisture pattern for a 9x9 km^2 Soil Moisture Active Passive (SMAP) grid cell. The seasonal dynamics of root-zone PAW for grassland and winter wheat were strongly asynchronous, so grassland soil moisture observations rarely reflect cropland soil moisture conditions in the region. The simple ANN approach facilitated efficient and accurate prediction of the simulated PAW under winter wheat, RMSE = 24 mm, using observed PAW under grassland as an input. This promising new approach for estimating soil moisture under adjacent, contrasting land covers at a relatively low computational cost may significantly enhance the applications of existing large-scale monitoring networks.

INTRODUCTION

The increasing relevance of soil moisture measurements for climate modeling (Hirschi et al., 2010; Koster and Suarez, 2001), hydrologic prediction (Houser et al., 1998; Western et al., 2004), and agricultural drought monitoring (Bolten et al., 2010; Mozny et al., 2012; Torres et al., 2013) has propelled the deployment of new observing systems including aerial and satellite remote sensing, emerging proximal sensing technologies, and large-scale in situ monitoring networks (Ochsner et al., 2013). While soil moisture observations using remote and proximal sensing are typically limited to the soil surface, in situ networks fill a unique niche by accurately monitoring both surface and root-zone soil moisture across relatively large spatial extents (e.g. watershed, state, or nation) at high temporal resolution (e.g. hourly) (Dorigo et al., 2011). These networks can provide soil moisture measurements for greater depths and higher temporal resolutions that can be achieved using satellites such as Advanced SCATterometer (ASCAT) (Gelsthorpe et al., 2000), Soil Moisture and Ocean Salinity (SMOS) (Kerr et al., 2010), and Soil Moisture Active Passive (SMAP) (Entekhabi et al., 2010). The in situ networks can also play a vital role in calibration and validation of satellite-derived soil moisture estimates if the points of measurements from the network can be effectively upscaled to the satellite footprint.

However, most existing large-scale networks share in common the limitation that stations have been deployed almost exclusively under grassland vegetation. Since soil moisture sensors are often associated with automated weather stations, grassland sites are usually chosen over forest sites where fetch is typically inadequate for above ground measurements. Grassland sites also offer greater long-term operational stability than

cropland, where farming operations make long-term deployment of automated soil moisture sensors impractical. The bias of in situ networks towards grassland sites and the presence of unmonitored contrasting land covers between the network stations create substantial uncertainty when estimating the soil moisture condition in landscapes with intermixed land covers. How well can grassland soil moisture observations represent the actual soil moisture patterns in landscapes with intermixed and contrasting land covers? To help answer this question, we explore here the relationship between grassland soil moisture measurements and soil moisture values in nearby cropland.

Soil moisture values under grassland and adjacent cropland can differ substantially, but the difference is not temporally stable. For example, 5-cm grassland soil moisture measurements from an NRCS-SCAN network station in the Walnut Creek watershed in Iowa overestimated soil moisture in nearby corn and soybean fields by 20% on average and the difference was not stable over time (Cosh et al., 2004). In the Upper Cedar Creek watershed in Indiana, sensors located under grassland at the edge of two soybean fields overestimated field average 5-cm soil moisture by 4-12% on average, but again the difference was not temporally stable (Heathman et al., 2012). For the same watershed, Han et al. (2012) found that the cumulative density function (CDF) matching operator was able to reliably translate soil moisture observations from permanent sensors at the edge of the field into average field soil moisture, but the CDF observation operator was not constant in time. The absence of a temporally stable relationship between soil moisture values under grassland and cropland is likely due to differences in phenology (Fig. 1) and growth habit between these land cover types, and this absence hinders the

use of data from in situ networks in a variety of contexts, from agricultural drought monitoring to soil moisture satellite validation.

There is a clear need to better understand how effectively grassland-based in situ networks can represent the soil moisture dynamics of landscapes with intermixed and contrasting land covers. There is also a need to develop upscaling methods that do not require temporally stable relationships between land covers in order to enhance the value and applications of large-scale soil moisture monitoring networks, particularly for validation of remote sensing soil moisture products. In this study set in the US southern Great Plains, we examine whether soil moisture observations in warm-season grassland can be used to effectively estimate soil moisture conditions of nearby winter wheat cropland. The specific objectives of this study were i) to compare root-zone soil moisture dynamics of two dominant and intermixed vegetation types in the southern Great Plains, grassland (measured) and winter wheat cropland (simulated); ii) to relate the soil moisture dynamics of grassland and cropland vegetation using a neural network as an observation operator; and iii) to apply the resulting neural network to estimate the soil moisture spatial patterns and spatial mean for a landscape of intermixed grassland and wheat cropland, specifically a 9x9 km^2 SMAP grid cell.

MATERIALS AND METHODS

Settings and Limitations

The study was conducted in Oklahoma, USA, where winter wheat is cultivated on approximately 2 million hectares, mostly in the western part of the state (Fig. 2). Grasslands cover approximately 8 million hectares in Oklahoma and are more evenly

distributed across the state (Fig. 2). As a result of the co-existence and predominance of these two land covers in central and western Oklahoma, the landscapes in this region often consists of intermixed grassland and winter wheat at spatial scales <1 km. Grassland soil moisture measurements are available through the Oklahoma Mesonet, an environmental monitoring network that spans the entire state with a total of 120 stations (McPherson et al., 2007). In the immediate vicinity of each station (≥ 25 m radius), the landscape is typically dominated by perennial warm-season grasses such as bermuda grass (*Cynodon dactylon* L.), big bluestem (*Andropogon gerardii* L.), and little bluestem (*Schizachyrium scoparium* L.), although species vary depending on the geographic location of the station.

All 120 stations monitor air temperature, relative humidity, wind speed and direction, rainfall, incoming solar radiation, and barometric pressure. For 78 out of the 120 stations, soil moisture observations are available from sensors installed at 0.05, 0.25, and 0.60-m depths (Fig. 2). We assumed each sensor to be located at the center of its representative soil layer (Scott et al., 2013). Thus, the sensor installed at 0.05 m depth was assumed to be representative of the layer between the soil surface and 0.10 cm depth. Similarly, the sensors located at 0.25 and 0.60-m depth were assumed to be representative of the 0.10 to 0.40 m and 0.40 to 0.80 m soil layers, respectively. We defined root-zone soil moisture as the plant available water (PAW) in the top 0.8 m of the soil profile. To allow direct comparisons of PAW between grassland and winter wheat, we assumed the root-zone for both was limited to a depth of 0.8 m. Although we acknowledge that 0.8 m is a relatively shallow rooting depth, we were constrained by the depth of soil moisture observations at the Oklahoma Mesonet stations. Nonetheless, shallow soils and root

restricting layers are common in the region and our choice of rooting depth is similar to that used in other related studies in the southern Great Plains (e.g. Heathman et al., 2003).

Plant available water under grassland was calculated from 18 years of soil moisture observations at 78 stations of the Oklahoma Mesonet, whereas PAW under winter wheat was simulated for the same 78 locations using a soil water balance model. The reason for relying on simulations of the soil moisture dynamics of wheat cropland was twofold: i) a modeling approach was the only way to obtain soil moisture estimates for the same points in space and time for both land covers; and ii) a modeling approach was the only practical alternative to conduct a soil moisture comparison among two land covers with adequate spatial and temporal extent to ensure the results are broadly applicable.

Plant available water observations under grassland

Daily values of plant available water under grassland were calculated from the output of the heat dissipation sensors (CS-229L, Campbell Scientific, Inc., Logan, UT) at the selected Oklahoma Mesonet sites following the steps detailed in Scott et al. (2013). Briefly, this approach consists of converting daily average normalized temperature differentials from the heat dissipation sensors into soil matric potential, which was subsequently converted into volumetric water content using a site- and depth-specific soil water retention parameters. For any given station, the days with missing temperature differentials were excluded from the analysis. Daily PAW was calculated by subtracting the lower limit (soil moisture at -1500 kPa) from the observed volumetric water content for each of the sensor depths, and then multiplying the resulting values by the thickness

of the corresponding soil layer. Root-zone PAW was calculated as the sum of the PAW in each the three layers.

Plant available water model for winter wheat

For each of the 78 selected locations, we simulated PAW in continuous winter wheat using the Food and Agriculture Organization (FAO) Irrigation and Drainage Paper No. 56 dual crop coefficient (dual K_c) method (Allen et al., 1998) with daily time steps. The dual K_c is a parsimonious and well established two-layer soil water balance model that has been calibrated and validated for wheat in several environments (Hunsaker et al., 2007; López-Urrea et al., 2009; Zhang et al., 2013; Zhao et al., 2013). The dual K_c model estimates crop evapotranspiration (ETc) based on the evapotranspiration of a hypothetical well-watered grass reference surface (ETo) and empirically determined basal crop coefficients (K_{cb}) that change with the different growth stages of the crop. For winter wheat we used crop coefficients for specific wheat growth stages derived from prior lysimeter studies in the southern Great Plains (Ko et al., 2009; Piccinni et al., 2007). Because these authors reported single crop coefficients rather than basal crop coefficients, values were adjusted following recommended methods (Allen et al., 1998) (Table 1).

We used the modified Wang-Engel (WES) quantitative wheat phenological model (Streck et al., 2003; Wang and Engel, 1998) to simulate wheat growth stages. The WES is a multiplicative phenological model that incorporates the effects of temperature and photoperiod to predict wheat stages. The WES model consists of three main developmental stages: emergence-terminal spikelet initiation (EM-TS), terminal spikelet-

anthesis (TS-AN), and anthesis-physiological maturity (AN-PM). Both vegetative (EM-TS and TS-AN) and reproductive (AN-PM) stages have maximum developmental rates that are modulated by non-linear functions that describe the effect of temperature and photoperiod on wheat development. We adopted the set of parameters (Table 2) for winter wheat used by Streck et al. (2003), who modeled wheat phenological stages in the central Great Plains using cultivars that are also common in the southern Great Plains.

To simulate daily PAW using the dual K_c model, daily precipitation data were obtained from the Oklahoma Mesonet station at each simulation site. Missing precipitation values were retrieved from the nearest neighboring station with available rainfall data. Daily surface runoff was approximated using the Soil Conservation Service Curve Number method (Hawkins et al., 2009). The curve number for each location was estimated based on land cover (i.e. winter wheat or fallow), an estimated residue cover of 50%, and the soil hydrologic group, which was retrieved from the Soil Survey Geographic Database (SSURGO, Soil Survey Staff, 2015). Upper and lower soil water retention limits, and percent clay and sand were obtained from prior measurements at each Oklahoma Mesonet site (Scott et al., 2013). Simulations of the winter wheat growing season started on 15 October across the entire state. Although average winter wheat planting dates for the southern and northern part of Oklahoma usually differ by about 10 days, the selected date represents a reasonable midpoint. Growing season simulations were terminated on 1 June, which is a reasonable date for physiological maturity in this region. Root growth was simulated using thermal time based on the empirical function proposed by Steduto et al. (2009).

Calibration and validation of the dual K_c model

The dual Kc model was calibrated using a set of soil moisture measurements collected under continuous no-till winter wheat from July 2009 to June 2011 at Lahoma, OK. Soil moisture was recorded every 15 days using a neutron probe soil moisture meter at 0.2-m intervals. For each soil layer, PAW was calculated by subtracting the lower limit from the daily volumetric water content and then multiplying the resulting value by the thickness of each layer. Root-zone PAW was then determined by adding up the PAW of the top four layers. Further details about this dataset were provided by Patrignani et al. (2012). Calibration of the dual K_c consisted of optimizing one model parameter that regulates the proportion of the plant available water capacity that can be depleted before plant stress occurs. Other parameters commonly included in the calibration process of the dual Kc model are the effective evaporative layer and the total and readily evaporable water (Allen et al., 2005; Zhao et al., 2013). In our study these parameters were not calibrated but were estimated using the fraction of sand and clay as described by Allen et al. (2005).

The calibrated dual K_c model was validated using three independent validation sets. The first validation set consisted of a time series of PAW in continuous no-till winter wheat from 2011 to 2013 recorded at Lahoma, OK. This validation set helped us to corroborate that the model was adequately predicting PAW at the calibration site. A second validation set was created using soil moisture observations from 2009 to 2011 at Lake Carl Blackwell, OK. This site was located on a side slope (5%), a landscape position on which winter wheat is sometimes cultivated in the southern Great Plains. Because of its topography, this site served as a challenging scenario to evaluate the dual

K_c model. At this location, soil moisture was also measured using a neutron probe soil moisture meter at 0.2-m intervals under continuous conventional and no-till wheat (Patrignani et al., 2012). The third validation set consisted of 23 measurements of PAW in the top 0.8 m from 8 site-years across the state of Oklahoma. From March to May of 2014 and 2015 four measurements per field were collected at each sampling date from large-scale (>0.5 ha) experimental fields and wheat producer fields. During 2014 volumetric water content was measured using an impedance probe (ML2x, Theta Probe, Delta-T Devices) with an attached extension to reach 0.8 m depth. A manual auger (Eijkelkamp, ~65 mm o.d.) was used to facilitate the access of the probe to 0.8 m depth. In each core, volumetric water content was recorded at six depths, approximately every 0.15 m. All volumetric water content values for each core were averaged to estimate the soil water content of the soil profile. In 2015, soil moisture was also measured in four cores per field of 0.8-m depth using the thermo-gravimetric method at each sampling date. Homogenized soil samples for each of the 0.8 m cores were used to estimate soil water content, particle size analysis (Gavlak et al., 2003), and soil water retention at 1500 kPa (i.e. lower limit). The upper limit for each soil was estimated by adding the available water holding capacity to the lower limit. The water holding capacity for each soil was retrieved from a previous study in the region where this variable was measured in field conditions (Lollato and Edwards, 2015 data not published). In this third validation set, the initial soil moisture condition of the sampled sites at the start of the winter wheat growing season was unknown. Therefore, simulations were started in 1 June of the preceding summer fallow period using an estimated initial PAW of 100 mm. Root mean squared error (RMSE), mean bias error (MBE), and Wilmott's index of agreement (Willmott,

1981) were used to describe the overall goodness of fit of the dual Kc against field observations of PAW.

Temporal and Spatial Soil Moisture Analyses

For the purpose of comparing the temporal dynamics of root-zone soil moisture in grassland and winter wheat, we computed the long-term (18-yr) mean PAW for four selected climate divisions of Oklahoma with contrasting precipitation regimes. These means were calculated by taking the arithmetic mean for each day of the year using PAW values from June 1997 to May 2015. Spatial soil moisture patterns were compared by generating state level maps of root-zone PAW for selected days. Maps were generated by: i) calculating an empirical semivariogram using PAW at each of 78 selected stations, ii) fitting an exponential model to the empirical semivariogram, and iii) interpolating PAW at the selected locations to a grid of 5000 points covering the state of Oklahoma using ordinary kriging. For each point in the grid, PAW was interpolated considering a maximum of eight nearest stations within a maximum radius of 200 kilometers. Although these maps ignore the spatial distribution of the land cover, they are useful to describe the spatial patterns imposed by the weather and vegetation (grassland vs winter wheat) across the state. We used the median to characterize the central tendency of root-zone PAW at state level and the highest density interval (HDI) as a measure of dispersion. The HDI is a concept commonly used in Bayesian analysis to represent the shortest interval that spans 95% of the values in a distribution (Kruschke, 2015).

Relating grassland and cropland soil moisture using an observation operator

To relate the soil moisture dynamics of grassland and winter wheat we developed an artificial neural network to serve as an observation operator (Drusch et al., 2005). This approach can be summarized as:

$$\phi_{wheat} = \mathcal{H}\left(\phi_{grass}, \theta_n\right) + \varepsilon$$

where ϕ_{wheat} represents the soil moisture time series under wheat cropland, ϕ_{grass} represents the soil moisture time series under grassland, $\mathcal{H}$ represents the observation operator, θ_n is the set of other covariates used to estimate cropland soil moisture, and ε is the error term. Although models based on first principles are often preferred to explain environmental processes, supervised machine learning techniques such as artificial neural networks are ideal in scenarios with complex non-linear interactions, unknown relationships, and abundant high quality data that can be used for proper training, validation, and testing (Abu-Mostafa et al., 2012). A key benefit of developing an observation operator capable of estimating cropland soil moisture from grassland soil moisture observations is that it would dramatically reduce computational burdens associated with operational large-scale, high-resolution soil moisture mapping.

We used a multi-layer feedforward neural network trained by a backpropagation algorithm with stochastic learning. This simple neural network consisted of: one input layer, one hidden layer, and one output layer. The input layer had seven neurons that corresponded to day of the year, latitude and longitude, observed root-zone PAW under grassland, and the percent of sand, silt, and clay in the top 0.8 m. The hidden layer had ten neurons and the output layer had one neuron representing the root-zone PAW in continuous wheat. The activation function between the input and the hidden layer was the following hyperbolic tangent function (LeCun et al., 2012):

$$f(x) = 1.7159\ tanh\left(\frac{2}{3}x\right)$$

This function has carefully selected parameter values so that saturation of the activation function is minimized, while still taking advantage of its non-linearity.

Since this is a regression rather than a classification problem, we used a linear activation function between the hidden and output layer. To improve training performance we added a learning rate with value of 0.01 and a momentum of 0.2 to help with escaping local minima (LeCun et al., 2012).

For training, validation, and testing of the neural network, a full dataset was created totaling 350,000 entries for each of the seven input and output variables (350,000 rows by 8 columns matrix) for the period of 2 June 1997 to 27 May 2015 for the 78 selected Oklahoma Mesonet stations. As output targets we used the PAW for winter wheat simulated with the dual Kc model. Rows with missing values in at least one input or the output variable were eliminated from the dataset. Then, we subdivided the full dataset to generate a training, validation, and testing set. We assigned 70% of the values in the full dataset to the training set. Assigning large fractions of the full dataset to the training set is a common practice to ensure that most plausible scenarios are presented to the network during the training stage. For better training performance, input values were shuffled using a pseudo random generator in Matlab (Mathworks, Nantick, MA). The randomization of the entries was performed for individual rows to keep inputs and outputs associated to each other. Then, inputs and outputs were standardized by centering the data with a mean of zero and a variance of one. The mean and variance were stored and were used to restore the standardized input and output values. The next step consisted in generating a validation set, which was composed of only 10% of the values in the full

dataset. The validation set is intended to evaluate the neural network during the training process to identify the set of training weights that minimized the error in the validation set, and thus, minimize the risk of over-fitting. We selected the training weights that minimized the root mean squared error (RMSE) of the validation set. Since the selected training weights were dependent on the validation set, a third independent set of information was required to assess the prediction power of the trained neural network. This was accomplished by creating a test set using the remaining 20% of the full dataset. The test set included a total of 70,000 entries encompassing 17 stations with different annual precipitation regimes and contrasting soil properties. Because only the entries of the training set were shuffled, none of the stations in the test set participated during the training process, resulting in a robust test for the neural network.

In light of the large number of values that were used for training, validation, and testing, we used a bivariate histogram to pictorially represent the performance of the network. The root mean squared difference (RMSD), the mean biased error (MBE), and the Pearson's correlation coefficient (r) were used to evaluate the predictions of the neural network relative to PAW simulated using the dual Kc model. For the evaluation of the neural network we used the term RMSD to emphasize that the differences were calculated relative to simulated, and thus uncertain, PAW in winter wheat instead of ground-truth field observations.

Application of the neural network to estimate root-zone PAW patterns across a heterogeneous SMAP grid cell

To demonstrate the significance of the observation operator, we used it, along with grassland soil moisture observations, to estimate the detailed soil moisture pattern for a 9x9 km^2 SMAP grid cell. For this example, we selected a grid encompassing an area dominated by winter wheat and grassland, and also including the Lahoma station of the Oklahoma Mesonet and the field site at which some of the calibration and validation data were recorded. To estimate the PAW under grassland and winter wheat cropland across the grid we followed these steps: i) identify locations of winter wheat cropland and grassland within the grid using the 2014 USDA cropland data layer (30x30 m resolution); ii) retrieve observations of temperature differentials for the Oklahoma Mesonet stations recording soil moisture at all three sensor depths for the selected date; iii) convert temperature differentials into root-zone PAW under grassland; iv) use an interpolation method (in this case ordinary kriging) to estimate grassland root-zone PAW for all locations (i.e. grassland and cropland) within the SMAP grid cell; v) collect and normalize inputs for the neural network including day of the year for the selected date, latitude and longitude of the wheat cropland, the interpolated grassland PAW for the wheat cropland, and the percent sand, silt, and clay for each wheat cropland location within the grid; and vi) estimate the PAW for the wheat cropland using the neural network as an observation operator that relates grassland and wheat cropland.

RESULTS AND DISCUSSION

Model calibration and validation

Considering all calibration and validation sets, modeling root-zone PAW of winter wheat cropland using the dual Kc model decreased estimation errors

approximately 60% compared to the default approach of assuming that soil moisture observations under grassland represent soil moisture conditions under winter wheat. The calibration of the dual K_c model using the data set for Lahoma 2009-2011 resulted in a RMSE of 21 mm relative to the measured PAW under winter wheat, whereas direct use of the observed grassland PAW at the nearest Mesonet station resulted in a RMSD of 50 mm (Fig 3A). Validation of the dual Kc model using the sets of winter wheat PAW measured at Lahoma 2011-2013 and Lake Carl Blackwell 2009-2011 (Fig. 3B and 3C) had RMSE ranging from 3 to 23 mm, MBE from 10 to 13 mm, and d from 0.82 to 0.85. As in the calibration set, prediction of winter wheat PAW using observed grassland PAW at the nearest Mesonet station had RMSD values ranging from 51 to 66 mm. In the validation set containing multiple sites from across the state (Fig. 3D), predictions of PAW resulted in a RMSE of 24 mm, a good result considering that the soil moisture condition at the beginning of the growing season was unknown and had to be estimated by initializing the model in the preceding summer fallow.

Although the model predictions were satisfactory, lower RMSE values for the dual Kc model have been reported for winter wheat in the literature. A study by Zhao et al. (2013) reported RMSE of approximately 7 mm in the top meter of the soil profile, a value three times lower than our study. Nonetheless, in that study the calibration and validation sets contained soil moisture collected only during two growing seasons at a single location. In contrast, the strength of our study relies on a calibration and validation set totaling 148 field observations over a period of six years across multiple locations with diverse soil properties, landscape positions, and climate conditions. Also our study requires year-round simulation of the winter wheat cropping system, which is a greater

challenge than simulating individual growing seasons. Under these circumstances, predictions of root-zone PAW may be improved using more advance models such as the Root Zone and Water Quality Model (RZWQM) or the Decision Support System for Agrotechnology Transfer (DSSAT), but a drawback associated with more sophisticated models is the large number of parameters requiring calibration.

Asynchronous soil moisture dynamics

Long-term mean root-zone PAW for grassland (measured) and winter wheat (simulated) displayed distinct sinusoidal seasonal cycles that were strongly asynchronous (Fig. 4). Winter wheat consistently had minimum PAW values at the end of the growing season in early June (DOY 112 to 152) and maximum PAW values at the end of the summer fallow (DOY 283 to 286). During the fallow period, summer rainfall, partial residue cover left from the prior wheat harvest, and the absence of an actively growing vegetation contribute to a slow but positive soil moisture recharge. On the other hand, grassland showed minimum PAW values from late July to mid-August (DOY 209 to 221) and maximum PAW values from early to late March (DOY 64 to 91). Clearly, the soil moisture dynamics under grassland were not representative of conditions under winter wheat. The seasonal soil moisture cycles of each land cover were closely linked with vegetation dynamics. While winter wheat is an annual cool-season (fall-winter-spring) crop, grasslands surrounding the stations of the Oklahoma Mesonet are predominantly composed of perennial warm-season (spring-summer-fall) grasses. In mid to late February, winter wheat reaches the end of its dormant growth stage with green canopy cover typically >75% (Fig. 1). Although dormant, the high percentage of green canopy

cover can become fully active with a few days of warm temperatures, explaining the typical rapid drying phase of winter wheat early in the spring compared to grassland (Fig. 4). At the same time, warm-season grasslands typically have almost no green canopy cover, which explains the lower soil moisture depletion rate in the early spring compared to continuous wheat.

Despite the contrasting temporal dynamics of soil moisture between these land covers, the mean annual PAW of winter wheat and grassland vegetation were similar within different climate divisions. Within each climate division, differences in mean annual PAW between grassland and winter wheat ranged from 5 mm in the south central division to only 9 mm in the north central division. Across climate divisions, mean annual PAW for continuous wheat ranged from 56 to 121 mm, while the mean annual PAW of grassland ranged from 50 to 115 mm. The lowest mean annual PAW for both land covers was in the Oklahoma Panhandle (460 mm 30-yr annual rainfall) and the greatest mean annual PAW was observed in the northeast division of Oklahoma (1200 mm 30-yr annual rainfall). While the seasonal variations of PAW within each climatic division were dominated by the land cover, the mean annual PAW values were dominated by the climate and precipitation regime.

The seasonal soil moisture patterns of winter wheat observed in this study were in agreement with a prior study conducted by Zhang (2004), who studied the soil moisture dynamics of continuous winter wheat in a watershed near El Reno, OK. Similarly, the soil moisture dynamics in grassland vegetation closely matched those found by Illston et al. (2004), who conducted an analysis of the soil moisture patterns for the Oklahoma Mesonet. The unique contribution of our study lies in the direct comparison of the soil

moisture dynamics of these two dominant land covers that are usually intermixed in the landscape of the southern Great Plains at scales <1 km. Our results shows that soil moisture observations from in situ networks deployed on warm-season grassland vegetation should not be used directly to assess the soil moisture conditions of winter wheat in the southern Great Plains or similar climatic conditions around the world. The asynchronous soil moisture patterns observed for grassland and winter wheat in Oklahoma would cause a lack of temporal stability in the relationship between edge of the field sensors and the actual soil moisture values under cropland, a phenomenon which has been reported in prior studies (e.g. Han et al., 2012; Heathman et al., 2012b).

Spatial pattern of vegetation impacts on soil moisture

State level interpolation of the long-term average root-zone PAW of grassland and wheat cropland for two contrasting dates revealed three distinct patterns as a consequence of the interaction between climate and land cover (Figure 5). In the western portion of the state, the low annual rainfall and the high atmospheric demand create soil moisture conditions that are typically in the dry range regardless of the land cover. Similarly, in the eastern part of the state, the average annual rainfall regime >1000 mm consistently generates the relatively wet soil moisture conditions regardless of the land cover. In contrast, the central portion of the state shows the greatest influence of the land cover on root-zone soil moisture. This is of particular relevance because a great portion of the wheat cropland in Oklahoma is concentrated in the central-western part of the state (Fig. 2), where using observed soil moisture under grassland vegetation as a surrogate of

the soil moisture condition under wheat cropland can induce substantial errors in root-zone PAW.

A highly instrumented watershed in southwest Oklahoma, called the Little Washita, has been the focus of numerous studies aimed at better understanding the spatio-temporal variability of soil moisture under varied topography and vegetation (Jackson et al., 1999; Mohanty and Skaggs, 2001; Starks et al., 2006). A study conducted by Mohanty and Skaggs (2001) using soil moisture observations collected during Southern Great Plains 1997 (SGP97) Hydrology Experiment showed that areas with intermixed grassland and cropland had the least temporally stability in soil moisture. The results in Figures 4 and 5 help explain that previous finding. The SGP97 experiment was conducted from mid-June through mid-July, a time when soil moisture conditions under grassland and winter wheat cropland are typically trending in opposite directions (Fig. 4).

Neural network-based observation operator

After training, the neural network effectively mimicked the soil moisture dynamics under winter wheat as simulated by the dual K_c model (Fig. 6). The only required inputs for operational use of the neural network are the day of the year, latitude and longitude, observed root-zone PAW under grassland, and percent of sand, silt, and clay. The neural network exploits information in grassland soil moisture observations to predict the soil moisture condition under winter wheat cropland. The training of the neural network using almost 250,000 simulated winter wheat PAW values from the dual K_c model resulted in MBE of 0 mm and Pearson's correlation coefficient of 0.91 (Fig. 6A). The ANN tended to slightly overestimate PAW values in the dry end and to under

estimate PAW in the wet end. In the validation set, the neural network resulted in MBE of -4.3 mm and correlation coefficient of 0.71. Despite the lower correlation coefficient, the validation set was effective to prevent overfitting of the neural network. The performance of the neural network in the test set showed a MBE of 0.4 mm, r equal to 0.78, and RMSD equal to 23.8 mm, values that are similar to those obtained with the dual K_c model when compared to field observations (compare Fig. 6C and D to Fig. 3B, C, and D). The soil moisture time series for a particular location, e.g. the Waurika Mesonet station, shows the relatively close match between simulated PAW dynamics using the dual K_c model and the neural network observation operator (Fig. 6D). Simply assuming that the grassland soil moisture observations were representative of neighboring winter wheat cropland would have resulted in RMSD of 50 mm relative to the dual K_c model at Waurika. This suggests that the neural network improves the prediction accuracy by >50% relative to the default assumption.

A limitation of using this neural network as an observation operator was its inability to exactly mimic the daily variations of PAW predicted by the dual K_c model, particularly the sharp rise of PAW as a consequence of rainfall events. Perhaps, the addition of other variables, such as daily precipitation, could improve the performance of the neural network. However, our intention was not to maximize similarity between the neural network and the mechanistic model, but to test whether observed PAW under grassland can be used to effectively estimate PAW under nearby winter wheat cropland. Due to the complexity of the problem and the few input variables provided to the neural network, it performed surprisingly well. The use of a neural network-based observation operator to relate the soil moisture of two different and adjacent land covers is a

departure from the use of mechanistic models that heavily rely on weather variables to model cropland soil moisture. Simulation of soil moisture using mechanistic crop models for a large number of fields can be computationally demanding and offers no guarantee of increased accuracy. The neural network is a faster computational alternative with limited requirements, which is well-suited for operational use to enhance the value of existing in situ soil moisture monitoring networks.

Application of the neural network to a SMAP pixel

One practical application of this approach can be demonstrated using a single 9x9 km^2 grid cell (FID: 153137, Row: 329, Column: 877) of the recently launched SMAP mission. This grid cell, which includes the Lahoma Oklahoma Mesonet station, has a total of 8,200 hectares including intermixed grassland (25% of the area) and winter wheat (47% of the area) as the dominant land covers (Fig 7A and 7B). The estimation of PAW at 30-m resolution for grassland (by ordinary kriging) and wheat cropland (by neural network) within the selected grid cell on 10 Oct. 2014, unveiled the strongly contrasting soil moisture patterns that can be present in intermixed landscapes (Fig. 7C). For the selected date, the median PAW under grassland in this domain was 18 mm, a value similar to the minimum long-term PAW presented in Figure 4B. This value seems reasonable since active grassland vegetation probably depleted a large portion of the soil moisture during the summer period. A completely different situation was predicted in the wheat fields, where the median PAW was 106 mm, a value almost six times higher than the median PAW in grassland. The median PAW in wheat cropland was also in agreement with the long-term mean PAW shown in Figure 4B for winter wheat. The

mean PAW across both land covers in the domain was 76 mm, or in other units, the mean root-zone soil moisture across both land covers was 0.073 cm^3 cm^{-3} [(76 mm – 18 mm)/800 mm] higher than the value which would have been estimated using the grassland observations alone. This bias in estimated soil moisture which would occur if grassland values were used directly for SMAP validation is large relative to the SMAP mission requirement of measuring 0-5 cm soil moisture to within 0.04 cm^3 cm^{-3}. Using the neural network allowed us not only to effectively translate root-zone soil moisture from the Oklahoma Mesonet stations to adjacent wheat fields, but also to estimate the weighted mean PAW of the grid without relying on identification of representative locations that exhibit temporally stable relationships to the grid mean (Vachaud et al., 1985; Chen, 2006).

CONCLUSION

The dual crop coefficient model was able to effectively predict the root-zone soil moisture dynamics of wheat cropland for a wide range of conditions. Simulations using the dual crop coefficient method allowed us to compare wheat cropland and grassland soil moisture at 78 stations of the Oklahoma Mesonet. Grassland and winter wheat had similar mean annual root-zone PAW across several climate divisions in Oklahoma, but the strongly asynchronous dynamics demonstrate that soil moisture observations under grassland vegetation should not be used to represent the soil moisture condition of nearby wheat cropland. A simple neural network proved to be an effective observation operator to translate soil moisture measurements under grassland into soil moisture estimates under nearby wheat cropland, demonstrating that it is possible to exploit embedded

information present in grassland soil moisture to predict wheat cropland soil moisture. The use of a neural network as an observation operator allowed us to identify and quantify the contrasting soil moisture patterns of intermixed grassland and cropland within a 9x9 km^2 SMAP grid cell. This promising new approach for estimating soil moisture under adjacent, contrasting land covers at a relatively low computational cost and without depending on the assumption of temporal stability may significantly enhance the applications of existing large-scale monitoring networks.

REFERENCES

Abu-Mostafa, Y.S., Magdon-Ismail, M., Lin, H.-T., 2012. Learning from data. A short course. AMLbooks.com.

Allen, R.G., Pereira, L.S., Raes, D., Smith, M., 1998. Crop evapotranspiration: guidelines fo computing crop water requirements. Irrigation and Drainage Paper 56. 300.

Allen, R.G., Pereira, L.S., Smith, M., Raes, D., Wright, J.L., 2005. Dual Crop Coefficient Method for Estimating Evaporation from Soil and Application Extensions. J. Irrig. Drain. Eng. 131, 2–13. doi:10.1061/(ASCE)0733-9437(2005)131:1(2).

Bolten, J.D., Crow, W.T., Zhan, X., Jackson, T.J., Reynolds, C.A., 2010. Evaluating the utility of remotely sensed soil moisture retrievals for operational agricultural drought monitoring. IEEE J. Sel. Top. Appl. Earth Obs. Remote Sens. 3, 57–66. doi:10.1109/JSTARS.2009.2037163.

Brocca, L., Hasenauer, S., Lacava, T., Melone, F., Moramarco, T., Wagner, W., Dorigo, W., Matgen, P., Martínez-Fernández, J., Llorens, P., Latron, J., Martin, C., Bittelli, M., 2011. Soil moisture estimation through ASCAT and AMSR-E sensors: An intercomparison and validation study across Europe. Remote Sens. Environ. 115, 3390–3408. doi:10.1016/j.rse.2011.08.003.

Brocca, L., Tullo, T., Melone, F., Moramarco, T., Morbidelli, R., 2012. Catchment scale soil moisture spatial-temporal variability. J. Hydrol. 422-423, 63–75. doi:10.1016/j.jhydrol.2011.12.039.

Cosh, M.H., Jackson, T.J., Bindlish, R., Prueger, J.H., 2004. Watershed scale temporal and spatial stability of soil moisture and its role in validating satellite estimates, in: Remote Sensing of Environment. pp. 427–435. doi:10.1016/j.rse.2004.02.016.

Cosh, M.H., T.J. Jackson, P. Starks, and G. Heathman. 2006. Temporal stability of surface soil moisture in the Little Washita River watershed and its applications in satellite soil moisture product validation. J. Hydrol. 323(1-4): 168–177.

Crow, W.T., Berg, A.A., Cosh, M.H., Loew, A., Mohanty, B.P., Panciera, R., De Rosnay, P., Ryu, D., Walker, J.P., 2012. Upscaling sparse ground-based soil moisture observations for the validation of coarse-resolution satellite soil moisture products. Rev. Geophys. 50. doi:10.1029/2011RG000372.

Dorigo, W.A., Wagner, W., Hohensinn, R., Hahn, S., Paulik, C., Xaver, A, Gruber, A., Drusch, M., Mecklenburg, S., Van Oevelen, P., Robock, A., Jackson, T., 2011. The International Soil Moisture Network: A data hosting facility for global in situ soil moisture measurements. Hydrol. Earth Syst. Sci. 15, 1675–1698. doi:10.5194/hess-15-1675-2011.

Drusch, M., Wood, E.F., Gao, H., 2005. Observation operators for the direct assimilation of TRMM microwave imager retrieved soil moisture. Geophys. Res. Lett. 32, L15403. doi:10.1029/2005GL023623.

Entekhabi, D., Njoku, E.G., O'Neill, P.E., Kellogg, K.H., Crow, W.T., Edelstein, W.N., Entin, J.K., Goodman, S.D., Jackson, T.J., Johnson, J., Kimball, J., Piepmeier, J.R., Koster, R.D., Martin, N., McDonald, K.C., Moghaddam, M., Moran, S., Reichle, R., Shi, J.C., Spencer, M.W., Thurman, S.W., Tsang, L., Van Zyl, J., 2010. The soil moisture active passive (SMAP) mission. Proc. IEEE 98, 704–716. doi:10.1109/JPROC.2010.2043918.

Famiglietti, J.S., Rudnicki, J.W., Rodell, M., 1998. Variability in surface moisture content along a hillslope transect: Rattlesnake Hill, Texas. J. Hydrol. 210, 259–281. doi:10.1016/S0022-1694(98)00187-5.

Gavlak, R., Horneck, D., Miller, R.O., Kotuby-Amacher, J., 2003. Soil, plant and water reference methods for the western region, 2nd Edition. ed. Fort Collins, CO.

Han, E., Heathman, G.C., Venkatesh M., and Cosh, M. 2012. Application of observation operators for field scale soil moisture averages and variances in agricultural landscapes. J. Hydrol. 444–445, 34–50. doi: /10.1016/j.jhydrol.2012.03.035.

Hawkins, R.H., Ward, T., Woodward, D.E., Van Mullem, J., 2009. Curve Number Hydrology: State of the Practice, ASCE, Journal of the hydraulic division.

Heathman, G.C., Cosh, M.H., Han, E., Jackson, T.J., McKee, L., McAfee, S., 2012a. Field scale spatiotemporal analysis of surface soil moisture for evaluating point-scale in situ networks. Geoderma 170, 195–205. doi:10.1016/j.geoderma.2011.11.004.

Heathman, G.C., Cosh, M.H., Merwade, V., Han, E., 2012b. Multi-scale temporal stability analysis of surface and subsurface soil moisture within the Upper Cedar Creek Watershed, Indiana. Catena 95, 91–103. doi:10.1016/j.catena.2012.03.008.

Heathman, G.C., Starks, P.J., Ahuja, L.R., Jackson, T.J., 2003. Assimilation of surface soil moisture to estimate profile soil water content. J. Hydrol. 279, 1–17. doi:10.1016/S0022-1694(03)00088-X.

Hirschi, M., Seneviratne, S.I., Alexandrov, V., Boberg, F., Boroneant, C., Christensen, O.B., Formayer, H., Orlowsky, B., Stepanek, P., 2010. Observational evidence for soil-moisture impact on hot extremes in southeastern Europe. Nat. Geosci. 4, 17–21. doi:10.1038/ngeo1032.

Houser, P.R., Shuttleworth, W.J., Famiglietti, J.S., Gupta, H. V., Syed, K.H., Goodrich, D.C., 1998. Integration of soil moisture remote sensing and hydrologic modeling using data assimilation. Water Resour. Res. doi:10.1029/1998WR900001.

Hunsaker, D.J., Fitzgerald, G.J., French, A.N., Clarke, T.R., Ottman, M.J., 2007. Wheat Irrigation Management Using Multispectral Crop Coedffients: I. Crop Evapotranspiraton Prediction. Trans. Asabe 50, 2017–2033. doi:10.13031/2013.24105.

Illston, B.G., Basara, J.B., Fisher, D.K., Elliott, R., Fiebrich, C.A., Crawford, K.C., Humes, K., Hunt, E., 2008. Mesoscale monitoring of soil moisture across a statewide network. J. Atmos. Ocean. Technol. 25, 167–182. doi:10.1175/2007JTECHA993.1.

Illston, B.G., Illston, B.G., Basara, J.B., Basara, J.B., Crawford, K.C., Crawford, K.C., 2004. Seasonal to interannual variations of soil moisture measured in Oklahoma. Int. J. Climatol. 24, 1883–1896. doi:10.1002/joc.1077.

Kerr, Y.H., Waldteufel, P., Wigneron, J.-P., Delwart, S., Cabot, F., Boutin, J., Escorihuela, M.-J., Font, J., Reul, N., Gruhier, C., Juglea, S.E., Drinkwater, M.R., Hahne, A., Martín-Neira, M., Mecklenburg, S., 2010. The SMOS Mission: New Tool for Monitoring Key Elements ofthe Global Water Cycle. Proc. IEEE 98. doi:10.1109/JPROC.2010.2043032.

Ko, J., Piccinni, G., Marek, T., Howell, T., 2009. Determination of growth-stage-specific crop coefficients (Kc) of cotton and wheat. Agric. Water Manag. 96, 1691–1697. doi:10.1016/j.agwat.2009.06.023.

Koster, R.D., Suarez, M.J., 2001. Soil Moisture Memory in Climate Models. J. Hydrometeorol. doi:10.1175/1525-7541(2001)002<0558:SMMICM>2.0.CO;2.

Kruschke, J.K., 2015. Doing Bayesian data analysis. A tutorial with R, JAGS, and Stan, 2nd editio. ed. Academic Press Elsevier.

Larson, K.M., Small, E.E., Gutmann, E., Bilich, A., Axelrad, P., Braun, J., 2008. Using GPS multipath to measure soil moisture fluctuations: Initial results. GPS Solut. 12, 173–177. doi:10.1007/s10291-007-0076-6.

LeCun, Y.A., Bottou, L., Orr, G.B., Müller, K.R., 2012. Efficient backprop. Lect. Notes Comput. Sci. (including Subser. Lect. Notes Artif. Intell. Lect. Notes Bioinformatics) 7700 LECTU, 9–48. doi:10.1007/978-3-642-35289-8-3.

Lollato, R.P., Edwards, J.T., 2015. Maximum attainable wheat yield and resource-use efficiency in the southern Great Plains. Crop Sci. doi:10.2135/cropsci2015.04.0215.

López-Urrea, R., Montoro, A., González-Piqueras, J., López-Fuster, P., Fereres, E., 2009. Water use of spring wheat to raise water productivity. Agric. Water Manag. 96, 1305–1310. doi:10.1016/j.agwat.2009.04.015.

McPherson, R.A., Fiebrich, C.A., Crawford, K.C., Elliott, R.L., Kilby, J.R., Grimsley, D.L., Martinez, J.E., Basara, J.B., Illston, B.G., Morris, D. a., Kloesel, K.A., Stadler, S.J., Melvin, A.D., Sutherland, A.J., Shrivastava, H., Carlson, J.D., Wolfinbarger, J.M., Bostic, J.P., Demko, D.B., 2007. Statewide monitoring of the mesoscale environment: A

technical update on the Oklahoma Mesonet. J. Atmos. Ocean. Technol. 24, 301–321. doi:10.1175/JTECH1976.1.

Mohanty, B.P., Skaggs, T.H., 2001. Spatio-temporal evolution and time-stable characteristics of soil moisture within remote sensing footprints with varying soil, slope, and vegetation. Adv. Water Resour. 24, 1051–1067. doi:10.1016/S0309-1708(01)00034-3.

Mozny, M., Trnka, M., Zalud, Z., Hlavinka, P., Nekovar, J., Potop, V., Virag, M., 2012. Use of a soil moisture network for drought monitoring in the Czech Republic. Theor. Appl. Climatol. 107, 99–111. doi:10.1007/s00704-011-0460-6.

Ochsner, T.E., Cosh, M.H., Cuenca, R.H., Dorigo, W.A., Draper, C.S., Hagimoto, Y., Kerr, Y.H., Njoku, E.G., Small, E.E., Zreda, M., 2013. State of the Art in Large-Scale Soil Moisture Monitoring. Soil Sci. Soc. Am. J. 77, 1888. doi:10.2136/sssaj2013.03.0093.

Palecki, M.A., Groisman, P.Y., 2011. Observing Climate at High Elevations Using United States Climate Reference Network Approaches. J. Hydrometeorol. 12, 1137–1143. doi:10.1175/2011JHM1335.1.

Patrignani, A., Godsey, C.B., Ochsner, T.E., Edwards, J.T., 2012. Soil Water Dynamics of Conventional and No-Till Wheat in the Southern Great Plains. Soil Sci. Soc. Am. J. doi:10.2136/sssaj2012.0082.

Patrignani, A., Ochsner, T.E., 2015. Canopeo: A powerful new tool for measuring fractional green canopy cover. Agron. J. doi:10.2134/agronj15.0150.

Piccinni, G., Ko, J., Wentz, A., Leskovar, D., Marek, T., Howell, T., 2007. Determination of crop coefficients (Kc) for irrigation management of crops. 28th Annu. Int. Irrig. Show 706–719. doi:https://watermgmt.tamu.edu/pdf/Research_Reports/DETERMINATION_OF_CROP_COEFFICIENTS_%28Kc%29.pdf.

Sayde, C., Gregory, C., Gil-Rodriguez, M., Tufillaro, N., Tyler, S., Van De Giesen, N., English, M., Cuenca, R., Selker, J.S., 2010. Feasibility of soil moisture monitoring with heated fiber optics. Water Resour. Res. 46. doi:10.1029/2009WR007846.

Schaefer, G.L., Cosh, M.H., Jackson, T.J., 2007. The USDA Natural Resources Conservation Service Soil Climate Analysis Network (SCAN). J. Atmos. Ocean. Technol. 24, 2073–2077. doi:10.1175/2007JTECHA930.1

Scott, B.L., Ochsner, T.E., Illston, B.G., Fiebrich, C.A., Basara, J.B., Sutherland, A.J., 2013. New Soil Property Database Improves Oklahoma Mesonet Soil Moisture Estimates*. J. Atmos. Ocean. Technol. 30, 2585–2595. doi:10.1175/JTECH-D-13-00084.1.

Soil Survey Staff, Natural Resources Conservation Service, United States Department of Agriculture. Web Soil Survey. Available online at http://websoilsurvey.nrcs.usda.gov/.

Steduto, P., Hsiao, T.C., Raes, D., Fereres, E., 2009. Aquacrop-the FAO crop model to simulate yield response to water: I. concepts and underlying principles. Agron. J. 101, 426–437. doi:10.2134/agronj2008.0139s.

Steele-Dunne, S.C., Rutten, M.M., Krzeminska, D.M., Hausner, M., Tyler, S.W., Selker, J., Bogaard, T.A., Van De Giesen, N.C., 2010. Feasibility of soil moisture estimation using passive distributed temperature sensing. Water Resour. Res. 46. doi:10.1029/2009WR008272.

Streck, N.A., Weiss, A., Xue, Q., Stephen Baenziger, P., 2003. Improving predictions of developmental stages in winter wheat: A modified Wang and Engel model. Agric. For. Meteorol. 115, 139–150. doi:10.1016/S0168-1923(02)00228-9.

Torres, G.M., Lollato, R.P., Ochsner, T.E., 2013. Comparison of Drought Probability Assessments Based on Atmospheric Water Deficit and Soil Water Deficit. Agron. J. 105, 428. doi:10.2134/agronj2012.0295.

Vachaud, G., Passerat De Silans, A., Balabanis, P., Vauclin, M., 1985. Temporal Stability of Spatially Measured Soil Water Probability Density Function1. Soil Sci. Soc. Am. J. doi:10.2136/sssaj1985.03615995004900040006x.

Wang, E., Engel, T., 1998. Simulation of phenological development of wheat crops. Agric. Syst. 58, 1–24. doi:10.1016/S0308-521X(98)00028-6.

Western, A.W., Zhou, S.L., Grayson, R.B., McMahon, T.A., Blöschl, G., Wilson, D.J., 2004. Spatial correlation of soil moisture in small catchments and its relationship to dominant spatial hydrological processes. J. Hydrol. 286, 113–134. doi:10.1016/j.jhydrol.2003.09.014.

Willmott, C.J., 1981. On the validation of models. Phys. Geogr. 2, 184–194. doi:10.1080/02723646.1981.10642213.

Zhang, B., Liu, Y., Xu, D., Zhao, N., Lei, B., Rosa, R.D., Paredes, P., Paço, T.A., Pereira, L.S., 2013. The dual crop coefficient approach to estimate and partitioning evapotranspiration of the winter wheat-summer maize crop sequence in North China Plain. Irrig. Sci. 31, 1303–1316. doi:10.1007/s00271-013-0405-1.

Zhang, X.C., 2004. Calibration, refinement, and application of the WEPP model for simulating climatic impact on wheat production. Trans. ASAE 47, 1075–1085.

Zhao, N., Liu, Y., Cai, J., Paredes, P., Rosa, R.D., Pereira, L.S., 2013. Dual crop coefficient modelling applied to the winter wheat-summer maize crop sequence in North China Plain: Basal crop coefficients and soil evaporation component. Agric. Water Manag. 117, 93–105. doi:10.1016/j.agwat.2012.11.008.

Zreda, M., Desilets, D., Ferré, T.P.A., Scott, R.L., 2008. Measuring soil moisture content non-invasively at intermediate spatial scale using cosmic-ray neutrons. Geophys. Res. Lett. 35. doi:10.1029/2008GL035655.

Table 1. Basal crop coefficients for the different winter wheat growth stages and equivalent Zadoks and Wang-Engel quantitative scales.

Growth stage	Zadoks	Wang-Engel†	K_{cb}
Planting	0	-1.00	0.40
Emergence	10	0.00	0.40
Early tiller	21	0.26	0.40
Mid tiller	26	0.37	0.65
Late tiller	30	0.45	0.90
Stem elongation	31	0.47	1.15
Heading	50	0.90	1.25
Flowering	60	1.00	1.20
Milk	71	1.20	1.00
Soft dough	85	1.75	0.80
Hard dough	87	1.82	0.60
Maturity	91	2.00	0.40

†Values were approximated using linear interpolation based on Wang and Engel 1998.

Table 2. Set of parameters used in the dual crop coefficient soil water balance model and the modified Wang-Engel phenological model.

Parameter	Description	Value	Units
Dual Kc model†			
$TT_{emergence}$	Cumulative thermal time to emergence	100	GDD
ptab	Factor that modulates available water	0.6	Dimensionless
K_{cb} fallow	Coefficient for diffusive losses	0.02	Dimensionless
Z_{max}	Maximum rooting depth	0.8	m
Z_{shape}	Shape factor for root growth	1.5	Dimensionless
TTZ_{max}	Thermal time to maximum rooting depth	900	GDD
Wang-Engel model‡			
R_{max} E-TS	Maximum development rate emergence-terminal spikelet	0.025	scale units per day
R_{max} TS-AN	Maximum development rate terminal spikelet -anthesis	0.049	scale units per day
R_{max} AN-PM	Maximum development rate anthesis-physiological maturity	0.038	scale units per day
T_{min} E-TS	Minimum temperature for emergence-terminal spikelet	0	°C
T_{min} DS-AN	Minimum temperature for terminal spikelet -anthesis	4	°C
T_{min} AN-PM	Minimum temperature for anthesis-maturity	8	°C
T_{min} Vernalization	Minimum temperature for vernalization	-1.3	°C
T_{opt} E-TS	Optimal temperature for emergence-terminal spikelet	19	°C
T_{opt} DS-AN	Optimal temperature for terminal spikelet-anthesis	24	°C
T_{opt} AN-PM	Optimal temperature for anthesis-physiological maturity	24	°C
T_{opt} Vernalization	Optimal temperature for vernalization	4.9	°C
T_{max} E-TS	Maximum temperature for emergence-terminal spikelet	30	°C
T_{max} DS-AN	Maximum temperature for terminal spikelet-anthesis	35	°C
T_{max} AN-PM	Maximum temperature for anthesis-physiological maturity	35	°C
T_{max} Vernalization	Maximum temperature for vernalization	15.7	°C
P_c	Critical photoperiod	7	hr
ω	Photoperiod sensitivity factor	0.16	h^{-1}
VD_{full}	Number of days to complete vernalization stage	40	days

†Parameters are similar to those of Steduto et al. (2009) and Allen et al. (1998).

‡ Parameters are equal to those suggested by Streck et al. (2003) for wheat cultivar Karl 92.

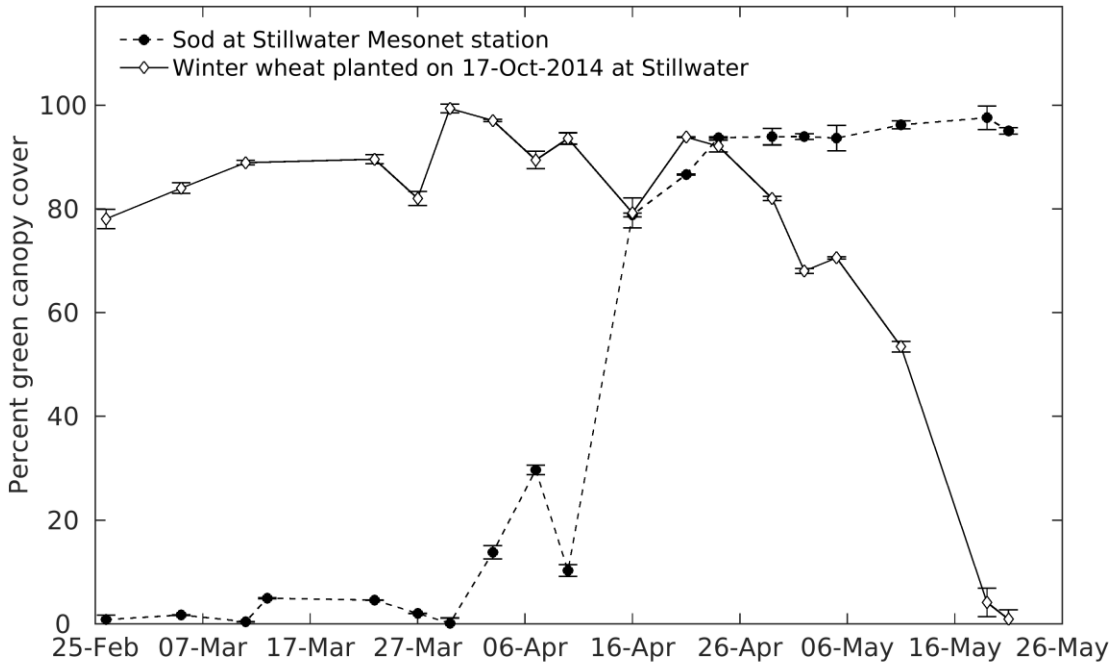

Figure 1. Field observations of green canopy cover in the grassland surrounding the Stillwater Oklahoma Mesonet station and an adjacent field of continuous winter wheat during the late winter and spring of 2015.

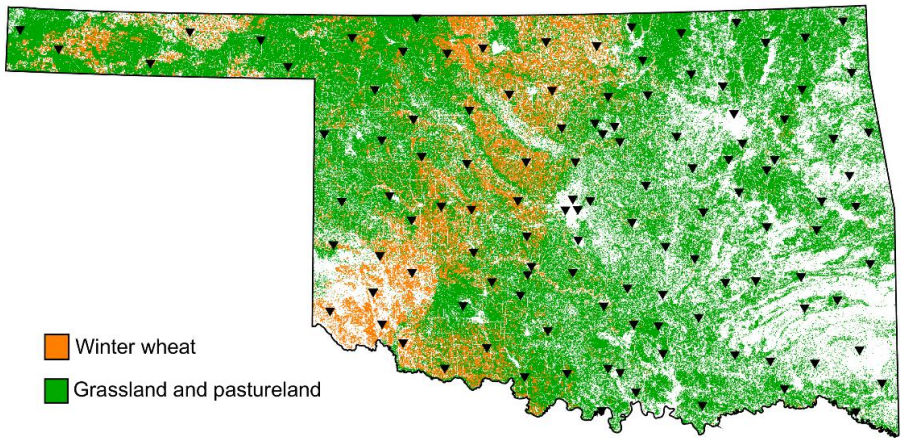

Figure 2. Map showing the spatial distribution of winter wheat cropland, grassland, and the 78 selected Oklahoma Mesonet stations (inverted black triangles) across the state of Oklahoma. Each point represents an area of 30 by 30 m. Source: USDA cropland data layer, 2014.

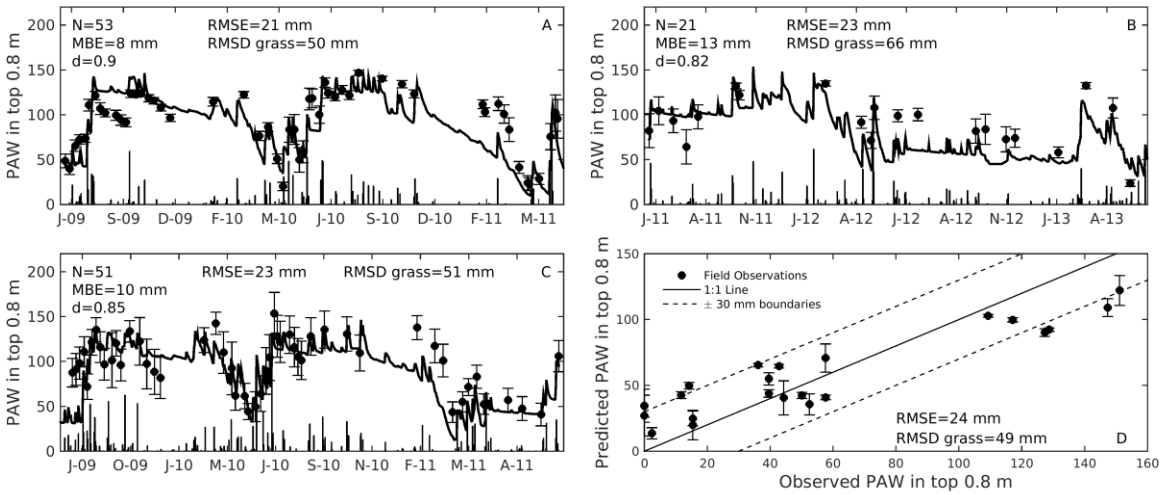

Figure 3. Calibration (A) and validation (B, C, D) of the dual crop coefficient model for different years and sites across the state of Oklahoma. Root mean squared error (RMSE), mean bias error (MBE), and the Wilmott index of agreement (d) were used to evaluate the model prediction of plant available water (PAW) in the top 0.8 m. The root mean squared difference (RMSD grass) was used to evaluate the difference between PAW field observations and the nearest Oklahoma Mesonet station. Bars in A, B, and C represent daily total precipitation.

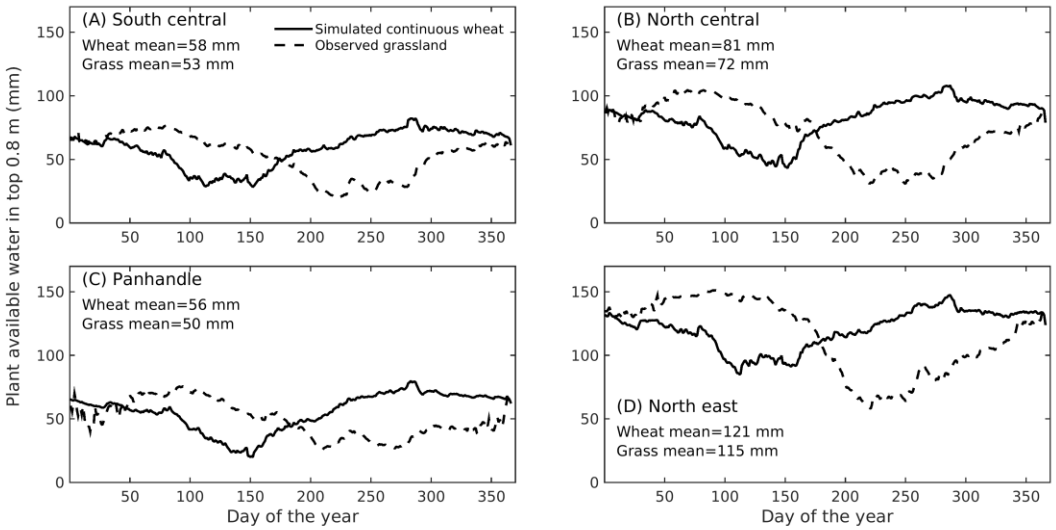

Figure 4. Long-term (18-yr) mean plant available water (PAW) in the top 0.8 m of continuous wheat and grassland across four Oklahoma climate divisions with contrasting annual precipitation.

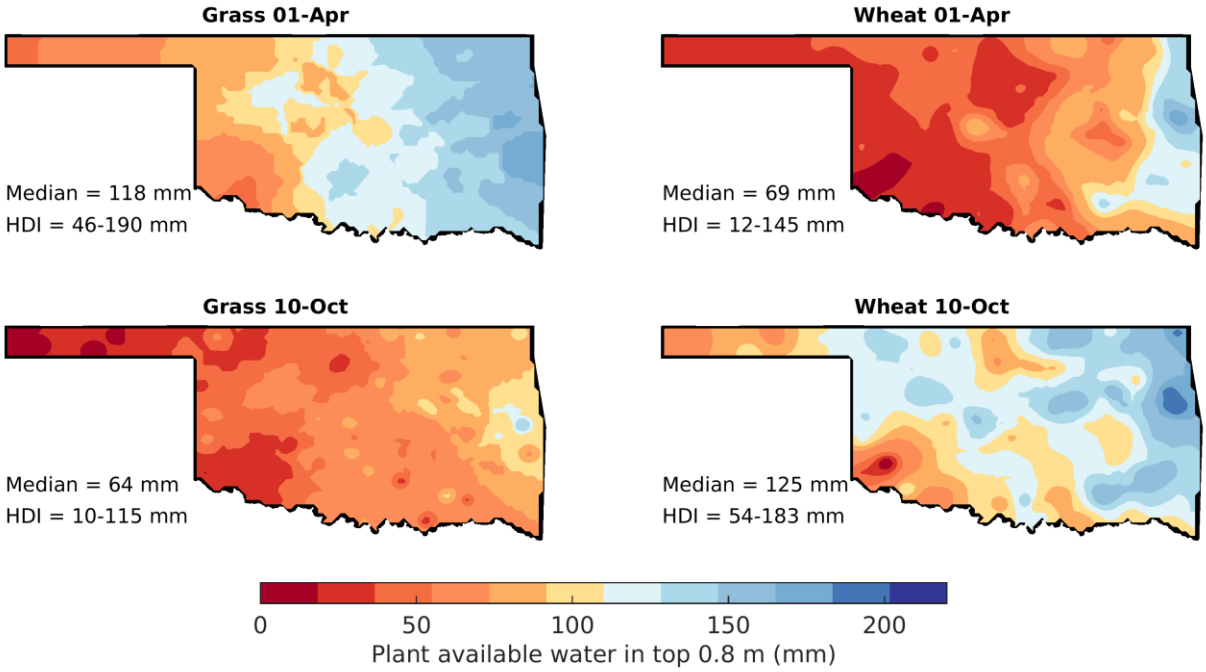

Figure 5. Selected dates of long-term (18-yr) mean plant available water (PAW) in the top 0.8 m of grassland (A and C) and continuous wheat (B and D) across Oklahoma.

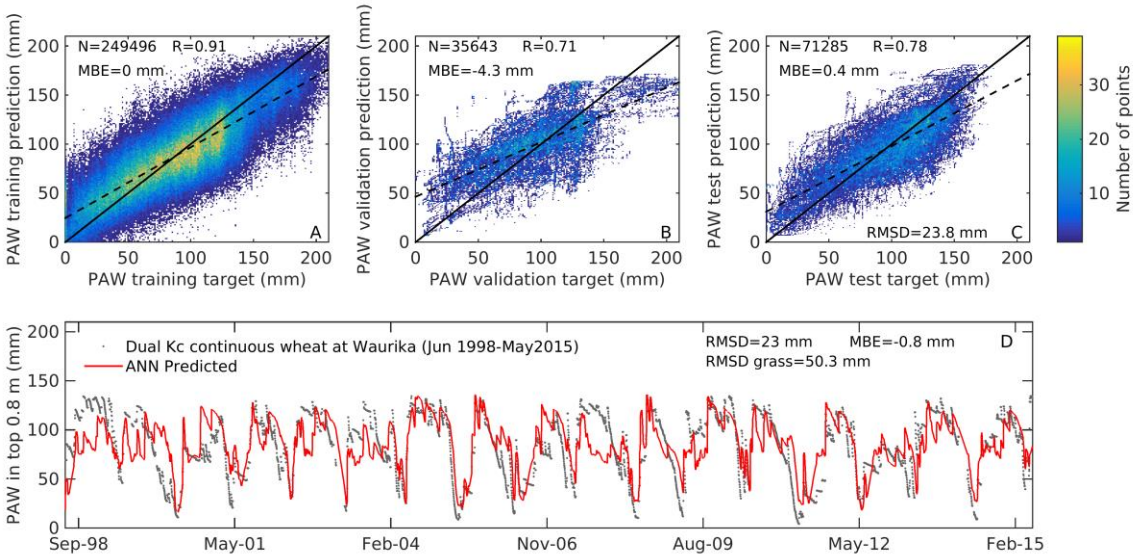

Figure 6. Training (A), validation (B), and testing (C) results of the feedforward-backpropagation artificial neural network (ANN) used to predict plant available water (PAW) in winter wheat based on observed soil moisture under grassland vegetation and six other inputs. The PAW dynamics for the Waurika station within the test set are displayed in (D). N represents the number of samples included in each set, MBE is the mean bias error, R is the correlation coefficient, and RMSD grass is the error between the simulated PAW in continuous wheat and the PAW at the Waurika Oklahoma Mesonet station.

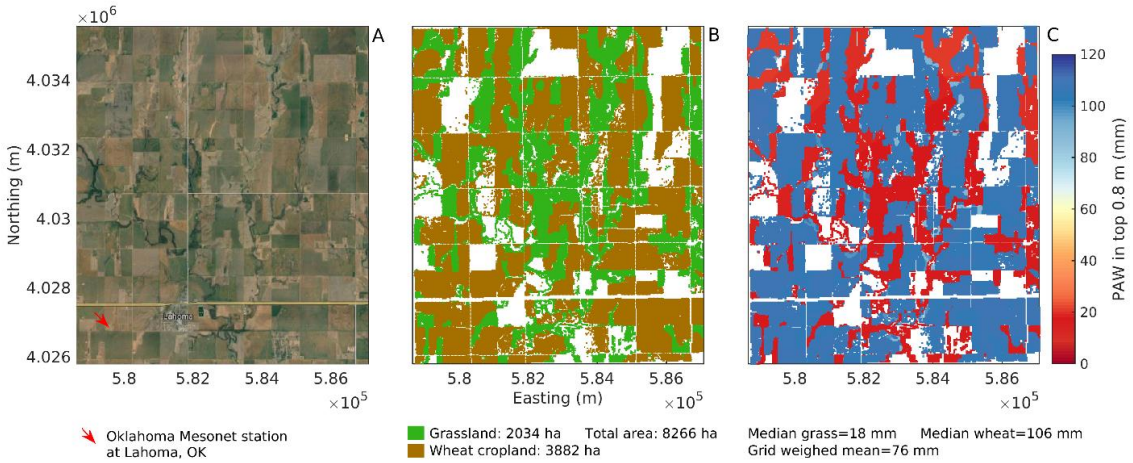

Figure 7. Orthophoto (A), grassland and winter wheat cropland area (B), and estimated plant available water (PAW) in the top 0.8 m of the soil profile on 10 Oct. 2014 for a SMAP grid cell (FID: 153137, row: 329, column: 877) near the Lahoma Oklahoma Mesonet station.

CHAPTER V

TRANSPIRATION RESPONSES TO SOIL DRYING UNDER HIGH ATMOSPHERIC DEMAND

Andres Patrignani and Tyson E. Ochsner

ABSTRACT

Quantitative relationships between plant transpiration and soil water are necessary to model vegetation dynamics in water-limited environments. It is a common practice to determine these relationships empirically by conducting field or pot experiments. However, most studies have only been conducted in low to moderate atmospheric demands adopting the concept of plant available water to describe the soil moisture condition, which relies on somewhat arbitrary lower and upper limits. The objectives of this study were: i) to compare transpirational responses of corn plants under a moderate and a high atmospheric demand for three soil textures, and ii) to investigate the application of a continuous double exponential function that relates relative plant transpiration to soil matric potential from saturation to oven-dryness without relying on lower and upper limits. Corn plants were grown in 7.8 L pots in a controlled-environment chamber under atmospheric demands of 4.8 and 8.4 mm d^{-1}. Actual transpiration rate was determined by differences in pot weight every 24 h. Potential transpiration was determined by estimating the maximum transpiration rate for a given fresh biomass. Relative plant transpiration was determined as the ratio between actual and potential transpiration rates. The soil matric potential at the inflection point of the soil water retention curve proved to be an effective and unbiased

point to generalize the relative transpiration response for different soil textures and both the moderate and high atmospheric demands. This generalized response was well represented by a double exponential model, which can be used within emerging quantitative frameworks such as the integral water capacity to determine the soil's plant available water capacity.

INTRODUCTION

Simulation of plant growth in water-limited environments requires expressions that quantitatively describe transpiration responses to different degrees of soil moisture content. As a consequence of the high complexity of the soil-plant-atmosphere continuum, these quantitative responses are usually determined empirically by conducting field, greenhouse, or controlled-environment chamber experiments that compare the transpiration rate of plants under different levels of soil water deficit with that of plants under well-watered conditions. The different levels of soil moisture content are often expressed as a fraction of the soil's plant available water capacity (PAWC), which is often defined by somewhat arbitrary lower and an upper retention limits. The threshold (PAWt) at which relative plant transpiration starts to rapidly decline as a function of plant available water is generally used to delimit the transition between well-watered and water-limited conditions.

Using the concept of PAW to describe plant transpiration responses to soil drying is attractive due to its simplicity. However, the arbitrary nature of the lower and upper limits prevent consistent determination of PAWC across field studies, laboratory routines, and pot experiments (Ratliff et al., 1983; Passioura, 2006). After an exhaustive review of the topic, Sadras and Milroy (1996) concluded that PAWt for different physiological processes is highly variable and that discrepancies in the determination of PAWt for a given plant under different conditions may be affected by the uncertainties in the determination of PAWC. Inspection of several studies (Denmead and Shaw, 1962; Ray and Sinclair, 1998; Fletcher et al., 2007; Gholipoor et al., 2010, 2013b) revealed that the procedures for determination of the drained upper limit (i.e. field capacity) to define PAWC are inconsistent. For instance, the study by Denmead and Shaw (1962) provides little information about the determination of the field capacity. It is unclear whether field capacity was determined using laboratory measurements at a given matric potential or was determined in field conditions. On the other hand, the determination of the drained upper limit in pot experiments (e.g. Ray et al., 2002; Gholipoor et al., 2013a) often is based on the soil moisture

content after thoroughly wetted pots drained overnight. This approach typically results in higher soil moisture contents compared to determinations in field conditions or by laboratory routines (Passioura, 2006).

The review by Sadras and Milroy (1996) also showed that a wealth of literature exists for transpiration responses in low (<3 mm d^{-1} reference evapotranspiration, ET_0) to moderate (3-6 mm d^{-1} ET_0) atmospheric demands, but there is lack of research under high (>6 mm d^{-1} ET_0) atmospheric demands, which are the environments that are most prone to experience soil water deficits and thus limit plant transpiration. We were unable to find any studies that investigated plant transpiration responses in environments with evapotranspiration demands exceeding 6.5 mm d^{-1}. A study conducted by Denmead and Shaw (1962) in Iowa, US explored the transpiration response of corn (*Zea mays* L.) plants growing in large pots buried in the field and subjected to different soil moisture treatments with atmospheric demands ranging from 1.4 to 6.4 mm d^{-1}. The authors found that the relative transpiration rate starts to decline at increasing soil moisture contents with increasing atmospheric demand. In contrast, a study conducted by Ray et al. (2002) showed that corn plants growing in a sandy loam soil under day-time vapor pressure deficits ranging from 1.1 to 3.6 kPa had stable transpiration responses regardless of the atmospheric demand. The authors found that relative transpiration started to consistently decline at PAWt ranging from 0.31 to 0.38. Despite its significance, the discrepancy of relative plant transpiration responses under contrasting atmospheric demands and its relationship to plant available water remains has not yet been clarified.

To solve some of these limitations, new methods such as the integral water capacity (Groenevelt et al., 2001) and the integral energy (Minasny and McBratney, 2003) have been proposed to estimate PAWC. The integral water capacity is a particularly attractive framework because of its flexibility to incorporate multiple weighting functions that describe different limitations to plant water uptake. Unfortunately, this flexibility is also a disadvantage, since the functions describing the limitations are unknown. In this study we explore the hypothesis that a

single continuous function could be used as a weighting function within the integral water capacity framework to describe the response of relative transpiration to soil moisture conditions without relying on arbitrary upper and lower limits. The objectives of this study were: i) to compare transpirational responses of corn plants under a moderate and a high atmospheric demand for three soil textures, and ii) to investigate the application of a continuous double exponential function that relates relative plant transpiration to soil matric potential from saturation to oven-dryness.

MATERIALS AND METHODS

Controlled-environment chamber

A walk-in growth chamber with an area of ~10 m^2 by 3 m tall with controlled air temperature, wind speed, and light was used to grow corn plants in a moderate and a high atmospheric demands (Table 1). The different atmospheric demands were generated by changing the air temperature and the wind speed during the day-time only. The day-time was set to 14 h and the night time was set to 10 h since these are representative of the growing season for corn. The moderate atmospheric demand was generated by setting the day-time air temperature to a target of 28 °C and the fan at its lowest speed (~ 1 m s^{-1}), while the highest atmospheric demand was generated by setting a target day-time air temperature of 38 °C and the fan was set to its highest speed (~ 3 m s^{-1}). The growth chambers successfully maintained the air temperature within ±1 °C from the specified values (Table 1). For each atmospheric demand we measured air temperature, relative humidity, and carbon dioxide concentration.

The chamber had a combination of metal halide and high pressure sodium lamps (400 Watts, Hortilife) that were used to maintain the photosynthetically active radiation (PAR) between 1200 and 1400 µmol cm^{-2} s^{-1} at the top of the canopy. To measure reference evapotranspiration (ET_0) we installed an atmometer (ETgage Co. Loveland, CO, USA) near the plants and its top part was kept aligned with the top of the canopy. Atmometers have been shown

to produce reliable estimates that closely match those of reference evapotranspiration by the Penman-Monteith method in Mediterranean (Magliulo et al., 2003), semi-arid (Gavilán and Castillo-Llanque, 2009), and humid (Knox et al., 2011) environments. Day-time, night-time, and weighted daily vapor pressure deficit for each atmospheric demand were estimated from air temperature and relative humidity.

Experiment setting

Corn plants were grown in the controlled-environment chamber using 7.8 L (0.3 m height) pots filled with homogenized silt loam, clay loam, and sandy loam soils. The silt loam soil was collected at Lahoma, OK (N 36.389642 W -98.105749), the clay loam soil was collected in Stillwater, OK (N 36.121377 W-97.094243), and the sandy loam was a commercially available soil (Timberline Top Soil acquired at Lowes). At the bottom of each pot we placed a mesh that held a thin layer of pea size gravel to improve drainage. Each soil was passed through the 2-mm sieve prior filling the pots. The filling process consisted of adding one third of the soil required to completely fill the pot at a time. After filling each third of the pot, the soil was irrigated using de-ionized water until drainage was evident. When completely filled, pots were left for one week prior to planting inside the growth chamber to experience several drying and wetting events that resulted in a homogeneous soil with mean bulk density of 1.17 g cm^{-3} with standard deviation of 0.05 g cm-3 across all pots and soils. During this period pots were irrigated two or three times. We adopted this packing technique to avoid the development of differentially compacted soil layers that can be present when manually packing the soil by layers. Initially, a total of 15 to 18 pots were planted with corn. Three seeds of similar weight (±0.01 g) were planted in each pot. After emergence, pots were thinned to leave only the most vigorous plant. When plants had five leaves fully expanded (V5), we selected the set of 12 plants with the lowest variance in plant height. To achieve this selection, we developed a routine in Matlab (Mathworks, Inc., Natick,

MA) that calculates the variance of all possible combinations of sets of 12 plants. This procedure ensured that comparisons of transpiration responses was for similar plants.

The day prior to initializing the treatments, pots were thoroughly wetted, sealed with white 150-µm thick polyethylene around the stem of the plants to prevent soil evaporation, and left draining overnight in order to reproduce the drained upper limit achieved by other researchers. At the beginning of the experiment eight plants were randomly selected as "stressed" and four plants were selected as "Non-stressed". The stressed plants received water only at the start of the experiment. The non-stressed plants received water periodically to avoid any visible stress. Soil water was replenished to ensure that well-watered pots had a soil matric potential of >-50 kPa based on tensiometers installed in the well-watered pots. To minimize nutritional deficiencies, pots were fertilized at planting and prior the initialization of the treatments by dissolving 22 g of a complete fertilizer (24-8-16, Miracle-Gro, Geneva, New York) in 10 L of water and then distributing this nutritive solution among the 12 pots in equal parts.

Determination of actual transpiration rates

Daily transpiration rate was calculated as the difference in pot weight between two successive daily weights using an Ohaus balance with minimum resolution of 1 g. Initial and final pot volumetric water content at the start and end of the experiment were estimated by taking three measurements in the top 0-6 cm per pot with a calibrated impedance probe (ML2x, Theta Probe, Delta-T Devices). From pilot experiments we learned that average 0-6 cm soil moisture was not different from the average of soil moisture measurements at several depths within the pot). Soil-specific soil water retention curves were used to convert volumetric water contents into soil matric potentials.

Determination of potential and relative transpiration rates

In many experiments non-stressed plants are referred to as “well-watered” plants. However, the definition of “well-watered” plants is seldom given. It is usually assumed that maximum transpiration rates occur at “field capacity”, but this term is loosely defined and often not consistent across experiment settings. Furthermore, because plant growth is affected by soil water stress, normalizations in the transpiration rates are often needed to account for the different sizes in well-watered and stressed plants. For these reasons, in this experiment we adopt a different approach to estimate the potential transpiration rates. Therefore, in this study we assumed that well-watered plants are those plants that exhibit the greatest transpiration rate for a given fresh biomass at each evapotranspiration demand. Our idea was not to achieve a given soil moisture content in the well-watered plants, but a range of well-watered conditions to determine the maximum transpiration rate. Our method was designed to account for subtle soil water excess or deficits under the so called “well-watered” conditions that may decrease the transpiration rate. Then, we used a 95th percentile quantile regression analysis (Cade et al., 2005) to determine the potential transpiration rate for any given fresh biomass. Quantile regression analysis allowed us to filter plants that were in the well-watered treatment but for some reason had lower transpiration rates as a consequence of soil water excess or deficits. Finally, the daily relative transpiration rate for each plant was calculated as the ratio between the actual transpiration rate of the plant and the corresponding potential transpiration rate according to its fresh biomass. This method allowed us to compare the actual and potential transpiration rates for plants of the same size.

Determination of aboveground and root biomass

Daily fresh and dry aboveground biomass were estimated by measuring stem diameter and plant height. Extra corn plants were grown to develop models for predicting fresh and dry biomass using multiple linear regression. At the end of each experiment, aboveground biomass was estimated destructively by harvesting the plants and drying them in an oven at 60 °C until constant weight (about 7 days). Plants were cut in small pieces to accelerate drying. Root dry

biomass was measured by first manually extracting the bulk of the root system from the soil. Then, a 2.0 mm-sieve was used to collect the remaining fine roots. Roots were soaked for 15 minutes to loosen up the soil in the rhizosphere, and then thoroughly washed. Similarly to the aboveground biomass, roots were dried until constant weight (about two to three days).

Soil properties

For each soil we sampled four cores from different pots using 100 cm^3 (50 mm i.d. and 50 mm height) stainless steel rings (Eijkelkamp sampling kit, Giesbeek, Netherlands). These samples were then used to measure the volumetric water content at soil matric potentials of 0, -5, -10, and -33 kPa using the pressure cell (Tempe cell) method (Dane and Hopmans, 2002) and at soil matric potentials of -100, -500, -1000, and -1500 kPa using the pressure plate extraction method (Dane and Hopmans 2002) (Table 2, Fig. 1). The Groenevelt-Grant (Groenevelt and Grant, 2004) soil water retention model was chosen because it allows multiple anchor points, does not rely on the assumption of residual water content, and explicitly provides the inflection point. In this case, we anchored the model to the saturation and oven-dryness points to fit the observed data. The equation of the models with two anchor points is:

$$\theta(h) = \theta_s - (\theta_s - \theta_{od}) \left\{ exp \left[\left(\frac{k_0}{h_{od}} \right)^n - \left(\frac{k_0}{h} \right)^n \right] \right\} \qquad \text{Eq. [1]}$$

where θ_s (cm3 cm^{-3}) is the volumetric water content at saturation, θ_{od} (cm3 cm^{-3}) is the volumetric water content at oven dryness (assumed to be zero), k_0 (kPa) and n (dimensionless) are fitting parameters, h_{od} (kPa) is the soil matric potential at oven dryness which is approximately $10^{5.9}$ kPa (Grant et al., 2010). The term $(\theta_s - \theta_{od})$ is equivalent to the k_1 parameter in the version of the equation with only one anchor point, since θ_{od} is assumed zero, then $k_1 = \theta_s$.

Double exponential stress function

Transpiration responses to soil water stress are usually modeled using piece-wise linear (Soltani et al., 2000; Ray et al., 2002) or single exponential functions (Muchow and Sinclair, 1991; Sadras and Milroy, 1996; Soltani et al., 2000). However, these functions are only able to represent the transpiration responses to soil drying from the point of maximum transpiration rate. We propose a flexible and continuous double exponential stress function that covers the entire range from saturation to oven dryness, which can be presented in its most general form as:

$$RT = RT_{max}\left\{\left[1 + exp\left(\frac{\psi_m}{\psi_{ip}} - \alpha\right)\right]^{-n} - exp\left[b\left(\frac{\psi_m}{\psi_{ip}} - c\right)\right]\right\} \qquad \text{Eq [2]}$$

where RT is the relative transpiration rate, RT_{max} is the maximum relative transpiration rate, α, b, c, and n are fitting parameters, ψ_m is the soil matric potential, and ψ_{ip} is the soil matric potential at the inflection point of the retention curve $\theta(log_{10}\psi_m)$. Although ψ_{ip} is equivalent to the parameter k_0 in the Groenevelt-Grant model, we adopt the more general symbolic representation, ψ_{ip}, because the inflection point can be obtained from other soil water retention models. Because a weighting function has a desired maximum of one, the parameter RT_{max} can be dropped. Also assuming that the transpiration rate is zero at the saturation point, the c parameter can also be dropped producing a more convenient three-parameter function of the form:

$$RT = \left[1 + exp\left(\frac{\psi_m}{\psi_{ip}} - \alpha\right)\right]^{-n} - exp\left(b\frac{\psi_m}{\psi_{ip}}\right) \qquad \text{Eq [3]}$$

An interesting feature about equation 3 is that the transpiration responses to soil water under wet and dry conditions can be controlled independently by different terms. The first part of the equation represents the responses to soil drying from the maximum transpiration rate, while the second part represents the plant transpiration responses from saturation to maximum transpiration rate. The parameter a (kPa) has the same unit as the soil matric potential and represents the inflection point of the drying portion of the curve, the n (dimensionless) parameter is related to the sensitivity of the plant to soil water stress in the drying portion of the curve, whereas the b

(kPa^{-1}) parameter controls the response of the plant at high soil moisture contents. The c (kPa) parameter may be considered in cases when there is plant transpiration even under saturated soil conditions. Plants such as rice and corn have specialized tissue (i.e. aerenchyma) that allows gaseous transport from shoot to root in hypoxic conditions, thus allowing transpiration. In equation 3 the maximum value is an asymptote, which may be a subtle limitation considering that a desirable property of weighting functions is to span the range from zero to one.

RESULTS AND DISCUSSION

Plant height and stem diameter proved adequate to nondestructively predict fresh and dry plant biomass during the experiments. All terms included in the full model for fresh biomass were significant with an R^2 of 0.92 (Table 3). For dry biomass, only stem diameter and the interaction of stem diameter x plant height were significant predictors, and therefore these terms were used to build a reduced model, which resulted in an R^2 of 0.79. The greater error in estimating dry biomass relative to fresh biomass may be related to our measurements. When plants are turgid, stem diameter and plant height can be measured with high precision, but when plants are wilted, accurate measurements become more difficult, particularly for stem diameter. For this reason, we employed fresh biomass to conduct our quantile regression analysis. In addition, using fresh biomass seems a better indicator of the current transpirational condition of the plant than dry biomass. A turgid plant and a stressed plant may have the same dry biomass, but dramatically different transpiration rates.

The use of quantile regression allowed us to determine the maximum plant transpiration rate as a function of fresh biomass for each soil and atmospheric demand. This method reduced the sensitivity to plants in the presumably well-watered treatment that had transpiration rates below the potential transpiration rate for a given plant fresh biomass. Transpiration rates below the potential rate may be present in “well-watered” plants that have excess of mild soil moisture deficits. This method has the advantage of not relying on the assumption that well-watered plants

are those at “field capacity” and avoids the double normalization used in other studies which sometimes mask the effect of lower transpiration rates as a consequence of overwatering pots. The maximum possible potential transpiration rate as a function of fresh biomass was effectively approximated using a power function (Fig. 2).

In order to demonstrate the limitations and the bias that can be introduced when determining PAWt based on arbitrary upper limits, we show in Figure 3 the transpiration response for corn plants growing in a sandy loam soil at an atmospheric demand of 8.4 mm d^{-1}. The determination of PAWC based on the soil moisture content at the saturation point, 10% air-filled porosity, -10 kPa, and -33 kPa resulted in dramatic changes of the PAWt with values ranging from approximately 0.4 to 1.0 PAWC. In the case of pot experiments where the drained upper limit can be close to 10% air-filled porosity (Passioura, 2006) the PAWt of the sandy loam soil occurred at values of 0.4 PAWC. This value closely matches the PAWt values obtained by other studies evaluating the transpiration response of corn in commercially available sandy loam soils (Ray et al., 2002). From this particular example, it is clear that using functions developed from pot experiments in models that are intended to simulate field conditions can result in considerable error. This example also highlights the large amount of water that can be held in the soil between -10 or -33 kPa and saturation or 10% air-filled porosity.

A simple alternative to using PAWC is to describe relative plant transpiration using soil matric potential. Using the soil matric potential is attractive since it has a direct relationship with the energy state at which water is held in the soil. The use of the soil matric potential to describe relative plant transpiration rate has been proposed by Feddes et al. (1978). While transpiration responses were consistent within a given soil texture for both moderate and high atmospheric demands (Fig. 4), the markedly different responses across soils implies that transpiration reduction curves need to be developed for each soil, which is certainly a disadvantage. The consistency of the transpiration responses within each soil under different atmospheric demands and the similarity between the transpiration responses in the clay loam and silt loam soils relative

to the sandy loam soil, inspired us to investigate the role of the inflection point of the soil water retention curve as a normalizing factor (Grant and Groenevelt, 2015).

Normalizing the soil matric potential (ψ_m) by the matric potential at the inflection point (ψ_{ip}) resulted in a generalized response describing relative transpiration and soil water content (Fig. 5). The double exponential equation (Eq. 3) presented in this study, can be used to relate relative plant transpiration to soil moisture with a single set of parameters across different soil types and atmospheric demands without relying on the arbitrary concept of "field capacity" or "drained upper limit". Parameters α, b, and n calculated for a particular variety or species grown in any given soil type could then be used be used to describe relative plant transpiration as a function of soil matric potential of any other soil by knowing the soil matric potential at its inflection point. The soil water retention model of Groenevelt and Grant (2004) explicitly provides with the inflection point, which is equal to one of the fitting parameters (i.e.k_0). Interestingly, the relative transpiration rate started to consistently decline when ψ_m/ψ_{ip} had an approximate value of one for all three soils. Our findings provide evidence supporting the hypothesis formulated by Grant and Groenevelt (2015) about the rapid decline in transpiration rate at, or nearby, the soil matric potential at the inflection point of the soil water retention curve.

The proposed continuous function describing plant transpiration responses to soil drying could also be used as a weighting function within the integral water capacity (Groenevelt et al., 2001) framework to estimate plant available water.

CONCLUSION

This study presented a set of observations that demonstrated the limitations of the often used PAWt framework which depends on assumption of "field capacity" or "drained upper limit" to represent transpiration responses to soil drying. For each of the three soil textures evaluated, the soil matric potential at the inflection point of the soil water retention curve proved to be an effective and unbiased point to generalize the relative transpiration response for different soil

textures, revealing that the relative transpiration rate started to decline at a soil matric potential near that at the inflection point. This generalized response can be represented by a double exponential model which describes the relative transpiration responses to different soil matric potentials for different soils and atmospheric demands. The proposed double exponential function can be used within emerging quantitative frameworks such as the integral water capacity to determine the soil's plant available water capacity.

REFERENCES

Cade, B.S., B.R. Noon, and C.H. Flather. 2005. Quantile regression reveals hidden bias and uncertainty in habitat models. Ecology 86(3): 786–800. doi:10.1890/04-0785.

Dane, J. H., and J. W. Hopmans, 2002: Water retention and storage. Methods of Soil Analysis: Physical Methods, J. H. Dane and G. C. Topp, Eds., Science Society of America Book Series, Vol. 5, Soil Science Society of America, Inc., 671–690.

Denmead, O.T., and R.H. Shaw. 1962. Availability of soil water to plants as affected by soil moisture content and meteorological conditions. Agron J 54(5): 385–

Feddes, R.A., P.J. Kowalik, and H. Zaradny. Simulation of field water use and crop yield. Centre for Agricultural Publishing and Documentation, 1978.

Fletcher, A.L., T.R. Sinclair, and L.H. Allen. 2007. Transpiration responses to vapor pressure deficit in well-watered "slow-wilting" and commercial soybean. Environ. Exp. Bot. 61(2): 145–151.

Gavilán, P., and F. Castillo-Llanque. 2009. Estimating reference evapotranspiration with atmometers in a semiarid environment. Agric. Water Manag. 96(3): 465–

Gholipoor, M., S. Choudhary, T.R. Sinclair, C.D. Messina, and M. Cooper. 2013a. Transpiration response of maize hybrids to atmospheric vapour pressure deficit. J. Agron. Crop Sci. 199(3): 155–160.

Gholipoor, M., P.V.V. Prasad, R.N. Mutava, and T.R. Sinclair. 2010. Genetic variability of transpiration response to vapor pressure deficit among sorghum genotypes. F. Crop. Res. 119(1): 85–90.

Gholipoor, M., T.R. Sinclair, M.A.S. Raza, C. Löffler, M. Cooper, and C.D. Messina. 2013b. Maize hybrid variability for transpiration decrease with progressive soil drying. J. Agron. Crop Sci. 199(1): 23–29.

Grant, C. D., P. H. Groenevelt, and N. I. Robinson. Application of the Groenevelt–Grant soil water retention model to predict the hydraulic conductivity. Soil Research 48.5 (2010): 447-458.

Groenevelt, P.H., and C.D. Grant. 2004. A new model for the soil-water retention curve that solves the problem of residual water contents. Eur. J. Soil Sci. 55(3): 479–485

Groenevelt, P.H., C.D. Grant, and S. Semetsa. 2001. A new procedure to determine soil water availability. Soil Res. 39(3): 577–598.

Knox, J.W., J.A. Rodriguez-Diaz, and T.M. Hess. 2011. Estimating evapotranspiration by using atmometers for irrigation scheduling in a humid environment. J. Irrig. Drain. Eng.Available at

Magliulo, V., R. d'Andria, and G. Rana. 2003. Use of the modified atmometer to estimate reference evapotranspiration in Mediterranean environments. Agric. Water Manag. 63(1): 1–14

Minasny, B., and A.B. McBratney. 2003. Integral energy as a measure of soil-water availability. Plant Soil 249(2): 253–262

Muchow, R.C., and T.R. Sinclair. 1991. Water deficit effects on maize yields modeled under current and "greenhouse" climates. Agron. J. 83(6): 1052.

Passioura, J.B. 2006. Viewpoint : The perils of pot experiments. Funct. Plant Biol. 33(12): 1075

Ratliff, L.F., J.T. Ritchie, and D.K. Cassel. 1983. Field-measured limits of soil water availability as related to laboratory-measured properties. Soil Sci. Soc. Am. J. 47(4): 770.

Ray, J.D., R.W. Gesch, T.R. Sinclair, and L. Hartwell Allen. 2002. The effect of vapor pressure deficit on maize transpiration response to a drying soil. Plant Soil 239: 113–121.

Ray, J.D., and T.R. Sinclair. 1998. The effect of pot size on growth and transpiration of maize and soybean during water deficit stress. J. Exp. Bot. 49(325): 1381–1386

Sadras, V.O., and S.P. Milroy. 1996. Soil-water thresholds for the responses of leaf expansion and gas exchange: A review. F. Crop. Res. 47(2-3): 253–266.

Soltani, A., F.R. Khooie, K. Ghassemi-Golezani, and M. Moghaddam. 2000. Thresholds for chickpea leaf expansion and transpiration response to soil water deficit. F. Crop. Res. 68(3): 205–210.

Table 1. Environmental conditions of the controlled-environment chamber at moderate and high atmospheric demands.

	Units	Moderate demand	High demand
Daily reference ETo†	mm d^{-1}	4.8	8.4
Day-time vapor pressure deficit	kPa	2.2	4.7
Night-time vapor pressure deficit	kPa	0.8	1.6
Daily weighted vapor pressure deficit	kPa	1.6	3.5
Photosynthetically active radiation	µmol $cm^{-2}s^{-1}$	1200-1400	1200-1400
Length day-time	h	14	14
Day-time air temperature	°C	29.0	37.9
Night-time air temperature	°C	21.2	20.6
Mean RH day	%	43.8	27.7
Mean RH night	%	70.4	31.8
Carbon dioxide concentration	ppm	595	588

† Determined by the atmometer.

Table 2. Saturated hydraulic conductivity (K_{sat}), bulk density (ρ_b), and the volumetric water content at saturation (θ_s), 10% air-filled porosity (θ_{AFP}), -10 kPa (θ_{10}), -33 kPa (θ_{33}), -1500 kPa (θ_{1500}), k_0, and n.

Soil texture	**K_{sat}**	**ρ_b**	**θ_{sat}**	**θ_{AFP}**	**θ_{10}**	**θ_{33}**	**θ_{1500}**	**k_0**	**n**
	cm h^{-1}	g cm^{-3}	——	——	cm^3	cm^{-3}	——	kPa	Unitless
Silty Loam	2.59	1.19	0.466	0.419	0.315	0.250	0.068	14.8	0.457
Clay Loam	1.79	1.22	0.466	0.420	0.268	0.222	0.102	12.7	0.349
Sandy Loam	22.7	1.10	0.495	0.445	0.198	0.177	0.062	3.81	0.559

Table 3. Parameter estimates, 95% confidence intervals, coefficients of determination (R^2), and F statistics for the full and reduced regression models. The independent variables are plant height, stem diameter (stemD), and their cross-products. The dependent variable is aboveground fresh (FB) and dry (DB) corn biomass (g).

		95% Confidence intervals			
Dependent variable	Parameter estimate	Lower	Upper	R^2	F
Full model FB					
Intercept	91.69	60.04	123.33	0.922	544***
Height, cm	-0.69	-1.05	-0.33		
StemD, cm	-255.37	-287.02	-223.72		
StemD X Height	2.47	2.23	2.70		
Full model DB					
Intercept	4.77	-1.57	11.10	0.797	179***
Height, cm	0.05	-0.02	0.12		
StemD, cm	-26.32	-32.66	-19.99		
StemD X Height	0.22	0.17	0.27		
Reduced model DB					
Intercept	8.04	3.98	12.09	0.794	266***
StemD, cm	-27.74	-33.73	-21.76		
StemD X Height	0.25	0.22	0.28		

***Significant at the 0.001 probability level.

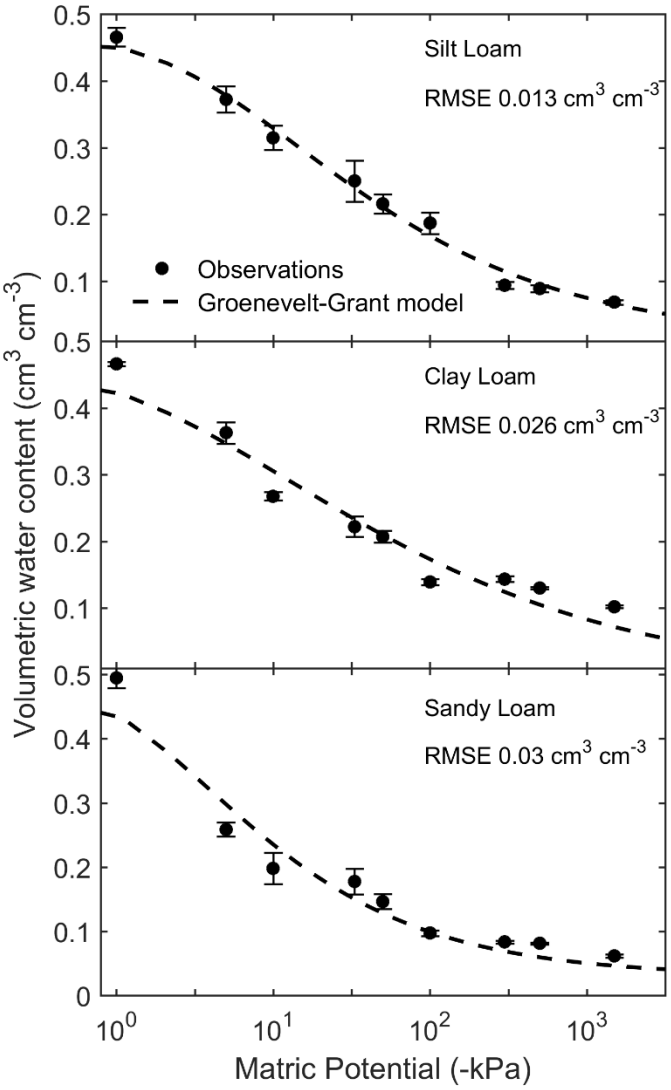

Figure 1. Laboratory observation and the fitted Groenevelt-Grant soil water retention model for the silt loam, clay loam, and sandy loams soils used in this study.

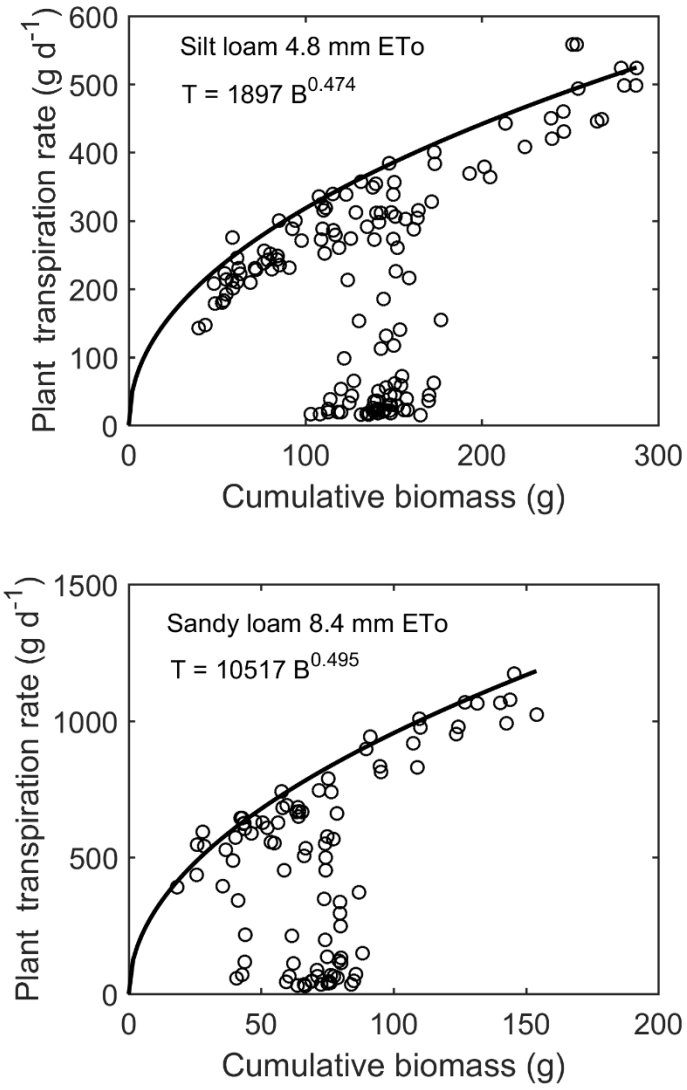

Figure 2. Example of the determination of the potential transpiration rate for a given plant fresh biomass using Quantile regression (95th percentile) for a silt loam at moderate atmospheric demand (4.8 mm d^{-1}) and a sandy loam at high atmospheric demand (8.4 mm d^{-1}).

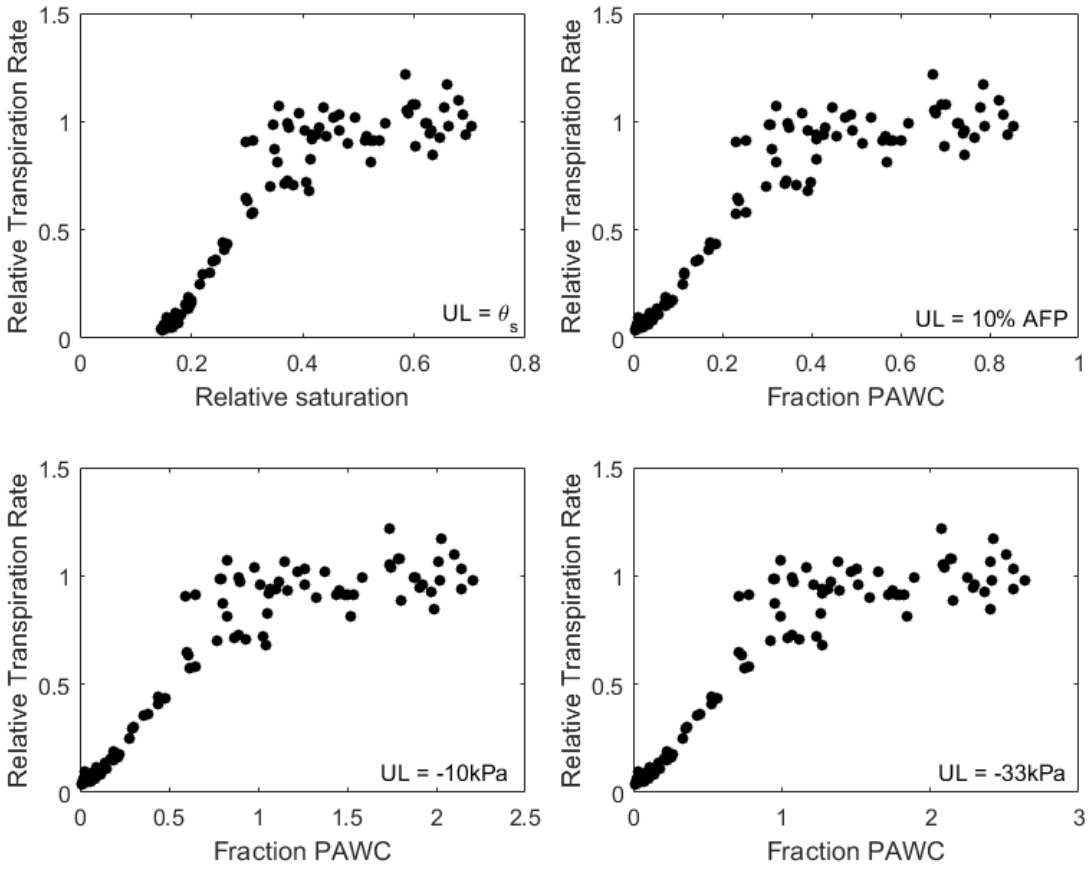

Figure 3. Relative transpiration rate as a function of the fraction of plant available water capacity (PAWC) for a sandy loam soil under an atmospheric demand of 8.4 mm d^{-1}. The value of PAWC=1 was defined by different common alternatives to estimate the upper limit (UL).

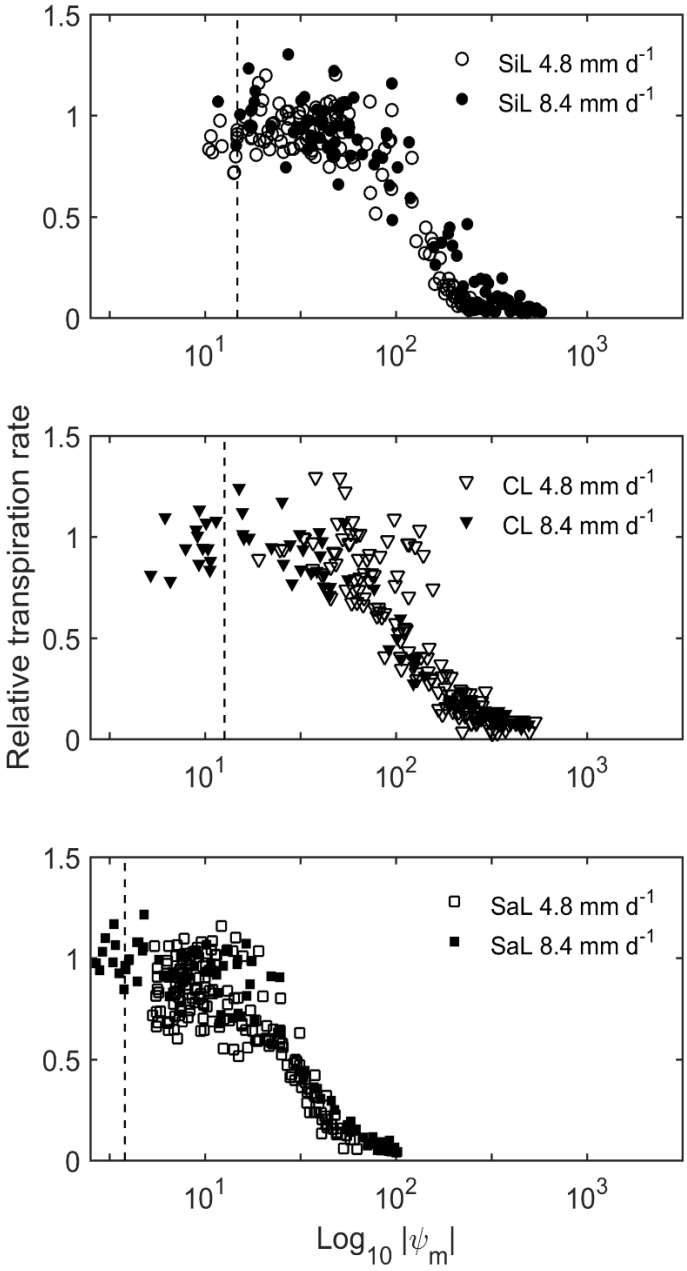

Figure 4. Transpiration responses as a function of the soil matric potential for a silt loam (SiL), clay loam (CL), and sandy loam (SaL) at atmospheric demands of 4.8 and 8.4 mm d^{-1} The vertical dashed line represents the inflection point of the soil water retention curve when plotted on a log10 scale. Soil matric potential was estimated from observations of volumetric water content and the fitted soil water retention curves.

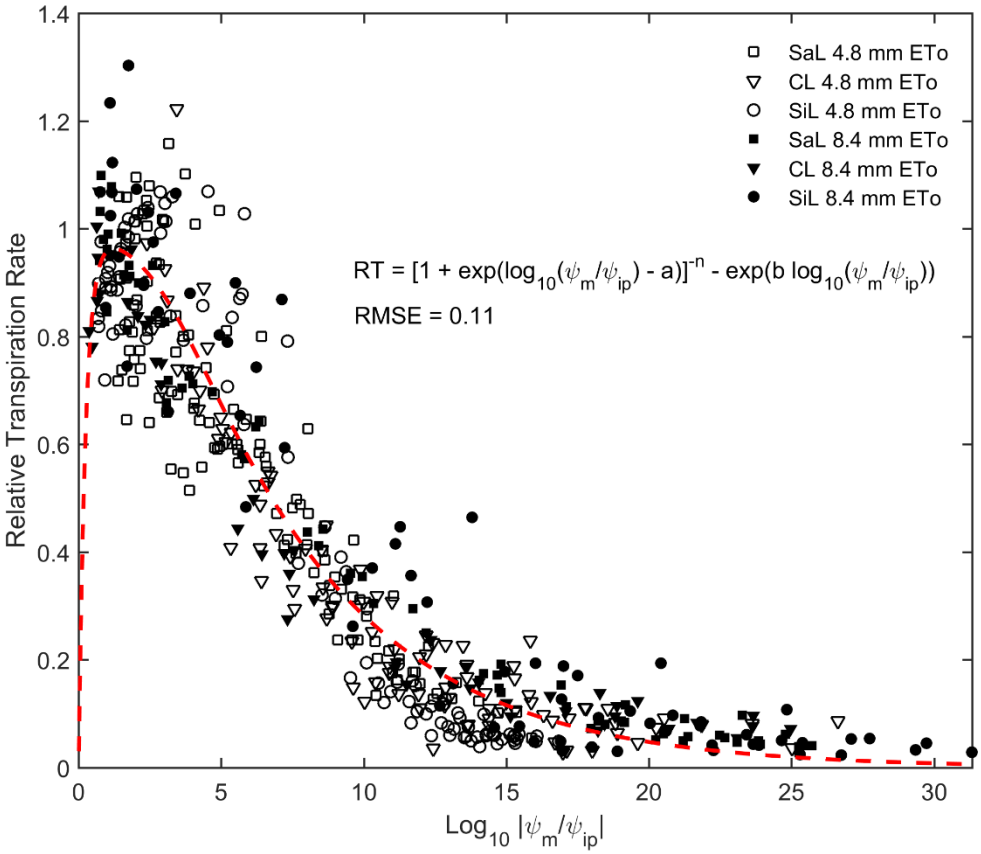

Figure 5. Relationship between the relative transpiration rate and the normalized soil matric potential by the soil matric potential at the inflection point for a sandy loam (SaL), clay loam (CL), and silt loam (SiL) at atmospheric demands of 4.8 and 8.4 mm d^{-1}. RT stands for relative transpiration, ψ_m/ψ_{ip} is the normalized soil matric potential, and a, b, and n are fitting parameters with value of 2.9 kPa, 4.06 kPa^{-1}, and 0.17, respectively.

CHAPTER VI

GENERAL CONCLUSION

Winter wheat is the predominant crop in the southern Great Plains of North America with about 8.5 million hectares planted every year. Winter wheat is predominantly grown in rainfed conditions and the frequent soil water deficits occurring during the growing season impose a limitation to crop production. The challenges that we addressed in this dissertation are related to i) the identification and quantification of the magnitude and possible reasons for state-level stagnation of wheat grain yields, ii) the development of a new tool to measure green canopy cover that can help improve crop models used for grain yield and root-zone soil moisture estimations, and thus aid wheat producers to make better in-season management decisions; iii) the need to increase the applications of large-scale soil moisture monitoring networks by translating soil moisture observations under grassland to estimate the soil moisture condition under wheat cropland, and iv) better understanding transpiration responses to soil water deficits under moderate and high atmospheric demands.

In the first study we investigated the magnitude of the yield and production gaps, and we tested the hypothesis that yield stagnation of wheat yields in the southern Great Plains is the result of a narrow yield gap. The study revealed that current average yield at state level are well below the maximum recorded yield at the plot level. Current yields represent 74% of the maximum attainable yield but only 30% of water-limited potential yield at state level. Wheat yields were often limited in growing seasons with total rainfall amount <250 mm, but average growing season rainfall was 471 mm, and yield was typically limited by factors. Production exhibited greater

temporal variability than yield, and production gap may be a better indicator than yield gap for regions with highest potential to increase production. We conclude that low yields and yield stagnation in Oklahoma cannot be attributed to a small remaining yield gap, nor to inadequate growing season rainfall amount. We suggest that low yields and yield stagnation may be related in part to past and present soil erosion.

The second study described a new tool to measure green canopy cover. This tool called Canopeo had an image processing speed 20 to 130 times faster than SigmaScan and 75 to 2500 times faster than SamplePoint, two existing image analysis tools. Canopeo correctly classified 90% of pixels when compared to SamplePoint, which was used as the "gold standard". The average root mean squared difference across several sets of images of corn, forage sorghum, bermuda grass, and switchgrass was 0.073. The unique capability of Canopeo to analyze video recordings proved to be useful to minimize sampling error and to quantify FGCC spatial variability. This analysis was simple and rapid with Canopeo but not possible with SamplePoint or SigmaScan. The rapid image processing and the accurate values of green canopy cover make Canopeo a useful tool to better manage grazing in dual purpose wheat systems. We also envision that Canopeo has potential for a variety of other applications in the field of agronomy and beyond.

The third study provided useful insights to estimate soil moisture under wheat cropland based on soil moisture observations under nearby grasslands. The use of an observation operator was proposed to translate root-zone soil moisture under grassland into root-zone soil moisture under wheat cropland. In this particular study we used a neural network as the observation operator, which proved to be effective to capture the main soil moisture dynamics simulated by the dual crop coefficient model. This study revealed that there is inscribed information in the soil moisture time series under grassland vegetation that allow estimates of soil moisture in nearby cropland. Potential applications of this approach involve the generations of more accurate large-

scale soil moisture maps and the possibility to determine the soil moisture patterns of landscapes with intermixed land covers for the ground-truthing remote sensing soil moisture estimations.

The fourth study focused on the transpiration responses of corn plants growing in different soils under moderate and high atmospheric demands. Relative plant transpiration rate (actual rate/potential rate) started to consistently decline at a soil matric potential similar to that at the inflection point of the soil water retention curve regardless of the atmospheric demand. This knowledge allowed us to generalize the transpiration response of corn plants by normalizing the soil matric potential by the soil matric potential at the inflection point. Using the normalized soil matric potential appears a better alternative to describe transpiration responses since it does not depend on arbitrary lower and upper limits to estimate plant available water. A double exponential function proved effective to describe the relationship between relative transpiration and the normalized soil matric potential for different soil and atmospheric demands. This function has the potential to be used within emerging quantitative frameworks to quantify the soil's plant available water capacity.

VITA

Andres Patrignani

Candidate for the Degree of

Doctor of Philosophy

Thesis: SOIL MOISTURE DYNAMICS IN WATER-LIMITED CROPPING SYSTEMS OF THE SOUTHERN GREAT PLAINS

Major Field: Soil Science

Biographical:

Education:

Completed the requirements for the Doctor of Philosophy in Soil Science at Oklahoma State University, Stillwater, Oklahoma in December, 2015.

Completed the requirements for the Master of Science in Plant and Soil Sciences at Oklahoma State University, Stillwater, Oklahoma in December 2011.

Completed the requirements for the Bachelor of Science in Agronomic Engineering at Universidad Nacional de Rosario, Zavalla, Santa Fe, Argentina in December 2008.

Experience:

Graduate Research Assistant, Ph.D. Department of Plant and Soil Sciences, Oklahoma State University, Stillwater, OK. Supervisor: Dr. Tyson Ochsner. 2012-2015.

Graduate Research Assistant, M.S. Department of Plant and Soil Sciences, Oklahoma State University, Stillwater, OK. Supervisors: Drs. Chad Godsey and Tyson Ochsner. 2010-2011.

Visitor Research Scholar. Department of Plant Science, South Dakota State University. Supervisor: Dr. Howard Woodard. 2009.

Professional Memberships:

American Geophysical Union; Soil Science Society of American; American Society of Agronomy; Crops Science Society of America